

# 國立交通大學

## 材料科學與工程學系 博士論文

碳奈米管之高效率離子與化學表面改質製程及其對碳  
奈米結構之影響

Study on highly efficient ion and chemical surface  
modification processes and their effects on carbon  
nanostructures

研究生：曾文綬

指導教授：郭正次 教授

中華民國九十八年六月

碳奈米管之高效率離子與化學表面改質製程及其對碳奈米結構之影響

Study on highly efficient ion and chemical surface modification processes and their effects on carbon nanostructures

研究生：曾文綬

Student: Wen-Shou Tseng

指導教授：郭正次 教授

Advisors: Prof. Chen-Tzu Kuo

國立交通大學

材料科學與工程學系

博士論文

A Thesis

Submitted to Department of Materials Science and Engineering

College of Engineering

National Chiao Tung University

in partial Fulfillment of the Requirements

for the Degree of

Doctor of Philosophy

in

Materials Science and Engineering

June 2009

Hsinchu, Taiwan, Republic of China

中華民國九十八年六月

# 碳奈米管之高效率離子與化學表面改質製程及其對碳奈米結構之影響

研究生：曾文綏

指導教授：郭正次 教授

國立交通大學  
材料科學與工程學系

## 摘要

為了提高碳奈米管(CNTs)應用之可能性，本研究主要目的為針對不同多壁碳奈米(MWCNTs)之表面改質技術進行研究，同時檢視其對碳奈米結構之影響。此製程包括利用提供不同氫/氧混合比例之氣體進行離子處理以及/或是使用兩種不同酸溶液進行酸處理。此實驗之離子乃藉由發散磁場以及施加於電漿區下 28 cm 處之樣品台偏壓自電漿萃取出，而此電漿由電子迴旋共振微波化學氣相沉積系統(ECR-MPCVD)所產生。而酸處理則使用 0.25 M 之稀釋硝酸溶液以及濃硝酸與濃硫酸之混合溶液( $\text{HNO}_3:\text{H}_2\text{SO}_4 = 1:3$  (v/v))，同時以不同的超音波震盪時間進行酸處理。經過處理後之碳奈米管，則藉由 X 射線光電子能譜儀(XPS)，掃描式電子顯微技術(SEM)，穿透式電子顯微技術(TEM)，拉曼光譜技術(Raman spectroscopy)，以及熱重分析法(TGA)進行結構及性質分析。

理想碳奈米管之官能基化本質上為藉由鍵結合氧官能基於碳管表面以便改變表面性質，而對奈米結構無太大之破壞。表面處理可能包括非結晶碳之消除、結構缺陷之形成或破壞。酸處理之效應，基本上藉由氧化碳管表面以產生自由基鍵並且稼接官能基於此鍵上，比較以濃硝/硫酸與稀釋硝酸處理之碳奈米管官能基化程度與結構之破壞，結果顯示以強酸進行酸處理，可使碳奈米管具較高的官能基化程度(高 $[\text{O}]/[\text{C}]$ 值，最高可至 52.7%)，但結構破壞過大(較高的  $I_D/I_G$  值至 0.96 以及較低的熱分解溫度至 638 °C)，由於 XPS 及 Raman 探測媒介的穿透深度限制，所量測之 $[\text{O}]/[\text{C}]$ 、 $sp^2$  以及  $I_D/I_G$  值，僅代表接近碳奈米管表面之量測結果。此外，傳統之酸處理亦具有汙染及處理時間過長(將近 9 小時)之缺點。

離子處理之效應本質上藉由使用高負偏壓值以便以較多陽離子轟擊碳奈米管並於碳管表面形成較多自由基鍵。同時，萃取自電漿具高還原電位之氧陽離子則易於此自由基鍵上鍵結而將碳管表面官能基化。實驗結果顯示，經離子處理後之碳奈米管，其 $[\text{O}]/[\text{C}]$ 、 $sp^2$  值對於氫/氧氣體流量比之曲線具有最大值而  $I_D/I_G$  具有最小值。最大官能基化程度之產生端賴於碳管表面之自由基鍵形成與萃取自電漿之氧化陽離子含量兩者間的競合關係。總言之，本研究之離子處理對於碳奈米管結構並無明顯之破壞，同時在中

間的氫/氧氣體流量比( = 25/25 (sccm/sccm))下,當離子處理時間為 5 分鐘及 20 分鐘時,官能基化程度之[O]/[C]值分別可達 31.1%及 59.8%.

而利用結合 5 分鐘之離子前處理與稀釋硝酸處理之兩階段製程來處理碳奈米管,結果顯示出,在中間的氫/氧氣體流量比( = 25/25 (sccm/sccm))下,經離子處理之碳奈米管,再經過稀釋硝酸處理兩小時後,由於可提高碳管提高管徑分布之尺寸,故可將碳奈米管之分解溫度自~ 595 °C 提高到至 684 °C,同時不會犧牲其官能基化之結果([O]/[C] = 52.4%)。比較不同的製程方法,在不使用離子處理下,濃硝/硫酸與稀釋硝酸製程處理皆可藉由減小雜質與減小小管徑之碳奈米管以提高管徑分布之尺寸來達到提升碳奈米管之分解溫度,但會造成碳奈米管之結構破壞過大或是製程時間過長的問題。總言之,結合離子前處理與稀釋硝酸後處理乃為一簡單且有效之官能基化方法,同時在不產生過大之結構破壞下提高碳奈米管之分解溫度。



# Study on highly efficient ion and chemical surface modification processes and their effects on carbon nanostructures

Student: Wen-Shou Tseng

Advisor: Prof. Cheng-Tzu Kuo

Department of Materials Science and Engineering  
National Chiao Tung University

## Abstract

For extending the potential applications of carbon nanotubes (CNTs), various processes to modify the surface of the multi-walled carbon nanotubes (MWCNTs) were studied, and effects on carbon nanostructure were examined. The processes included the ion treatment by using various flow ratios of  $H_2/O_2$  gas mixtures and/or acid treatment of two different compositions. The ions for treatment were extracted from the plasma, generated by an electron cyclotron resonance assisted microwave plasma chemical vapor deposition (ECR-MPCVD) system, through the divergent magnetic flux and the bias voltage application on the specimen stage at the position 28 cm below the plasma zone. The solutions for acid treatment included 0.25 M nitric acid or nitric/sulfuric ( $HNO_3:H_2SO_4=1:3$  (v/v)) acids. The acid treatments were conducted under various sonication times. The MWCNTs after each processing step were characterized by X-ray photoelectron spectroscopy (XPS), scanning electron microscopy (SEM), transmission electron microscopy (TEM), Raman spectroscopy, and thermogravimetric analysis (TGA).

Optimum functionalization of CNTs is essentially to bond more oxygen-containing functional groups on the surface to vary their surface properties without too much damage to the nanostructures. The surface treatment may include amorphous carbon elimination, structure defect formation or damage. Effect of acid treatment is basically to oxidize the surface of the nanotubes to create free radical bonds and to graft polar functional groups to the free bonds. By comparing the degree of functionalization and structure damage of CNTs of nitric/sulfuric acid with the dilute nitric acid treatments, the results show that former treatment results in a greater functionalization (i.e. higher  $[O]/[C]$  values, up to 52.7%) but too much structure damage (i.e. higher  $I_D/I_G$  ratios and lower decomposition temperatures, up to 0.96 and down to 638 °C), though the values of  $[O]/[C]$ ,  $sp^2$  and  $I_D/I_G$  merely represent the near surface features due to limitation of penetration depth of XPS and Raman probes. Other

drawbacks of the traditional acid treatment are its pollution issue and too long treating time (up to 9 h).

Effect of the ion treatment by using high negative substrate bias (-250 V) is essentially to bombard CNTs by more positive ions and create more free radical bonds on their surface. Meanwhile, the oxygen cations extracted from plasma can readily be bonded with these free radical bonds to functionalize the surface. The results indicate that there are existence of maximum values of  $[O]/[C]$  and  $sp^2$ , and minimum values of  $I_D/I_G$  values at medium  $H_2/O_2$  ratios. The existence of maximum functionalization is due to the competition between the amount of free radical bonds on nanotube surface and oxygen cations in the plasma stream. In summary, at medium  $H_2/O_2$  ratio (= 25/25 (sccm/sccm)), the ion treatment in the present cases causes no significant structure damage, and at treatment times of 5 and 20 minutes, the  $[O]/[C]$  values of the functionalization degree, are 31.1% and 59.8% , respectively.

For process combining the 5 min ion pretreatment and a post dilute nitric acid treatment, the results show that the ion-treated MWCNTs at medium  $H_2/O_2$  ratio (= 25/25 (sccm/sccm)) can be further treated by the dilute acid to increase the decomposition temperature from ~ 595 °C up to 684 °C without sacrificing the functionalization ( $[O]/[C]$  =52.4%) owing to the increase of size distribution change of the nanotube. By comparing different process methods, both nitric/sulfuric and dilute nitric acid treatment, without the ion treatment can also enhance decomposition temperature by eliminating the impurities and the smaller CNTs to vary the size distribution of the tubes but it causes either too much structure damage or too long treating time. In summary, the process with the ion pretreatment and followed by a dilute acid treatment is relative simple and efficient to functionalize CNTs, simultaneously enhance the decomposition temperature and cause no significant structure damage.

## Acknowledgements (謝辭)

在經歷了跨越不惑之年的這段起伏的全職學生生活後，讓我對於人生有著全然不同的體會與感受，沒有成功或者完成的喜悅，卻有著謙卑與眾多的感謝。能走過這段路，我想我該感謝的人、事、物是相當多的，然而最感謝的是郭正次教授在學習、研究及寫作方面的指導與協助。

另外，由於有 University of Manchester 的課程指導教授 Dr. Marrow 及中央大學董必正教授協助，我才能進入交大就讀。而研究主題則非常感謝台大凝態中心王立義教授與明新科大陳密教授的啟發，讓我找到最適合的方向。好友周宜衡經理及北科大賀瀚旭則一路情義相挺，讓我能一路完成各項實驗之數據分析。尤其感謝屏科大車輛系主任曾全佑教授的資源支持及寫作指導，讓我能順利完成相關的論文發表。並且感謝實驗室安亞及必愷漏夜擷取數據、威翔的鼓勵、以及學弟妹的共同生活經歷。而好友吳漢同則在我經濟困頓時給予相當的協助，使我能撐過這幾年的經濟真空期。

由於離開工作全心於學業，在這段期間歷經了許許多多的波折與障礙，因此，在此謝謝林秋萬老師在各方面適時的提醒與指點，讓我突破這許許多多的困難。而署立新竹醫院眼科主任柯美蘭醫師，總在最需要的時候給予我最大的關懷與鼓勵。最後，我特別要感謝的是我的太太欣怡，以及我親愛的女兒韻庭及兒子彥萌對我一直以來的精神支持及諒解，有了你們無怨無悔的支持才能讓我越過許許多多的茫然與內心的掙扎。



# Acknowledgements

After many years of working, the return to campus for studying the PhD program means a series of challenges and difficulties, but finally has brought me a wholly different experience of successfully dealing with many perplexities and obstacles. However, the finish of the student life seems to bring me nothing proud and arrogant but only appreciation in my heart.

The first I would like to thank is Prof. Kuo for his kind help and guidance in learning, research and writing skills. Meanwhile, owing to the references of Dr. James Marrow at the University of Manchester in the UK and Prof. Pi-Cheng Tung at National Central University, I could get the chance to study further in Chiao Tung University. Prof. Leeyih Wang at National Taiwan University and Prof. Mi Chen at MUST, inspired me the research topics. Yi-Hung Chou, Mr. He, An-Ya Lo, and Pi-Kai Chuan helped me doing the data collection and calculation. Particularly, I would like to thank Prof. Chyuan-Yow Tseng at National Pingtung University of Science and Technology for his direction on paper writing and sponsor for experiments and Han-Tung Wu for his assistance in supporting my live hood. Mr. Lin and Dr. Mai-Lan Ko at Hsin-Chu Hospital suggested me the invaluable solutions to deal with many challenges.

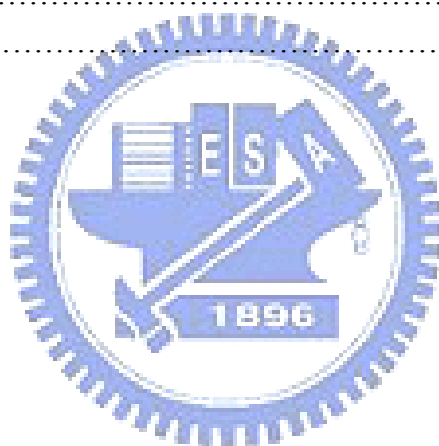
Very special thanks are due to the support and tolerance of my wife, Hsin-Yi, my daughter, Yun-Ting, and my son, Yen-Meng, letting me concentrate on my study for the years.



# Contents

Abstract in Chinese.....	I
Abstract in English.....	III
Acknowledgements (謝辭).....	V
Acknowledgements .....	VI
Contents.....	VII
List of symbols.....	IX
Table captions.....	X
Figure captions.....	XI
<b>Chapter 1 Introduction.....</b>	<b>1</b>
<b>Chapter 2 Literature review.....</b>	<b>4</b>
2.1 Structures and properties of CNTs.....	4
2.2 Synthetic methods of CNTs.....	10
2.2.1 Arc-discharge method.....	11
2.2.2 Laser ablation.....	12
2.2.3 Chemical vapor deposition.....	12
2.3 The proposed growth mechanisms of catalyst-assisted CVD.....	15
2.4 The proposed surface modification processes of CNTs.....	17
2.4.1 Chemical processes.....	18
2.4.2 Plasma processes.....	18
2.5 The characterization methods.....	19
2.5.1 Scanning electron microscopy (SEM).....	19
2.5.2 Transmission electron microscopy (TEM).....	21
2.5.3 X-ray photoelectron spectrometry (XPS).....	22
2.5.4 Raman spectroscopy.....	24
2.5.5 Thermogravimetric analysis (TGA).....	29
<b>Chapter 3 Experimental methods.....</b>	<b>32</b>
3.1 Experimental flow chart.....	32
3.2 Raw materials and processing apparatus.....	34
3.3 Acid treatment procedures.....	38
3.4 ECR plasma system for ion treatment.....	38
3.5 Ion treatment procedures.....	41
3.6 CNTs characterization.....	41
3.6.1 Scanning electron microscopy (SEM).....	41
3.6.2 Transmission electron microscopy (TEM).....	41

3.6.3	X-ray photoelectron spectrometry (XPS).....	42
3.6.4	Raman spectroscopy.....	42
3.6.5	Thermogravimetric analysis (TGA).....	42
<b>Chapter 4</b>	<b>Results and discussion</b> .....	<b>43</b>
4.1	Effect of treatment time and solution composition on morphologies of the acid-treated MWCNTs.....	43
4.2	Effect of H <sub>2</sub> /O <sub>2</sub> flow ratio on morphologies of the ion-treated MWCNTs.....	47
4.3	Effect of ion pretreatment on MWCNTs morphologies by two-step process.....	47
4.4	TEM microstructures.....	50
4.5	XPS spectra.....	51
4.6	Raman spectra.....	57
4.7	TGA results.....	62
<b>Chapter 5</b>	<b>Conclusions</b> .....	<b>69</b>
<b>Chapter 6</b>	<b>Future Prospects</b> .....	<b>72</b>
<b>References</b>	.....	<b>73</b>
<b>Vita</b>	.....	<b>84</b>



## List of symbols

$a_{c-c}$	Lattice constant	晶格常數
$C_h$	Chiral vector $C_h = na_1 + ma_2 \equiv (n, m)$ ( $n, m$ : integral) $a_1$ and $a_2$ : graphite lattice unit vectors	旋度向量 $n, m$ : 整數 $a_1$ 與 $a_2$ : 石墨烯單位向量
CNTs	Carbon nanotubes	碳奈米管
CVD	Chemical vapor deposition	化學氣相沉積法
$d_t$	The diameter of nanotube	碳奈米管直徑
$d_R$	The greatest common divisor of $(2n+m, 2m+n)$	$(2n+m, 2m+n)$ 的最大公約數
$E_L$	Excitation energy	激發能
ECR	Electron cyclotron resonance	電子迴旋共振
ECR-MPCVD	Electron cyclotron resonance chemical vapor deposition	電子迴旋共振化學氣相沉積法
$I_D/I_G$	The intensity ratio of G and D band of Raman spectrum	拉曼光譜之 D 峰和 G 峰的強度比
$K_1, K_2$	$K_1 = \frac{1}{N}(-t_2b_1 + t_1b_2), K_2 = \frac{1}{N}(mb_1 - nb_2)$	倒晶格向量
M	Molarity	莫耳濃度
MPCVD	Microwave plasma chemical vapor deposition	微波電漿化學氣相沉積法
MWCNTs	Multi-walled carbon nanotubes	多壁碳奈米管
PECVD	Plasma enhanced chemical vapor deposition	電漿輔助化學氣相沉積法
RBM	Radial breathing mode	徑向呼吸模式
RF	Radio frequency	射頻
sccm	Standard cubic centimeter per minute	標準狀態毫升/分
SEM	Scanning electron microscopy	掃描式電子顯微鏡
SWCNTs	Single-walled carbon nanotubes	單壁碳奈米管
T	Translation vector $T = (t_1a_1 + t_2a_2) \equiv (t_1, t_2)$ $t_1 = (2m+n)/d_R, t_2 = -(2n+m)/d_R$	平移向量
TEM	Transmission electron microscopy	穿透式電子顯微鏡
TGA	Thermogravimetric analysis	熱重分析法
$\theta$	Chiral angle	旋度角
XPS	X-ray photoelectron spectrometry	X 射線光電子能譜儀

# Table Captions

**Table 3-1** Specimen designations and their treatment conditions and sequences.....40

**Table 4-1** Comparisons of the XPS, Raman  $I_D/I_G$ , and TGA peak temperature for MWCNTs specimens merely treated by acid or ion treatments.....54

**Table 5-1** Comparisons of the performance of the modification processes on structure damage and the ranges of [O]/[C] ratio,  $sp^3$  percentage, and decomposition temperature.....70



# Figure Captions

<b>Fig. 2-1</b>	(a) Chiral type CNT, (b) Armchair CNT , and (c) Zigzag CNT <a href="http://en.wikipedia.org">[http://en.wikipedia.org]</a> .....	4
<b>Fig. 2-2</b>	(a) The unrolled honeycomb lattice of a nanotube and (b) (4, 2) SWCNT, showing the translation vector $\mathbf{T}$ . <a href="#">[Dresselhaus 2005-47]</a> .....	5
<b>Fig. 2-3</b>	(a) The unit cell, (b) the Brillouin zone of a graphene, and (c) the cutting lines for (4,2) nanotube <a href="#">[Dresselhaus 2005-47]</a> .....	6
<b>Fig. 2-4</b>	Electronic density of states for two (n, m) zigzag nanotubes: (a) (10, 0) and (b) (9, 0) <a href="#">[Saito 1992-2204]</a> .....	9
<b>Fig. 2-5</b>	Schematic of arc-discharge system <a href="#">[Saito-1995-3062]</a> .....	11
<b>Fig. 2-6</b>	Schematic of laser ablation system <a href="#">[Guo 1995-49]</a> .....	12
<b>Fig. 2-7</b>	Schematic of thermal CVD system <a href="#">[Lee 2001-245]</a> .....	13
<b>Fig. 2-8</b>	Schematic of MPCVD apparatus <a href="#">[Qin 1998-3437]</a> .....	14
<b>Fig. 2-9</b>	Schematic of PE-HF-CVD apparatus <a href="#">[Kurt 2001-1723]</a> .....	14
<b>Fig. 2-10</b>	SEM purity grading system <a href="#">[Itkis 2005-3439]</a> .....	20
<b>Fig. 2-11</b>	TEM images of (a) SWNTs (b) SWNT bundles (c) DWNT (d) MWNT <a href="#">[Flahaut 2000-249]</a> .....	21
<b>Fig. 2-12</b>	XPS survey spectrum of CNT treated by oxygen plasma <a href="#">[Felten 2005-074308]</a> .....	22
<b>Fig. 2-13</b>	XPS $C_{1s}$ spectra of the as-purchased MWCNTs and the five chemical species: (1) graphite; (2) $sp^3$ carbons; (3) hydroxyl groups; (4) carbonyl groups; and (5) carboxyl groups <a href="#">[Felten 2005-074308]</a> .....	22
<b>Fig. 2-14</b>	Schematic of state change of Raman scattering <a href="#">[Rao 1997-187]</a> .....	25
<b>Fig. 2-15</b>	The left panel shows the electronic transition energies $E_{ii}$ vs. nanotube diameter $dt$ . The right panels show schematic figures defining the SWNT classes: MOD0 — metallic, where one cutting line crosses the $K$ point; MOD1 and MOD2 — semiconducting <a href="#">[Dresselhaus 2005-47]</a> .....	25
<b>Fig. 2-16</b>	Raman spectra from a metallic (top) and a semiconducting (bottom) SWNT at the single nanotube <a href="#">[Dressehaus 2005-47]</a> .....	26
<b>Fig. 2-17</b>	The Raman vibration modes of CNTs (a) G-band mode (b) D-band mode (c) Radial breath mode <a href="#">[Raravikar 2002-235424]</a> .....	27
<b>Fig. 2-18</b>	(a) The revised $E_{ii}$ vs $\omega_{RBM}$ plot comparing experimental results from experiments on SDS wrapped SWNTs in solution. (b) The revised Kataura plot <a href="#">[Jorio 2005-075401]</a> .....	29
<b>Fig. 2-19</b>	The weight loss (solid) and weight derivative (dash) curves of TGA <a href="#">[Harutyunyan 2002-8671]</a> .....	30
<b>Fig. 3-1</b>	Experiment flowchart.....	33

<b>Fig. 3-2</b>	SEM image of as-purchased CNTs.....	34
<b>Fig. 3-3</b>	TEM images of as-purchased CNTs: (a) at lower magnification, (b) at higher magnification.....	34
<b>Fig. 3-4</b>	XPS C <sub>1s</sub> spectrum of the as-purchased CNTs.....	35
<b>Fig. 3-5</b>	Raman spectrum of the as-purchased CNTs.....	36
<b>Fig. 3-6</b>	TGA curve for the as-purchased CNTs.....	37
<b>Fig. 3-7</b>	Schematic of the ECR plasma system for ion treatment.....	39
<b>Fig. 4-1</b>	SEM morphologies of MWCNTs after different acid treatment times, (a) 6 h; (c) 9 h (Specimens A1 and A2, respectively), where (b) and (d) are corresponding SEM images of (a) and (c) respectively at higher magnification.....	44
<b>Fig. 4-2</b>	SEM images of the 0.25 M HNO <sub>3</sub> acid-treated MWCNTs (Specimen A3)...	44
<b>Fig. 4-3</b>	SEM images for the ion-treated MWCNTs specimens for different H <sub>2</sub> /O <sub>2</sub> flow ratios, (a) 50/0, (b) 40/10, (c) 25/25, (d) 10/40, (e) 0/50 and (f) 25/25 (sccm/sccm), (Specimen B1 to B6, respectively).....	45
<b>Fig. 4-4</b>	SEM images for the ion-treated MWCNTs specimens for different H <sub>2</sub> /O <sub>2</sub> flow ratios, (a) 50/0, (b) 40/10, (c) 25/25, (d) 10/40, (e) 0/50 and (f) 25/25 (sccm/sccm) (Specimen B1 to B6, respectively) at higher magnification.....	46
<b>Fig. 4-5</b>	SEM images for the ion-pretreated MWCNTs specimens for different H <sub>2</sub> /O <sub>2</sub> flow ratios, (a) 50/0, (b) 40/10, (c) 25/25, (d) 10/40 and (e) 0/50 (sccm/sccm) (Specimen C1 to C5, respectively), and followed by a 0.25 M HNO <sub>3</sub> acid-treatment.....	48
<b>Fig. 4-6</b>	SEM images for the ion-pretreated MWCNTs specimens for different H <sub>2</sub> /O <sub>2</sub> flow ratios, (a) 50/0, (b) 40/10, (c) 25/25, (d) 10/40 and (e) 0/50 (sccm/sccm), (Specimen C1 to C5, respectively), and followed by a 0.25 M HNO <sub>3</sub> acid-treatment at higher magnification.....	49
<b>Fig. 4-7</b>	TEM image of merely ion-treated MWCNT (Specimen B3) at higher magnification.....	50
<b>Fig. 4-8</b>	TEM image ion-treated MWCNT (Specimen B3) at higher magnification.....	50
<b>Fig. 4-9</b>	XPS C <sub>1s</sub> spectra of the acid-treated MWCNTs under different treatment times, (a) 6h, and (b) 9 h (for Specimens A1 and A2, respectively).....	52
<b>Fig. 4-10</b>	XPS survey spectra of the 5 min ion-treated MWCNTs under different H <sub>2</sub> /O <sub>2</sub> flow ratios (for Specimens B1 to B5).....	53
<b>Fig. 4-11</b>	XPS C <sub>1s</sub> spectra of the 5 min ion-treated MWCNTs under different H <sub>2</sub> /O <sub>2</sub> flow ratios (for Specimens B1 to B5).....	53
<b>Fig. 4-12</b>	XPS C <sub>1s</sub> spectrum of the 20 min ion-pretreated MWCNTs (Specimen B6)	

	and its deconvoluted spectra.....	53
<b>Fig.4-13</b>	XPS C <sub>1s</sub> spectra of the 5 min ion-pretreated MWCNTs and followed by a 0.25 M HNO <sub>3</sub> acid treatment (for Specimens C1 to C5).....	56
<b>Fig. 4-14</b>	Raman spectra of the acid-treated MWCNTs under different treatment times (for Specimens A1 and A2).....	57
<b>Fig. 4-15</b>	Raman spectra of the 5 min ion-treated MWCNTs under different H <sub>2</sub> /O <sub>2</sub> flow ratios (for Specimens B1 to B5).....	58
<b>Fig. 4-16</b>	I <sub>D</sub> /I <sub>G</sub> ratio of the 5 min ion-treated MWCNTs vs. H <sub>2</sub> concentration in H <sub>2</sub> /O <sub>2</sub> flow.....	59
<b>Fig. 4-17</b>	Raman spectra of the 5 min ion-pretreated MWCNTs and followed by a 0.25 M HNO <sub>3</sub> acid treatment (for Specimens C1 to C5).....	61
<b>Fig. 4-18</b>	TGA curves for the acid-treated MWCNTs under different treatment times, (a) 6 h, and (b) 9 h (for Specimens A1 and A2, respectively).....	62
<b>Fig. 4-19</b>	TGA curves for the ion-treated MWCNTs under different H <sub>2</sub> /O <sub>2</sub> gas flow ratio.....	63
<b>Fig. 4-20</b>	Weight-derivative TGA curves for the 5 min ion-treated MWCNTs under different H <sub>2</sub> /O <sub>2</sub> flow ratios (for Specimens B1 to B5).....	64
<b>Fig. 4-21</b>	TGA curves for 0.25M HNO <sub>3</sub> acid-treated MWCNTs.....	65
<b>Fig. 4-22</b>	TGA curves of the 5 min ion-pretreated MWCNTs and followed by a 0.25 M HNO <sub>3</sub> acid treatment (for Specimens C1 to C5).....	66
<b>Fig. 4-23</b>	Weight-derivative TGA curves of the 5 min ion-pretreated MWCNTs and followed by a 0.25 M HNO <sub>3</sub> acid treatment (for Specimens C1 to C5).....	66
<b>Fig. 4-24</b>	TGA curves of MWCNTs for different conditions, (a) as-purchased, (b) 5 min ion-treated (Specimen B3), (c) merely 0.25 M HNO <sub>3</sub> acid-treated (Specimen A3), (d) 5 min ion-pretreated and 0.25 M HNO <sub>3</sub> acid-treated (Specimen C3), and (e) merely acid-treated MWCNTs (Specimen A2).....	67
<b>Fig.4-25</b>	Weight-derivative TGA curves of MWCNTs for different conditions, (a) as-purchased, (b) 5 min ion-treated (Specimen B3), (c) merely 0.25 M HNO <sub>3</sub> acid-treated (Specimen A3), (d) 5 min ion-pretreated and 0.25 M HNO <sub>3</sub> acid-treated (Specimen C3), and (e) merely acid-treated MWCNTs (Specimen A2).....	67

# Chapter 1

## Introduction

A single-walled carbon nanotube (SWCNT) can be described as a layer of hexagonal graphene sheet rolled into a seamless cylinder whilst a multi-walled carbon nanotube (MWCNT) is formed with multiple graphene layers. This results in a nanostructure with high aspect ratio (length—to—diameter) exceeding up to 100,000 [Saito 2004-p35]. Such cylindrical carbon molecules have novel properties that make them potentially useful in many applications, such as biosensors, drug and vaccine delivery vehicles, protein transporters, artificial muscles, novel biomaterials, and solar power [Venkatesan 2005- 7154, Bianco 2005-674, Smart 2006-1034, Chiu 2008-3024, Landi 2005-165]. To date, in order to fulfill many application requirements, variety methods have also been proposed for the synthesis of CNTs, e.g. arc discharge [Saito 1995-979], laser ablation [Guo 1995-49] and chemical vapor deposition (CVD) [Lee 2001-245].

As mentioned by previous study, the resulting products often contain unwanted carbon impurities such as nanocrystalline graphite and fullerene [Landi 2005-9952]. In addition, the inactive layer formed by amorphous carbon on the outer surface has been suggested as the main cause of bundling [Felten 2005-074308-1, Ionescu 2006-36]. Because most applications of CNTs involve their dispersion in polymer or aqueous matrices, the agglomeration of CNTs can significantly reduce their usefulness [Fu 2003-351, Liu 1998-1253]. Therefore, post-synthesis treatments are often called for in order to remove the byproducts or graft covalent bonding on their sidewall without damaging the CNTs structure. To date, many researchers are resorting to the use of strong acids that can have a serious impact on the integrity of nanotubes. Acid treatment is based on selective oxidation to remove amorphous carbon through sonicating or refluxing the nanotubes in a strong acid. It is found to effectively remove metals from the



reaction products [Tohji 1996-679, Hou 2002-81, Park 2001-655] and introduce oxygenated groups such as carboxylic acids (-COOH), carbonyls (-C=O), and hydroxyls (-OH) on the surface of the nanotubes. This enhances the polarity of the nanotubes which is an advantageous property [Fu 2003-351, Ovejero 2006-2206, Dujardin 1998-1472, Li 2003-858, Park 2006-141]. However, the drawbacks of this method include degradation of the length of the CNTs and oxidative damage to the nanotubes [Fu 2003-351, Ovejero 2006-2206, Dujardin 1998-1472, Li 2003-858, Park 2006-141].

Recent studies have shown that plasma treatment can be used to facially modify CNTs and to remove amorphous carbon from the surface of nanotubes [Felten 2005-074308-1, Ionescu 2006-36, Xu 2007-8945, Wu 2007-1336, Khare 2004-8166, Khare 2005-23466, Ahn 2003-2481]. During the treatment, the generated particles and UV light may create free radical bonds on the surface and, additionally, form polar functional groups on the radical bonds [Felten 2005-074308-1]. In addition, the amorphous carbon layer is more active than the cylindrical walls for the formation of volatile products with the oxygen cations which are then removed by the pumping system. Although many results have shown that plasma treatment is effective in facial modification of CNTs, it is also mentioned that the high energy and temperature of the plasma may cause serious structural damage through overheating and over-etching within a short process time [Felten 2005-074308-1, Xu 2007-8945]. Therefore, placing nanotubes away from plasma, and reducing the treatment time and temperature would be the optimal ways to circumvent these issues.

In this study, in order to find a method to efficiently functionalize CNTs with insignificant structure damage and to extend the potential applications of carbon nanotubes (CNTs), various processes to modify the surface of the multi-walled carbon nanotubes (MWCNTs) were studied, and effects on their nanostructure were examined. The processes included the ion treatment of various flow ratios of H<sub>2</sub>/O<sub>2</sub> gas mixtures and/or acid treatment of two different compositions. The ions for treatment were extracted from the plasma, generated by an electron cyclotron resonance assisted microwave plasma chemical vapor

deposition (ECR-MPCVD) system, through the divergent magnetic flux and the bias voltage application on the specimen stage at the position 28 cm below the plasma zone. The solutions for acid treatment included 0.25 M nitric acid or nitric/sulfuric ( $\text{HNO}_3:\text{H}_2\text{SO}_4=1:3$  (v/v)) acids. The acid treatments were conducted under various sonication times. The MWCNTs after each processing step were characterized by X-ray photoelectron spectroscopy (XPS), scanning electron microscopy (SEM), transmission electron microscopy (TEM), Raman spectroscopy, and thermogravimetric analysis (TGA).



# Chapter 2

## Literature review

### 2.1 Structures and properties of CNTs

CNTs are one of the most exciting new materials for the past decades in the field of nanoscience and nanotechnology. CNTs are giant fullerenes which, by definition, is a closed convex cage molecule containing only hexagonal and pentagonal faces [Pillai 2007-3011]. Formed from essentially the graphite sheets (or graphene sheets), CNTs normally exists with varied structures, differed in length, type of chirality, and number of layers [Saito 2004-p35, Pillai 2007-3011].

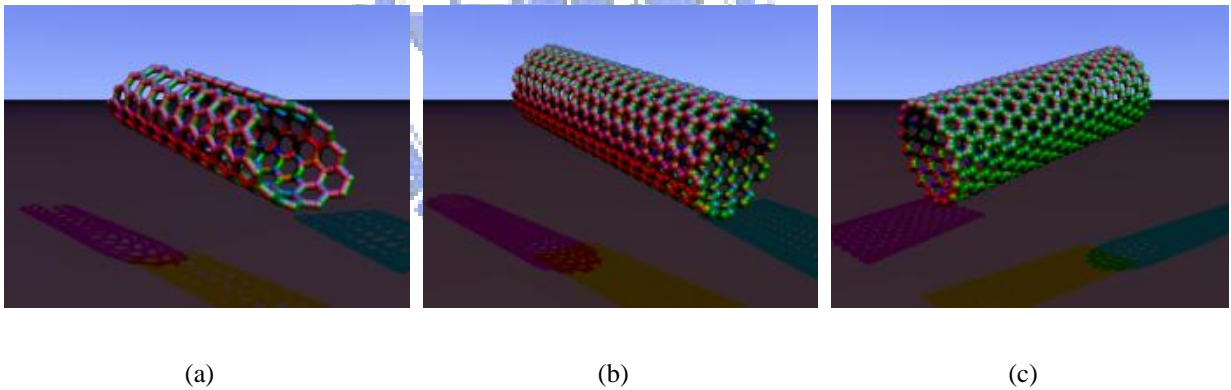


**Fig. 2-1** (a) Chiral type CNT, (b) Armchair CNT, and (c) Zigzag CNT [http://en.wikipedia.org]

Theoretically, a single-walled carbon nanotube (SWCNT) can be described as a layer of hexagonal graphene sheet rolled into a seamless cylinder whilst a multi-walled carbon nanotube (MWCNT) is formed with multiple graphene layers [Saito 2004-p35]. This leads to different types of structural arrangements, which are typically classified as non-chiral and chiral structural types, due to different rolling direction [Saito 2004-p35]. In non-chiral structures of SWCNTs, the honey comb lattices of the nanotube are parallel to the tube axis and these

are known as armchair (Fig. 2.1(b)) and zigzag (Fig. 2.1(c)) arrangements [Saito 1992-2204]. In armchair structure, two C-C bonds on opposite sides of each hexagonal lattice are perpendicular to nanotube axis; in zigzag structure, the bonds are parallel to nanotube axis. Different from non-chiral structures, the C-C bonds in chiral structures (Fig. 2.1(a)) are with an angle to nanotube axis.

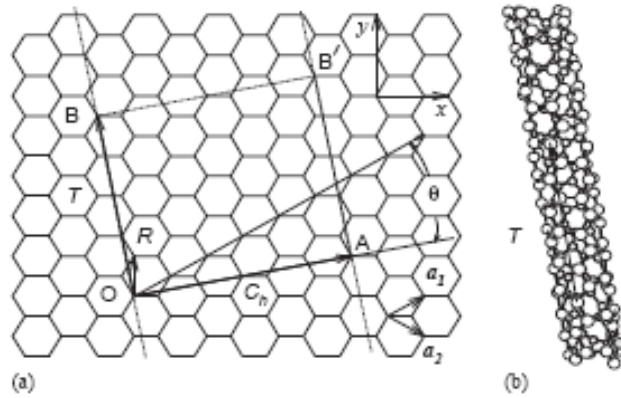


**Fig. 2-2** (a) The unrolled honeycomb lattice of a nanotube and (b) (4, 2) SWCNT, showing the translation vector  $T$ . [Dresselhaus 2005-47]

As shown in Fig. 2.2, when sites O and A, and B and B' are connected, respectively, a portion of a graphene sheet can thus be rolled seamlessly to form a SWCNT. Meanwhile, vectors OA and OB are defined as the chiral vector,  $C_h$ , and the translational vector  $T$  of the nanotube, respectively [Saito 2004-p38]. This rectangle portion, OAB'B, is then defined as a unit cell for the nanotube. Generally, a SWCNT is mathematically specified by a chiral vector,  $C_h$ , (Fig. 2.2(a)) and the  $C_h$  is given by [Dresselhaus 2005-47, Saito 2004-p46]

$$C_h = na_1 + ma_2 \equiv (n, m) \quad (1)$$

where  $a_1$  and  $a_2$  are unit vectors in two-dimensional (2D) hexagonal lattice and  $n$  and  $m$  are integers. Meanwhile, chiral vector is often described by a pair of indices  $(n, m)$ . With chiral vector,  $C_h = (n, m) = (4, 2)$ , the nanotube in figure Fig. 2.2 is described as a (4, 2) nanotube. A

chiral angle,  $\theta$ , is defined as the angle between  $C_h$  and  $a_1$  and given by [Dresselhaus 2005-47]

$$\theta = \tan^{-1} \left( \frac{\sqrt{3}m}{2n+m} \right) \quad (2)$$

When a graphene sheet is rolled into a nanotube, the  $C_h$  (or vector  $OA$ ) forms the circumference of the circular cross-section of the nanotube with the ends of the vector superimposing with each other. Different pairs of integers  $(n, m)$  define a different rolling way to form a nanotube. This means the chiral vector determines the rolling direction of a graphene sheet to form a nanotube. Note that a lattice point  $(n, m)$  is superimposed with an origin  $(0, 0)$ . In this sense, a diameter,  $d_t$ , of the nanotube can be expressed as [Dresselhaus 2005-47, Saito 2004-p46]

$$d_t = \frac{|C_h|}{\pi} = \frac{\sqrt{3}a_{c-c} \sqrt{n^2 + nm + m^2}}{\pi} \quad (3)$$

where  $a_{c-c} = 1.44 \text{ \AA}$  is the nearest neighbor C–C distance in the graphene sheet [Saito 2004-p46]. When  $n = m$  and  $\theta = 30^\circ$ , armchair nanotubes are obtained while zigzag nanotubes correspond to either  $n$  or  $m$  are equal to 0 and  $\theta = 0$ . In addition, all other nanotubes have  $\theta$  values ranging from 0 to  $30^\circ$ .

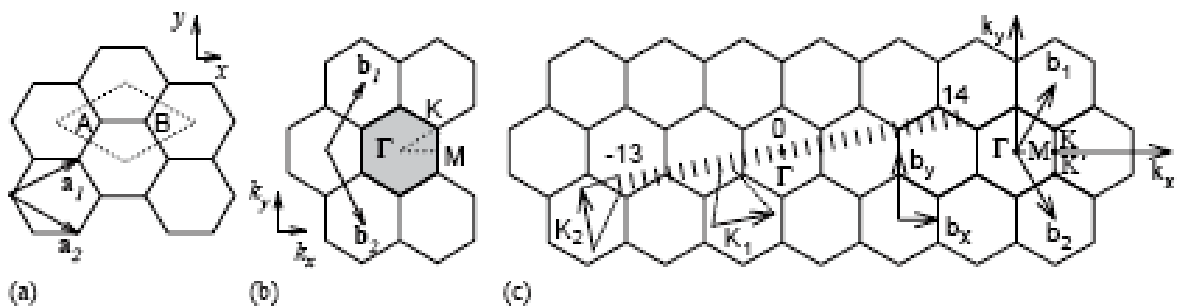


**Fig. 2-3** (a) The unit cell, (b) the Brillouin zone of a graphene, and (c) the cutting lines for  $(4,2)$  nanotube [Dresselhaus 2005- 47]

As shown in Fig. 2.3(a) a unit cell is plotted as a dotted rhombus in real space with

containing the sites A and B, where carbon atoms are located [Dresselhaus 2005-47]. Fig. 2.3 (b) reveals the Brillouin zone, i.e. the shaded hexagon, in reciprocal space of the 2D graphite layer. Meanwhile,  $\mathbf{a}_i$  and  $\mathbf{b}_i$ , where  $i = 1$  and  $2$ , in the figure are the basis vectors and reciprocal lattice vectors, respectively. It is shown that the direction of the reciprocal vectors,  $\mathbf{b}_1$  and  $\mathbf{b}_2$ , of the reciprocal hexagonal lattice are rotated by  $30^\circ$  from the basis vectors,  $\mathbf{a}_1$  and  $\mathbf{a}_2$ , of the hexagonal lattice in real space. Three high symmetry points,  $T$ ,  $K$  and  $M$  are also indicated in Fig. 2.3 (b) [Dresselhaus 2005-47]. As shown in Fig. 2.3 (c), some parallel cutting lines are plotted in circumferential direction and labeled by the cutting line index  $\mu$ , which assumes the integer values from  $1 - \frac{N}{2} = -13$  to  $\frac{N}{2} = 14$  [Dresselhaus 2005-47]. Each of the discrete values of the circumferential wave vectors, one-dimensional (1D) energy bands will appear (one  $\pi$ -band and one  $\pi^*$ -band) [Saito 2004-P47].

From the theoretical viewpoint, carbon nanotubes are interesting as a 1D periodic graphene structure along the tube axis [Saito 1992-2204]. The confinement in the radial direction can be induced by the 1D monolayer nanotube [Saito 1992-2204]. In order to define a unit cell for the 1D nanotube, the vector  $OB$  in Fig. 2.2(a) is defined as the shortest repeat distance along the nanotube axis [Dresselhaus 2005-47].

The translation vector  $T$  is then defined as [Dresselhaus 2005-47, Saito 2004-p46]

$$\mathbf{T} = t_1 \mathbf{a}_1 + t_2 \mathbf{a}_2 \equiv (t_1, t_2) \quad (4)$$

where  $t_1$  and  $t_2$  are given by

$$t_1 = \frac{2m+n}{d_R}, \quad t_2 = -\frac{2n+m}{d_R} \quad (5)$$

where the greatest common divisor,  $d_R$ , of  $(2m+n, 2n+m)$  is given by

$$d_R = \begin{cases} d, & \text{when } n - m \text{ is not a multiple of } 3d \\ 3d, & \text{when } n - m \text{ is a multiple of } 3d \end{cases} \quad (6)$$

Both translation vector,  $\mathbf{T}$ , and chiral vector,  $\mathbf{C}_h$ , determine the unit cell of the carbon nanotube in real space. The reciprocal lattice vectors  $\mathbf{K}_2$  along the nanotube axis and  $\mathbf{K}_1$  in the circumferential direction are the corresponding vectors in reciprocal space and  $\mathbf{K}_1$  vector gives the discrete  $k$  values in the direction of the chiral vector  $\mathbf{C}_h$  [Dresselhaus 2005-47]. The vectors  $\mathbf{K}_1$  and  $\mathbf{K}_2$  can be obtained from the relation  $\mathbf{R}_i \cdot \mathbf{K}_j = 2\pi\delta_{ij}$ , where  $\mathbf{R}_i$  and  $\mathbf{K}_j$  are the lattice vectors in real and reciprocal space and should follow the relations [Dresselhaus 2005-47]

$$\mathbf{C}_h \cdot \mathbf{K}_1 = 2\pi, \mathbf{T} \cdot \mathbf{K}_1 = 0, \mathbf{C}_h \cdot \mathbf{K}_2 = 0, \mathbf{T} \cdot \mathbf{K}_2 = 2\pi \quad (7)$$

From Eq. (7),  $\mathbf{K}_1$  and  $\mathbf{K}_2$  can be written as

$$\begin{cases} \mathbf{K}_1 = \frac{1}{N}(-t_2\mathbf{b}_1 + t_1\mathbf{b}_2) \\ \mathbf{K}_2 = \frac{1}{N}(m\mathbf{b}_1 - n\mathbf{b}_2) \end{cases} \quad (8)$$

The  $N$  wave vectors  $\mu\mathbf{K}_1$  ( $\mu=1-N/2, \dots, N/2$ ) may lead to  $N$  discrete  $k$  vectors or cutting lines as mentioned previously [Saito 2004-P47]. For a particular  $(n, m)$  nanotube, when a cutting line passes through a  $\mathbf{K}$  point in the 2D Brillouin zone, where the  $\pi$  and  $\pi^*$  energy bands of 2D graphite are degenerate by symmetry, the 1D energy bands will be with a zero energy gap and show a metallic behavior [Saito 2004-P60]. On the other hand, it is expected to show semiconducting behaviors if no cutting line passes through the point [Saito 2004-P60]. Owing to the translation symmetry of  $\mathbf{T}$ , there are continuous wave vectors in the direction of  $\mathbf{K}_2$  for CNT with infinite length [Saito 2004-P47]. However, when a nanotube is with finite length of  $L$ , the spacing between discrete wave vectors along the tube axis is thus  $2\pi/L$  [Saito 2004-P47].

Considering the tube geometry, some mixing of the  $\pi$  ( $2p_z$ ) and  $\sigma$  ( $2s$  and  $2p_{x,y}$ ) carbon orbitals may appear owing to the tube curvature [Saito 1992-2204]. However, the mixing is

marginal near the Fermi level and, therefore, only  $\pi$  orbitals are required to be considered [Saito 1992-2204]. Therefore, the 2D energy dispersion relations for  $\pi$  bands of graphene layer can be obtained by the equation [Saito 2004-P62]

$$E_{2D} = \pm \gamma_0 \left[ 1 + 4 \cos\left(\frac{\sqrt{3}k_x a_{c-c}}{2}\right) \cos\left(\frac{k_y a_{c-c}}{2}\right) + 4 \cos^2\left(\frac{k_y a_{c-c}}{2}\right) \right]^{\frac{1}{2}} \quad (9)$$

where  $\gamma_0$  is the nearest-neighbor overlap integral [Jishi 1994-2252] and  $a_{c-c}$  is a lattice constant as mentioned previously. When  $k_x$  or  $k_y$  are eliminated by using the periodic boundary condition [Saito 1992-2204],

$$C_h \cdot k = 2\pi q \quad (10)$$

where  $q$  is an integer, 1D energy bands can be thus obtained for general chiral structures through slicing the 2D energy dispersion relations of Eq. (9) in the directions expressed by Eq. (10) [Saito 1992-2204].

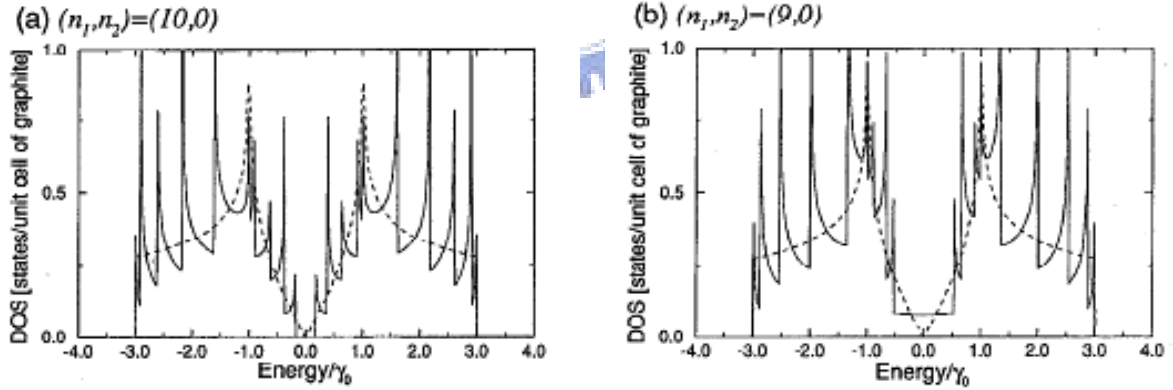


**Fig. 2-4** Electronic density of states for two  $(n, m)$  zigzag nanotubes: (a)  $(9, 0)$  and (b)  $(10, 0)$

[Saito 1992-2204]

As shown in Fig. 2.4, the density of states for two zigzag nanotubes with  $(n, m) = (10, 0)$  and  $(9, 0)$  are plotted according to the units of states per unit cell of 2D graphite. For comparison purpose, the corresponding density of states of 2D graphite is also plotted with



dotted lines. Meanwhile, the  $1/\sqrt{E}$  singularities of 1D energy bands can be observed at the band edges of each energy band [Saito 1992-2204]. As shown in Fig. 2.4 (a), it is also observed that there is an energy gap at the Fermi level, where  $E = 0$ , while there is a finite density of states in Fig. 2.4 (b), and semiconducting (Fig. 2.4(a)) and metallic (Fig. 2.4(b)) nanotube are thus present. Normally, to determine a nanotube as a metallic type should follow the condition [Saito 1992-2204]

$$2n + m = 3b \quad (11)$$

where  $b$  is an integer. This condition can be obtained by substituting the  $k$  vector of the degenerate point of 2D graphite at the corner of the Brillouin zone into Eq. (10). Normally, the chiral vectors are only located in the range,  $-30^\circ < \theta < 0^\circ$ , as shown in Fig. 2.2 [Saito 1992-2204]. It is suggested that all armchair nanotubes and zigzag nanotubes should be metallic when  $n$  is a multiple of three [Saito 1992-2204].

Interestingly, it is proposed that if the distribution of  $C_h$  vectors shown in Fig. 2.2 is uniform,  $1/3$  of the nanotubes will be with metallic behaviors and  $2/3$  of those will be with semiconducting behaviors [Saito 1992-2204]. However, a larger fraction of metallic CNTs may be obtained if the initial seed of the tube caps is centered on a pentagon. This leads to an armchair nanotube [Saito 1992-2204]. On the other hand, if the initial seed is a hexagon other than a pentagon, the nanotube might be grown with a planar graphite structure [Saito 1992-2204]. Based on this point, it is suggested that nature might prefer armchair-type nanotubes [Saito 1992-2204].

## 2.2 Synthetic methods of CNTs

Until recently, many methods have been developed to synthesize CNTs in three primary approaches including arc-discharge, laser ablation and chemical vapor deposition (CVD) [Lee 2001-245; Pillai 2007-3011]. In these methods, carbon sources are normally provided in gas or solid

states. Meanwhile, the morphology and properties of CNTs are often controlled with the process parameters including substrate temperature, precursor gases and gas ratio, catalyst, pretreatment conditions, and bias voltage, etc. However, the proposed methods still suffer from the problems, such as low yielding and low uniformities in structure and property.

### 2.2.1 Arc-discharge method

CNTs were first synthesized by arc-discharge method and identified by Iijima [Iijima 1991-56]. As shown in Figure 2.5 [Saito 1995-979], two graphitic rods are used as anode and cathode in this arc-discharge system. In the process, arcing occurs when DC voltage is applied between these two electrodes. With containing small amount of catalysts, such as Fe, Co, Ni, and Y, the SWCNTs can be synthesized at the anode [Bethune, 1993-605] whilst MWNTs can be fabricated using pure graphite as two electrodes.

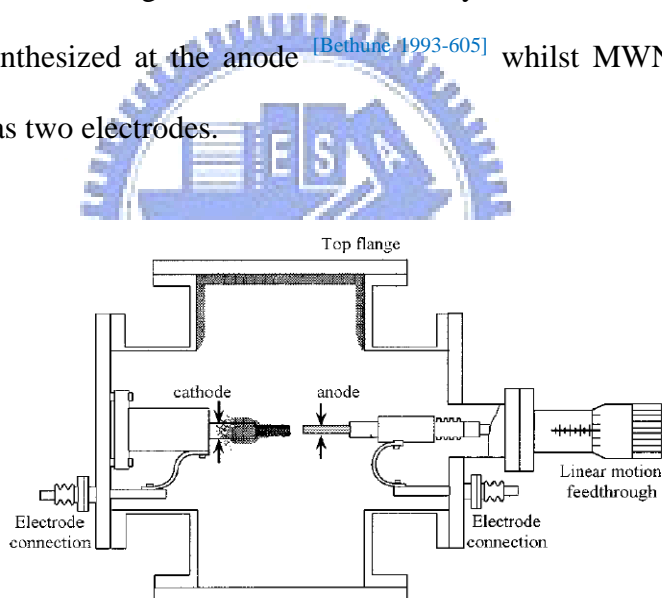


**Fig. 2-5** Schematic of arc-discharge system [Saito-1995-3062]

The discharge system is normally operated with voltages ranging from 20 to 40 V and current from 40 to 100 A under He or Ar gas pressure of 10 ~ 500 Torr. Carbon clusters, collided out from the anodic graphite rod through electron bombardment, are deposited on the cathode surface. The products on the cathode may include amorphous carbon, fullerenes, carbon cluster, carbon nanotubes, and other carbon structures. Therefore, post treatment to purify the nanostructures is often required for practical uses. Another drawback is its low

yielding in producing CNTs.

### 2.2.2 Laser ablation

Laser ablation was first reported by Guo's group in 1995 <sup>[Guo 1995-49]</sup>, as shown in Fig. 2.6. An incident laser beam is used to vaporize graphite target under helium or argon gas atmosphere with pressure of 500 Torr. The products are swept out by the flowing gas and to be deposited on the water cooled collector. Therefore, it is also named as laser vaporization method. Normally, the graphite target used in this method often containing Co, Ni, Fe, or Y and this is a favorable condition of forming SWCNTs.

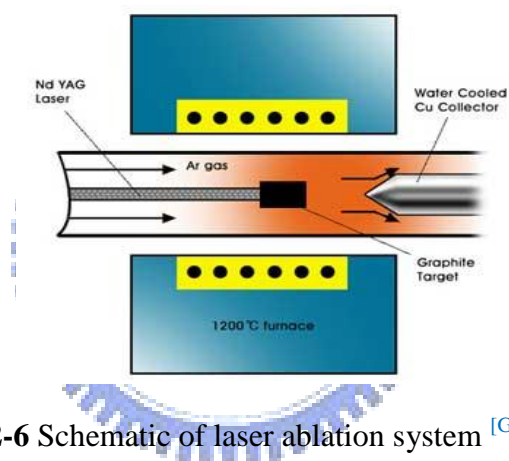
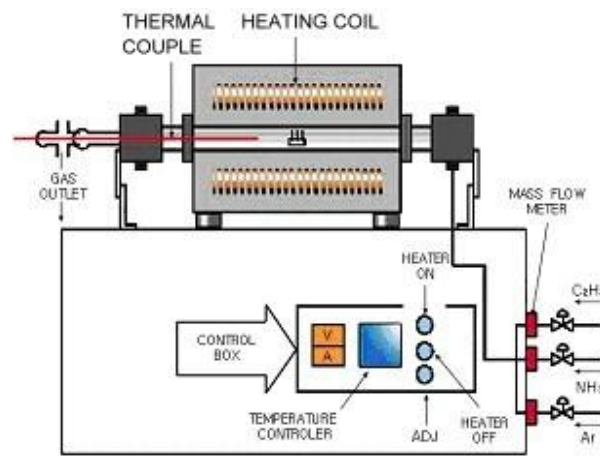


Fig. 2-6 Schematic of laser ablation system <sup>[Guo 1995-49]</sup>

### 2.2.3 Chemical vapor deposition

As shown in Fig. 2.7, thermal chemical vapor deposition <sup>[Lee 2001-245]</sup> applies the pyrolysis of hydrocarbon source to synthesize the CNTs. This method is also a catalyst-assisted SWCNTs growth method and is one of the most commonly used methods. Meanwhile it is considered the best solution for nanoscale device fabrication because it not only allows a scalable process but also enables selective growth on patterned catalyst film <sup>[Golovko 2005-1636]</sup>. The formation of CNTs using CVD involves the formation of small catalyst nanoparticles, decomposition of hydrocarbon gases such as  $\text{CH}_4$  and  $\text{C}_2\text{H}_2$ , and then growth of the nanotubes on the metal catalysts. Normally, the catalyst particles are coated on substrate and reduced by

CVD using hydrogen plasma to form well-distributed and active metallic nanoparticles. Nanosized catalytically metal particles are formed after the catalytic metal film is etched with  $\text{NH}_3$  gas at a temperature ranging from 750 to 1050°C. Reaction gas is supplied from one end of the apparatus and evacuated from the outlet on the other side. The merit of this method is capable of depositing large area, and uniform as well as good quality of SWNTs. However the drawback of this method is not compatible with IC (integrated circuit) process due to the high working temperature over 600 °C.



**Fig. 2-7** Schematic of thermal CVD system [Lee 2001-245]

PECVD system is the most employed method for depositing CNTs [Qin 1998-3437] compared with the other methods because this method can be compatible to IC process for its low process temperature and a cheap, less contamination, and high yielding process. Meanwhile, this process is highly capable of producing controlled alignment of SWCNTs. Therefore, many new techniques have been developed to prepare vertically aligned SWCNTs through using this method.

In practical uses, the plasma is activated by a microwave plasma apparatus using RF or DC discharged system, microwave plasma assisted hot filament, and electron cyclotron resonance (ECR) plasma source. In general, the typical power supplies used in this method are DC bias, radio frequency (RF) (13.56 MHz) and microwave (2.45 GHz). During the

process, SWCNTs are produced by the decomposition of hydrocarbon (such as  $\text{CH}_4$ ,  $\text{C}_2\text{H}_2$ ,  $\text{C}_2\text{H}_4$  and  $\text{C}_6\text{H}_6$ ) or monoxide, and then deposition on nanoparticles of transition-metal.

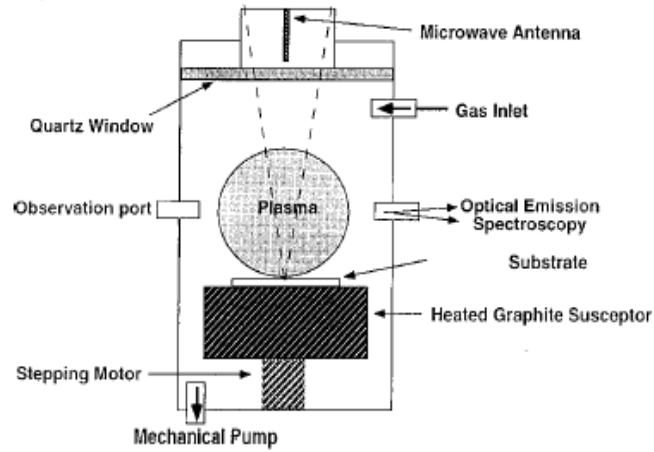


**Fig. 2-8** Schematic of MPCVD apparatus [Qin 1998-3437]

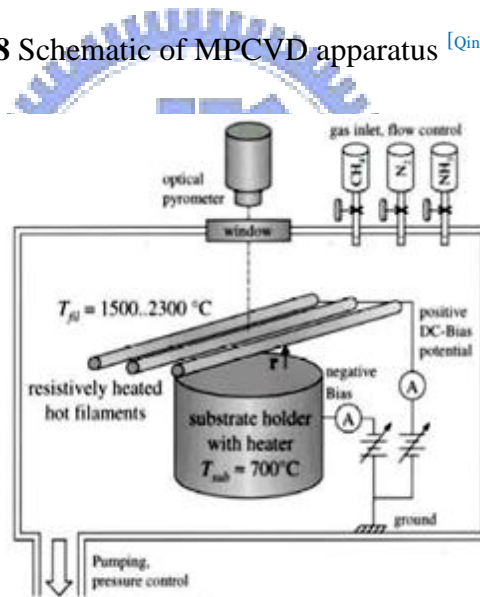


**Fig. 2-9** Schematic of PE-HF-CVD apparatus [Kurt 2001-1723]

As shown in Fig. 2.8, with the high density of plasma, the MP-CVD system [Qin 1998-3437] is a contamination-free process and the plasma shape can be regulated through adjusting the cavity. The PE-HF-CVD system applies the current of the tungsten filament to efficiently increase the temperature in the process chamber [Kurt 2001-1723] as depicted in Fig. 2.9. As shown in Fig. 2.10, ECR-CVD system is well known for its advantages of high dissociation percentage of the precursor gas, high uniformity of plasma energy distribution and large area

of CNTs deposition [Tsai 2001-NCTU].

### 2.3 The proposed growth mechanisms of catalyst-assisted CVD

In order to well control the synthesizing process of CNTs, it is very important to understand of the growth mechanism of CNTs. Until recently, although many detailed and precise growth have been proposed, most of them are still in controversy [Kuo 2004-p9-2]. However, it is believed that the application of catalyst is required to synthesize CNTs in diameter ranging from 0.7 to 2 nm for the growth process [Kuo 2004-p9-9]. It is also known that the application of alloy catalyst can increase the growth quantity of SWCNTs significantly. Some of the growth mechanisms of SWCNTs are demonstrated as blew:

#### (a) Root growth model

Proposed by Saito et al., this model is used to explain the growth mechanism of radiate sea-urchin-like SWCNTs by using arc-discharge [Saito 1994-L526]. In their study, numerous SWCNTs grow from single catalyst particles and their resulting diameters are much smaller than the particles. It is proposed that carbon-metal alloy can be formed by vaporization during arc discharge process; this alloy posses higher carbon solubility than in a solid state. Therefore, the liquid alloy particles tend to segregate excess carbon on their surface with the decrease of temperature of the cathode.

Two possible occasions can be observed in process. The first is that the cooling rate of the particles proceeds with a moderate rate and the supersaturated carbon in metal particles is not high so that carbon is gradually segregated on the particle surface, forming graphitic layer.

Alternatively, the cooling rate is so rapid that the dissolved carbon in a particle is very high. Supersaturated carbon could cause numerous nucleation sites of graphite on the particle

surface. A large number of tiny flakes are thus forming and subsequently closing their open ends in order to saturate dangling bonds at their periphery. SWCNTs can then be formed on the random graphitic flake assembly.

### **(b) Ball-and-stick catalyst scooting model**

This model can be used to explain the phenomenon when catalyst is not found at the tip of SWCNTs [\[Birkett 1997-111\]](#). According to the proposal, transition metals show a high propensity for decoration fullerene surfaces. A carbon fragments bind to the metal clad fullerene and they may self-assemble as a surrounding circular hexagonal chicken-wire-like fence. Once they are formed as a belt, the network could propagate as a cylinder. This is so called open edge growth.

Another similar model, scooter mechanism, considers that a few metal atoms are chemisorbed and scooted around the open edge of the sheet, and this keeps the tube open and grows. SWCNT will stop when the metal atoms aggregate and lose their kinetic energy for scooting.



### **(c) Vapor-liquid-solid growth mechanism**

According to this proposed model [\[Gorbunov 2002-113\]](#), a molten catalyst nanoparticle penetrates an amorphous carbon aggregate dissolving it and precipitating carbon atom. These atoms arrange in a graphene sheet whose orientation parallel to the supersaturated metal-carbon melt is not energetically favorable. Any local defect of this graphene sheet will result in its buckling and formation of a SWCNT nucleus. Further precipitating carbons incorporate in edges of growing nanotube, which are anchored to the catalyst nanoparticle by overlapping its unsaturated  $sp^2$  orbital with the metal orbital of the catalyst nanoparticles.

#### (d) Yarmulke mechanism

Proposed by Dai et al. [\[Dai 1996-471\]](#), this model explains the growth mechanism of CNTs synthesizing on molybdenum nanoparticles by the disproportionate of CO at 1200 °C and concludes that catalyst size determines the tube diameter. It is also proposed that tubes are close end and carbon atoms are chemisorbed on the catalyst to for yarmulke first. Subsequently, carbon source decomposes and defuses into catalyst, making SWCNTs longer.

### 2.4 The proposed surface modification processes of CNTs

Owing to many unique fascinating properties, many recent studies are devoted to employ CNTs for various novel applications such as biosensors, drug and vaccine delivery vehicles, protein transporters, artificial muscles, novel biomaterials, and solar power [\[Venkatesan 2005- 7154, Bianco 2005-674, Smart 2006-1034, Chiu 2008-3024, Landi 2005-165\]](#). Because most applications of CNTs involve their dispersion in polymer or aqueous matrices, some existing challenges of CNTs can hinder their success. These challenges result from the presence of an amorphous layer on nanotube surface, the nonreactive nature of the CNT surface, the nature of agglomeration of CNTs into bundles, and almost insolubility in any solvent [\[Felten 2005-074308; Fu 2003-351\]](#). This can significantly reduce their usefulness [\[Fu 2003-351, Liu 1998-1253\]](#). To overcome this issue, a modification of the CNTs by changing their surface chemical composition has proven to be efficient. Meanwhile, oxygen functionalization can also serve as a purification method for the carbon nanotubes [\[Lian 2004-8848\]](#). Furthermore, functionalizing the CNTs with a number of functional groups is known for increasing their chemical reactivity and can be used as a starting point for further chemical modification [\[Boul 1999-367\]](#) for some specific applications.

To date, many functionalization methods, such as electrochemical functionalization [\[Bahr 2001-6542\]](#), fluorination [\[An 2002-4235, Mickelson 1998-188\]](#), Polymer wrapping [\[O'connel 2001-265\]](#), chemical



functionalization [Cao 2002-8971, Ago 1999-8116] and plasma treatment, have been developed to improve the solubility and to achieve dispersion of CNTs in water or polymers. Among these techniques, chemical functionalization can be the most common and important way for surface modification of CNTs [Fu 2003-351].

### 2.4.1 Chemical processes

The theory behind modification processes is that the formation of polar functional groups on the surface of CNTs enhances their solubility and dispersion abilities in water or polymers. At present, the chemical method [Fu 2003-351] is the most common; in this process, CNTs are normally refluxed or sonicated in a strong acid, such as HNO<sub>3</sub> and/or H<sub>2</sub>SO<sub>4</sub>, to produce free radical bonds in sp<sup>2</sup> structure on nanotube surface and introduce oxygen containing functional groups, such as carboxylic acids (-COOH), carbonyls (-C=O), and hydroxyls (-OH), to the radical bonds [Dumitrescu 2007-12944]. However, the harsh conditions inherent in this method may introduce wall damage, decreasing their stability and even cleaving them into shorter pieces [Harutyunyan 2002-8671, Zhang 2004-149, Dumitrescu 2007-12944]. These processes may also give rise to some unfavorable issues such as waste treatment, as well as time and cost efficiency issues. Treating nanotubes in mild acid may be an alternative to avoid these issues but this results in a very low production efficiency.

### 2.4.2 Plasma processes

Compared with the chemical processes, plasma treatment has gained lots of attention recently since it is a solvent-free, time efficient, versatile, and environmentally friendly procedure for surface modification [Wu 2007-1336, Khare 2005-23466, Hassanien 2005-278, Zheng 2007-1622]. In addition, this method can provide the greatest opportunity to scale up the production if the system is optimized. Therefore, plasma treatment has been used for a long time in deposition

and etching processes in many industrial fields. To date, many approaches have been investigated to demonstrate the viability and performance of plasma treatment for surface modification of CNTs. Among these studies, various gases, such as N<sub>2</sub> [Yu 2004-380], H<sub>2</sub> [Zhang 2004-54], O<sub>2</sub> [Felten 2005-074308, Ionescu 2006-36, Juan 2005-8231], NH<sub>3</sub> [Zheng 2007-1622, Felten 2005-074308, Ionescu 2006-36], and CF<sub>4</sub> [Felten 2005-074308, Khare 2004-8166] have been used. Generally, the plasma is generated using glow discharge, radio frequency discharge, or microwave discharge at low-vacuum pressure. The generated ions, radicals, and UV light in plasma interact with the CNT surface, creating free radical bonds on nanotube surface and bonding functional groups to the radical bonds [Felten 2005-074308]. Although plasma treatment has been shown to be effective in facial modification of CNTs, some have mentioned that it may cause serious structural damage due to the high energy and temperature plasma within very short time [Felten 2005-074308, Xu 2007-8945]. An alternative that circumvents these issues is placing the nanotubes away from plasma sheath and extracting plasma ions by applying a bias voltage so as to reduce temperature, radiation, and ion density. However, in most designs, plasma sources are working at around 0.1 to 1 Torr pressure which leads to low mean-free-path; this in turn leads to low etching efficiency if the alternative is applied. Active plasma at higher-vacuum pressure may be an optimal solution but this results in a low density plasma that cannot be activated. Therefore, to seek an optimal method with generating high density plasma in high-vacuum is very important.

## 2.5 The characterization methods

### 2.5.1 Scanning electron microscopy (SEM)

As shown in Fig. 2-10, after Knoll developed the first Scanning electron microscope (SEM) [Newbury 2000-323], demonstrating most of the basic principles of operation, and a surprisingly modern SEM instrument was subsequently described by Zworykin et al. at RCA

[Newbury 2000-323], the SEM has been the most versatile and widely used electron beam instrument in material characterizations [Joy 1997-465] for their abilities to produce high resolution and magnification images. In the research filed of CNTs, SEM has traditionally been an important technique for the characterization of CNTs to monitor the bulk-scale production of CNTs by a variety of synthetic techniques. It is also the most popular tool to evaluate the quality of as-grown CNT soot [Itkis 2005-3439].

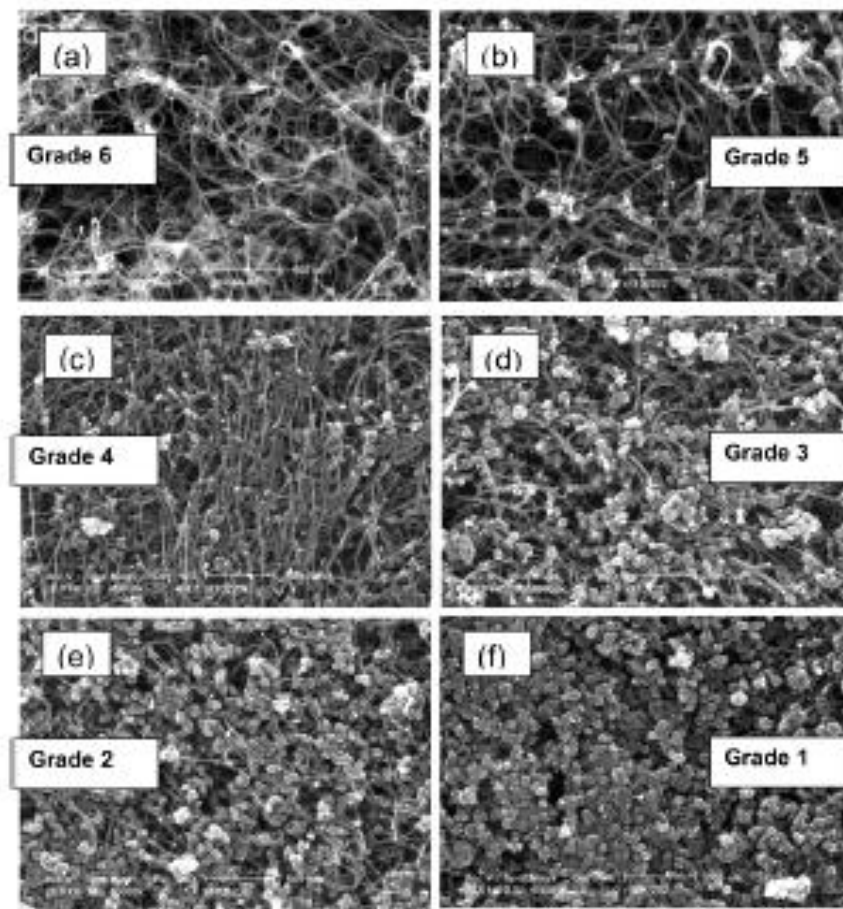


**Fig. 2-10** SEM purity grading system [Itkis 2005-3439]

On the other hand, some drawbacks can be brought while SEM is used to generate high quality image to evaluate the quality of CNTs [Itkis 2005-3439]. It is mentioned that the metal catalyst contained in nanotube and a thin coating of amorphous carbon on CNTs are invisible to SEM technique but easily observed by Transmission electron microscopy (TEM) technique

[Itkis 2005-3439]. Meanwhile, limited by observation scale, more frames with various magnifications is necessary to provide reliable characterization information [Itkis 2005-3439].

## 2.5.2 Transmission electron microscopy (TEM)

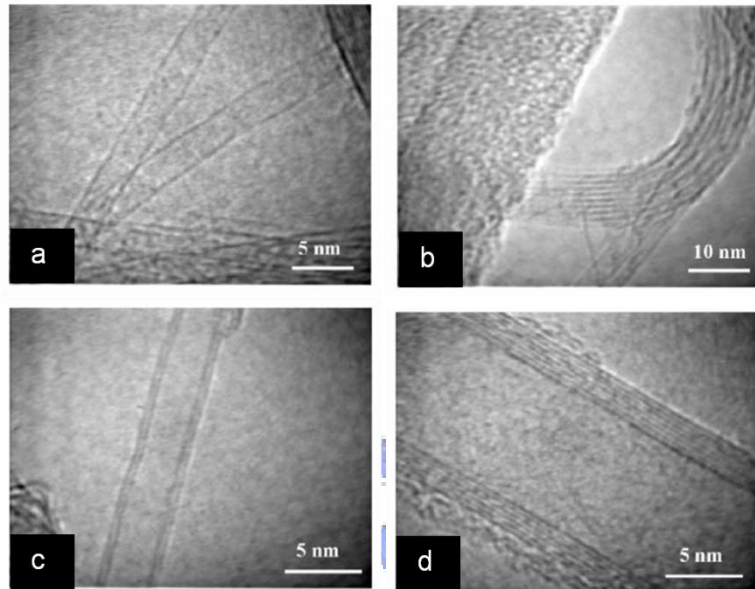


**Fig. 2-11** TEM images of (a) SWNTs (b) SWNT bundles (c) DWNT (d) MWNT [Flahaut 2000-249]

TEM technique can reveal the interior microstructure of the specimen, and produce the high-resolution lattice image and the electron diffraction pattern as well. However, in practical use, some drawbacks can be happened. When TEM is used to directly analyze the structure of SWCNT, it is difficult to obtain a clear image of one SWCNT. The main reasons are the structure of SWCNT is easily destroyed by high energy electron beam and electron scattering are not apparent because of SWCNT is composed of so few carbon atoms. Furthermore, SWNT is hard to be built on stilts to avoid the background interference from copper grid and SWNTs dispersion is also an important problem. Figure 2-11 shows the HRTEM images of (a) SWNTs (b) SWNT bundles (c) DWNT (d) MWNT [Flahaut 2000-249]. A thin layer of amorphous carbon on nanotube surface may be observed by TEM. However, it is difficult to predict the precise quantity of the layer amount because the TEM energy is so high that the layer structures are easily destroyed and subsequently more amorphous carbon are generated. The

same as SEM technique, with the observation limitation, more frames with various magnifications is often required to provide homogeneous characterization information.

### 2.5.3 X-ray photoelectron spectrometry (XPS)

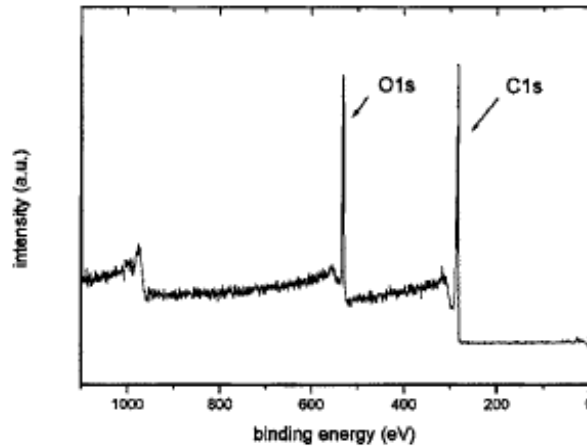


**Fig. 2-12** XPS survey spectrum of CNT treated by oxygen plasma [Felten 2005-074308]

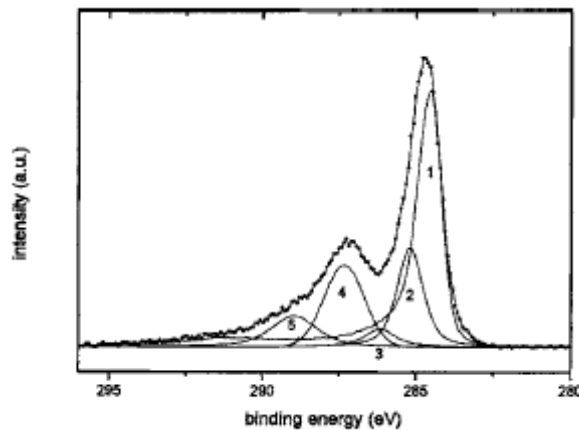


**Fig. 2-13** XPS  $C_{1s}$  spectra of the as-purchased MWCNTs and the five chemical species: (1) graphite; (2)  $sp^3$  carbons; (3) hydroxyl groups; (4) carbonyl groups; and (5) carboxyl groups [Felten 2005-074308]

XPS has its origins in investigations of photoelectric effect in which X-ray is used as the exciting source [Briggs 1996-p7]. Based on the equation as below, XPS spectra are obtained by irradiating a material with a beam of X-rays while simultaneously measuring the kinetic

energy ( $E_k$ ) and number of electrons that escape from the surface of material being analyzed.

$$E_k = h\nu - E_B \quad (12)$$

where  $h\nu$  is the incident photo energy, and  $E_B$  is the electron binding energy. The heart of this technique is the measurement of an electron energy spectrum by using an electron energy analyzer, also called a spectrometer. It is often used to estimate that all aromatic sites at the surface of the oxidized nanotubes [Felten 2005-074308, Ago 1999-8116, Xu 2007-8945, Ionescu 2006-36, Zhang 2007-2366, Wiltner 2004-881]. This technique can also be used to identify chemical composition on material surface and functional groups attached to CNTs. According to the research of Felten et al. [Felten 2005-074308], MWCNTs are modified by inductive coupled rf-plasma with applying  $O_2$ ,  $CF_4$  and  $NH_3$  gases and then investigated by XPS to analysis and quantify the chemical composition on nanotube surfaces so as to support their experimental results. Figures 2-12 and 2-13 give their XPS investigation results of the oxygen plasma-treated nanotubes. The XPS survey spectrum in Fig. 2-12 is used to confirm the chemical elements on the surface of nanotubes. The XPS  $C_{1s}$  spectrum in Fig. 2-13 is deconvoluted into five Gaussian peaks centered at 284.5, 285.1, 286.2, 287.2, and 288.9 eV after the background are subtracted. The main peak at 284.5 eV originates from the graphite signal. The peak at 285.1 eV is attributed to  $sp^3$  carbon atoms. The peaks at 286.2, 287.2, and 288.9 eV correspond to hydroxyl, carbonyl (or ether), and carboxyl (or ester) groups respectively. The XPS results show that after the nanotubes are treated by the oxygen plasma under various process conditions, the [O]/[C] ratio which is the relative percentage of the oxidized carbon species to total number of carbon species detected is can be increased [Ago 1999-8116].

## 2.5.4 Raman spectroscopy

Raman spectroscopy provides information about molecular vibrations that can be used for sample identification and quantification. Normally, a monochromatic light (laser) incident on a sample, the photons which make up the light may be absorbed or scattered, or may not interact the material and may pass through it. When light is scattered from an atom or molecule, most photons are elastically scattered (Rayleigh scattering), such that the scattered photons have almost the same frequency as the incident photons. However, a small fraction of the scattered light (approximately 1 in  $10^6 - 10^8$  photons) is scattered by an excitation, with the scattered photons having a frequency different from, and usually lower than, the frequency of the incident photons [Smith 2005-p2]. The energy difference between the monochromatic light and the Raman scattered light is equal to the energy involved in changing the molecule's vibration state [Smith 2005-p2]. This energy difference is then called the Raman shift [Smith 2005-p2]. Several different Raman shifted signals will often be observed; each being associated with different vibrational or rotational motions of molecules in the sample. Figure 2-14 shows the schematic diagram of state change of Raman scattering [Rao 1997-187]. In CNTs research field, the Raman scattering from SWCNTs is resonantly enhanced if the excitation energy ( $E_L$ ) matches the separations between the pairs of Van Hove singularities ( $E_{ij}$ ) in the one-dimensional electronic density of states of the SWCNTs, as shown in Fig. 2-4 [Itkis 2005-3439] and Fig. 2-15. It is widely used as a sensitive prober to analysis the electronic structure in carbon nanotubes and presence of defects [Dresselhaus 2005-47].



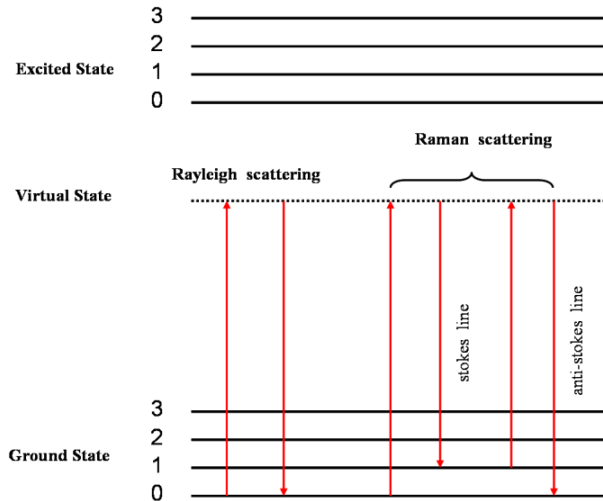


**Fig. 2-14** Schematic of state change of Raman scattering [Rao 1997-187]

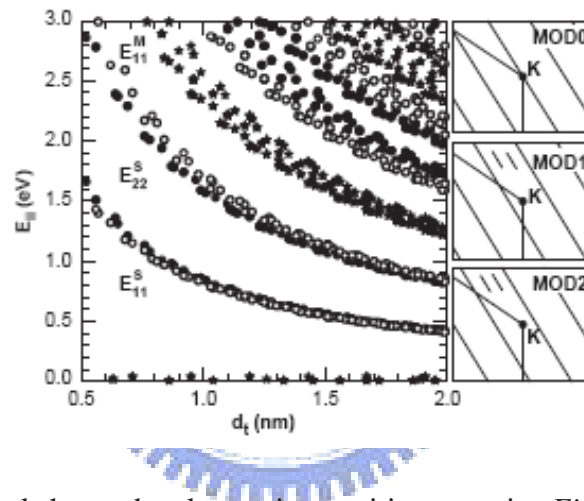


**Fig. 2-15** The left panel shows the electronic transition energies  $E_{ii}$  vs. nanotube diameter  $d_t$ . The right panels show schematic figures defining the SWNT classes: MOD0 — metallic, where one cutting line crosses the  $K$  point; MOD1 and MOD2 — semiconducting [Dresselhaus 2005-47]

In the inspection of carbon nanostructures, there are two characteristic peaks in Raman spectrum represented as D and G bands. The  $D$  mode at around  $1300 \text{ cm}^{-1}$  is correlated with structural disorder of CNTs, which originates from the defects including disordered materials, poor graphitization, functionalized carbon, and the amorphous carbon on the sidewall of nanotubes [Shaijumon 2007-75, Dillon 2004-691, Jian 2008-230]. The relative intensity of this mode can provide direct evidence of covalent modification and defect concentration. When estimating the defect concentration, the  $D$  mode intensity is usually normalized with respect to the intensity of the  $G$  mode at around  $1600 \text{ cm}^{-1}$ . This approach relies on the assumption that the



intensity of the  $G$  mode is independent of defect concentration and originates from a single resonant Raman process [Jian 2008-230]. On the other hand, if the  $G$  mode is induced by defects, this procedure for normalizing the intensity is no longer correct [Maultzsch 2002-2647].

The radial breathing mode (RBM) can be used to study nanotube diameter through its frequency ( $\omega_{\text{RBM}}$ ) and to perform  $(n, m)$  assignment of SWCNTs by analyzing both  $d_t$  and  $I_{\text{RBM}}$  [Dresselhaus 2005-47]. As shown in Fig. 2-16, the RBM of Raman spectrum is a unique feature to SWNTs and involves a collective vibrational movement of the carbon atoms towards and away from the central axis of a SWCNT. It occurs with  $\omega_{\text{RBM}}$  ranging from 120 to 350  $\text{cm}^{-1}$  for diameters,  $d_t$ , ranging from 0.7 nm to 2 nm [Dresselhaus 2005-47]. It is therefore very useful for indentifying if a given carbon materials contains SWCNTs.

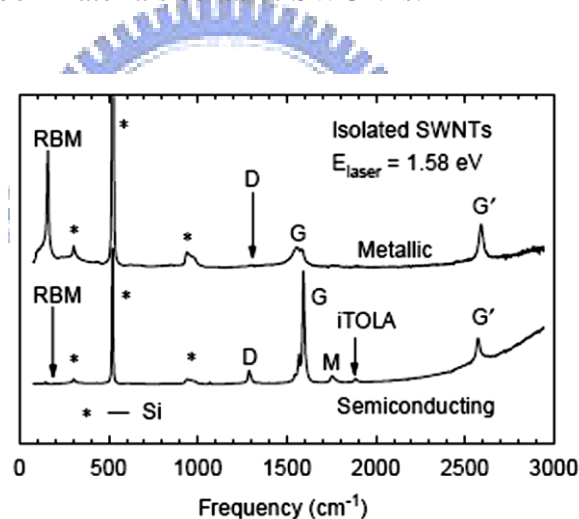


**Fig. 2-16** Raman spectra from a metallic (top) and a semiconducting (bottom) SWNT at the single nanotube [Dresselhaus 2005-47]

### ● RBM frequency for nanotube diameter

The RBM oscillations strongly correlate with a periodicity imposed on a graphene sheet by wrapping it into a finite-size nanotube with small diameter. Consequently, the associated RBM wavelength and frequency are directly related to the perimeter of the nanotube [Dresselhaus 2005-47], as shown in Fig. 2-17. Based on this relationship, as the diameter of the nanotube increases, the RBM frequency decreases to lower wave numbers. On the other hand, for larger

nanotubes and MWCNTs the RBM frequency becomes very small and, at the same time, the intensity of the RBM decreases and ultimately becomes undetectable by Raman spectroscopy measurements. Hence Dresselhaus et al. [Dresselhaus 2002-2043] proposed that the frequency of the RBM are :

$$\omega_{RBM} = \frac{A}{d_t} + B \quad (13)$$

where  $A = 234$  or  $248 \text{ cm}^{-1} \text{ nm}$  and  $B = 10$  or  $0 \text{ cm}^{-1}$  for bundle or isolated SWCNTs on silicon wafer, respectively [Dresselhaus 2005-47]. Note that, for larger diameter tubes ( $d_t > 2 \text{ nm}$ ), the intensity of the RBM is very weak and hardly detected. Meanwhile, it should be noted that a single Raman measurement can give an idea of the nanotubes that are resonance with the laser line. However, this cannot give a complete characterization of the diameter distribution of the sample. Alternatively, using many laser lines with different excitation energies can obtain a good characterization of the diameter distribution in the sample.

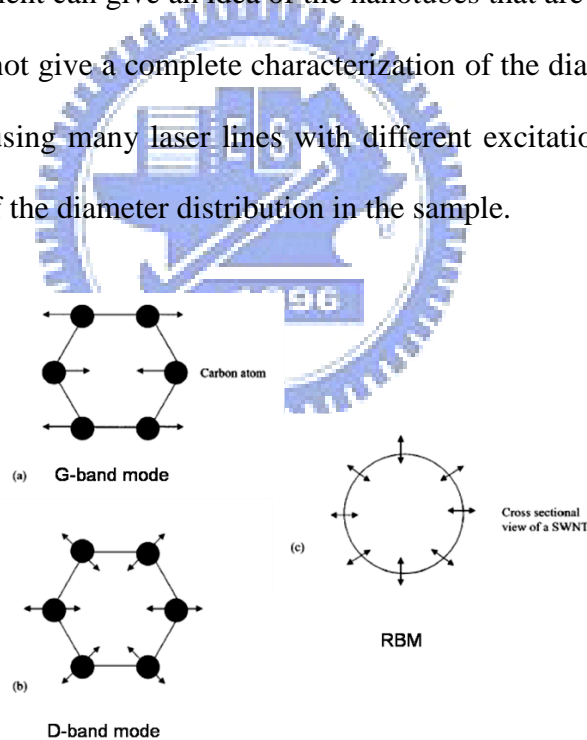


**Fig. 2-17** The Raman vibration modes of CNTs (a) G-band mode (b) D-band mode (c) Radial breath mode [Raravikar 2002-235424]

● **RBM for nanotube electronic structure** [Dresselhaus 2005-47]

SWCNTs can be classified into three different classes, according to whether MOD

$(2n+m, 3) = 0, 1, \text{ or } 2$ . Here MOD 1 and MOD 2 are two types of semiconducting nanotubes owing to no  $k$  vector crosses the  $k$  point as shown in Figs. 2-3 and 2-15 [Dresselhaus 2005-47]. For MOD 0, a cutting line crosses the K point. Thus, the SWCNTs are classified as metallic type nanotubes. It is noted that only armchair ( $n = m$ ) SWCNTs are truly metallic whilst other MOD 0 SWCNTs, i.e.,  $n \neq m$ , are metallic at room temperature but exhibit a small chirality-dependent energy gap at lower temperature [Dresselhaus 2005-47]. Fig. 2-15 shows the  $E_{ii}$  values for all  $(n, m)$  SWCNTs with different diameter ranging from 0.5 to 2.0 nm. Meanwhile, according to Tight-binding method the  $E_{ii}$  values should follow eq. (9) [Kataura 1999-2555]. This results in a so-called Kataura plot and the plot is widely used to interpret the Raman spectra measured from CNTs. Superscript S or M are used to denote whether the electronic transition energies  $E_{ii}^M$  for metallic SWCNTs else for semiconducting SWCNTs [Dresselhaus 2005-47]. The RBM spectra for SWCNT bundle contain an RBM contribution from different SWCNTs in resonance with the excitation laser energy. Therefore, it is useful to probe the electronic data with having a Kataura plot when the RBM spectra from SWCNTs are obtained. It is suggested that, because semiconducting and metallic nanotubes of similar diameters cannot occur at similar  $E_{ii}$  values,  $\omega_{\text{RBM}}$  measured from several laser energies  $E_L$  can thus be used to characterize the ratio of metallic to semiconducting SWCNTs in the nanotube sample [Dresselhaus 2005-47].

● **RBM for chirality assignment** [Dresselhaus 2005-47, Jorio 2005-075401]

When the  $d_t$  values are obtained from  $\omega_{\text{RBM}}$  under the  $E_{ii} - E_L$  resonance conditions, RBM can be used for nanotube chirality  $(n, m)$  assignment with the application of Kataura plot. As shown in Fig. 2-16, the spectra are obtained from using a laser excitation energy of  $E_L = 1.58$  eV (wavelength = 785 nm). The observed result for in upper spectrum present in the figure can be assigned as metallic SWCNT (13, 10) with  $d_t$  of 1.59 nm, where the  $E_L$  is resonance with  $E_{11}^M$ . By contrast, the lower spectrum is assigned as (23, 1) SWCNT where  $E_L$

is resonance with  $E_{33}^S$ .

As shown in Fig. 2-18(a), some experimental results obtained for  $E_{ii}$  vs.  $\omega_{\text{RBM}}$  for each (n, m) resonant nanotube are provided. Meanwhile, in this figure, the  $E_{ii}$  for nanotubes are clearly seen with the relation of  $2n + m = \text{constant}$ . Meanwhile, as mentioned by Jorio et al. [Jorio 2005-075401], the Kataura plot should be revised when it is applied on nanotubes in small diameters, as shown in Fig. 2-18b. With the aid of Fig. 2-18(a) and eq. (3), the corresponding values of  $d_t$  and  $2n+m$  can be obtained. The chiral vector,  $C_h = (n, m)$  can thus be calculated.

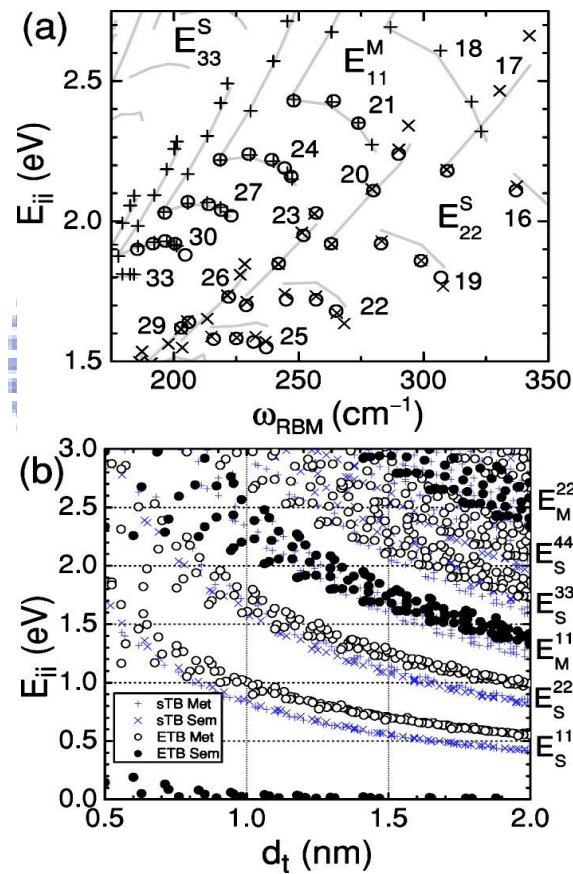


**Fig. 2-18** (a) The revised  $E_{ii}$  vs  $\omega_{\text{RBM}}$  plot comparing experimental results from experiments on SDS wrapped SWNTs in solution. (b) The revised Kataura plot [Jorio 2005-075401]

### 2.5.5 Thermogravimetric analysis (TGA)

TGA is an analytical technique used to determine a material thermal stability has been used to characterize carbon nanotubes for over a decade [Landi 2005-6819]. It is often used to

analyze the resulted SWCNT samples by synthesis and purification methods and is also a popular technique for the determination of the amount of metal catalyst in CNT sample. The widespread acceptance of this method is mainly resulted from the simplicity of using a representative sample and evaluating the changes in weight loss in a flowing air as a function of temperature. In addition, it is the most common used method for calculating the metal-catalyst impurity levels.

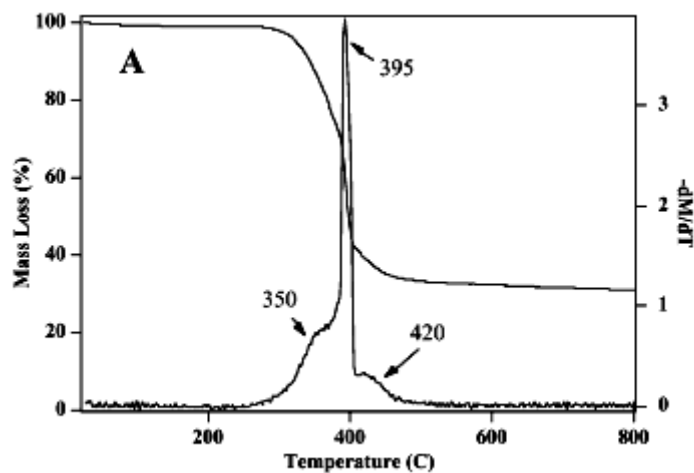


**Fig. 2-19** The weight loss (solid) and weight derivative (dash) curves of TGA [Harutyunyan 2002-8671]

As shown in Fig. 2-19, the relative amount of different fraction in CNT sample are normally identified from interpretation for TGA data if their different fractions in sample are well separated, and the weight derivative curve have been used to analyze their fractions in terms of CNTs, amorphous carbon, and graphitic nanoparticles according to their various decomposition temperatures obtained from the peak value of the weight derivative curve [Zhang 2004-149, Hu 2003-13838, Harutyunyan 2002-8671, Shi 1999-35, Landi 2005-6819]. SWCNTs could decompose in the range from 300 to 500 °C [Zhang 2004-149]. HiPco MWCNTs could decompose at temperature approximately ~ 600 °C [Musso 2007-1183, Dileo 2007-064307]. Besides the main combustion temperature, some satellite peaks could be observed at lower temperature. suggested from previous studies, when MWCNTs are treated by various acid treatments, it is suggested that

derivative peak temperatures observed at  $\sim 350$  °C might have resulted from additional carbonaceous impurities which are introduced by the destruction of nanotubes during acid treatments [Zhang 2004-149, Hu 2003-13838, Harutyunyan 2002-8671, Shi 1999-35]. Additionally, the peak below 300 °C is typical of residual acid and absorbed water in the sample after treatment [Landi 2005-6819].

According to the study of Zhang et al., when SWCNTs are sonicated in nitric acid up to 4 h, the derivative peak increases from 450 to 480 °C as the treatment time increases to 2 h, and the peak decreases to 420 °C as the treatment time increases to 4 h [Zhang 2004-149]. The peak temperature of MWCNTs also change according to various treatment conditions [Musso 2007-1183].



# Chapter 3

## Experimental methods

Various processes were used to facially modify the MWCNTs. The processes included the ion treatment, a two-step process combining the ion pretreatment and followed by a dilute nitric acid (0.25 M HNO<sub>3</sub>) treatment, and the acid treatments which sonicated CNTs in nitric/sulfuric (HNO<sub>3</sub>/H<sub>2</sub>SO<sub>4</sub>=1/3 (v/v)) or dilute nitric (0.25 M HNO<sub>3</sub>) acids with various process times. The details of the experimental flow chart, the experimental procedures, and surface and structure characterizations are illustrated in the following sections.

### 3.1 Experimental flow chart

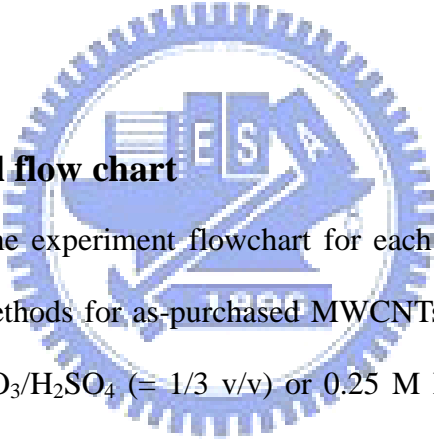
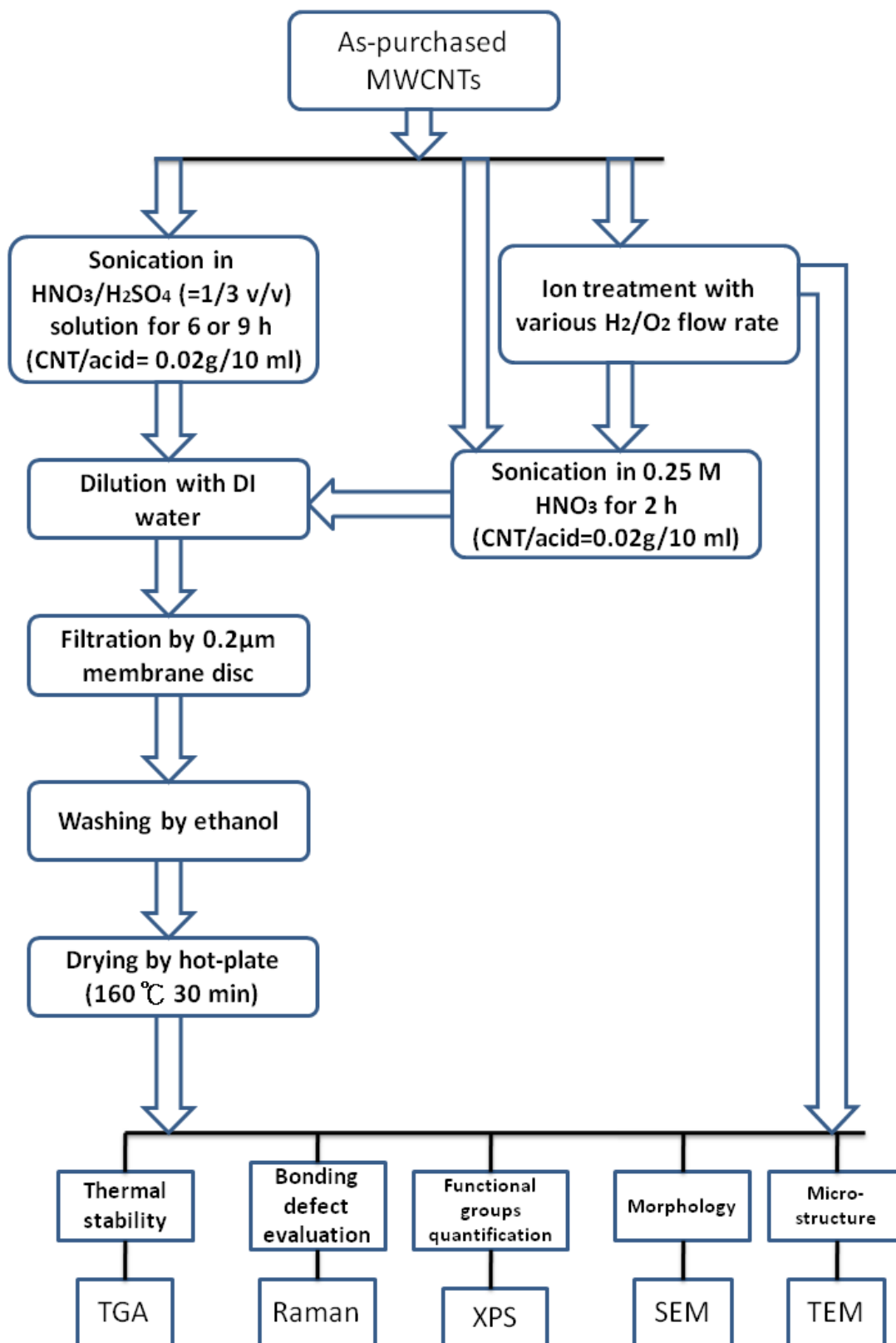


Figure 3-1 depicts the experiment flowchart for each step of the surface modification processes and analysis methods for as-purchased MWCNTs. The MWCNTs were treated by acid treatment using HNO<sub>3</sub>/H<sub>2</sub>SO<sub>4</sub> (= 1/3 v/v) or 0.25 M HNO<sub>3</sub> acid solution with various process time, the ion treatment applying H<sub>2</sub>/O<sub>2</sub> gas mixture with various gas flow ratios, and the ion pretreatment and followed by a 0.25 M HNO<sub>3</sub> acid treatment. Each acid treatment was followed by a cleaning and drying procedures in air.



**Fig. 3-1** Experiment flowchart



## 3.2 Raw materials and processing operators

- SEM and TEM images of as-purchased CNTs

The CNTs, provided by a commercial company, were grown by thermal chemical vapor deposition. As shown in Fig. 3-2 and 3-3, the SEM and TEM images shows that the CNTs are highly tangled with multiple layers and diameters ranging from 15 to 40 nm.

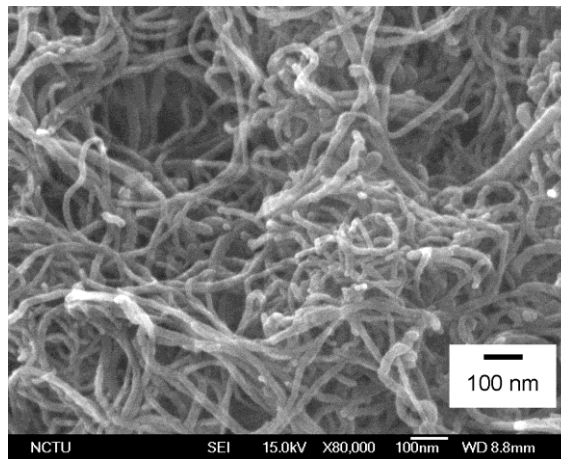


Fig. 3-2 SEM image of as-purchased CNTs

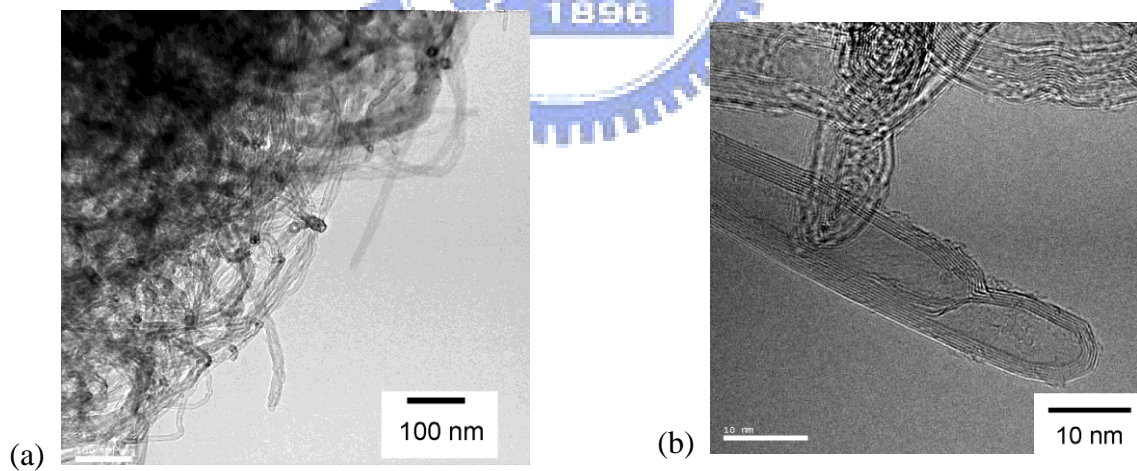
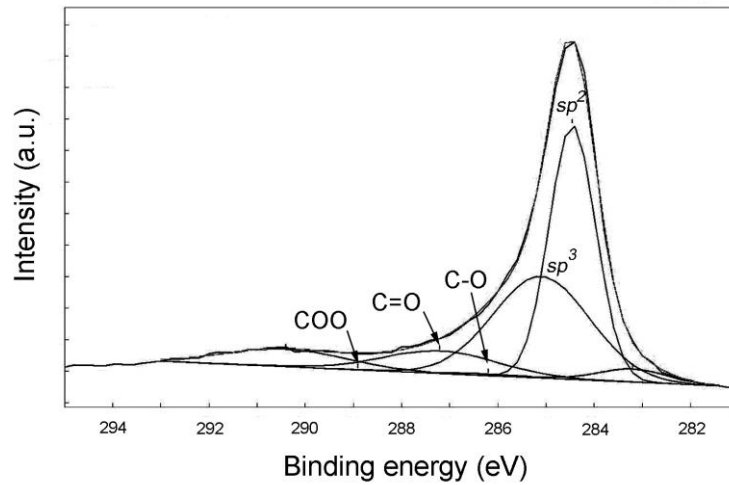


Fig. 3-3 TEM images of as-purchased CNTs: (a) at lower magnification, (b) at higher magnification

- XPS analysis of as-purchased CNTs



**Fig. 3-4** XPS C<sub>1s</sub> spectrum of the as-purchased CNTs

The XPS C<sub>1s</sub> spectrum of the as-purchased CNTs was recorded and is shown in Fig. 3-4. Based on the previous studies [\[Felten 2005-074308, Ago 1999-8116\]](#), the spectra are deconvoluted into five Gaussian peaks centered at 284.5, 285.1, 286.2, 287.2, and 288.9 eV. Here, the main peak at 284.5 eV originates from a graphite signal. The peak at 285.1 eV is attributed to sp<sup>3</sup> carbon [\[Felten 2005-074308, Xu 2007-8945\]](#). The peaks at 286.2, 287.2, and 288.9 eV correspond to hydroxyl, carbonyl (or ether), and carboxyl (or ester) groups respectively. A peak attributed to  $\pi$ - $\pi^*$  shake-up bonds is observed at 290.4 eV [\[Ionescu 2006-36, Zhang 2007-2366\]](#); and the peak at 283.2 eV originates from carbidic carbon [\[Wiltner 2004-881\]](#). Meanwhile, the deconvolution results also show that the oxygen functional groups have been grafted onto the surface of the pristine MWCNTs with a concentration of approximately 11.2 %. This is consistent with the description provided by the vendor that the raw materials were treated using mild acids prior

to shipment. Furthermore, the results show that the CNTs are still composed of approximately 40 %  $sp^3$  content as shown in table 4-1.

- Raman spectra of as-purchased CNTs

As shown in Fig. 3-5, with two characteristic peaks , D and G bands, the Raman spectrum shows that the  $I_D/I_G$  of the as-purchased CNTs is approximately 0.89. Due to the absence of RBM signal, the Raman spectra further confirms that the CNTs are MWCNTs.

- TGA of as-purchased CNTs

The TGA curve in Fig. 3-6 reveals that the as-purchased CNTs are oxidized from approximately 450 to 650 °C. It also shows that the catalyst shares around 5 wt. % in the material. Meanwhile, the weight derivative TGA curve shows a main decomposition peaked at 600 °C.

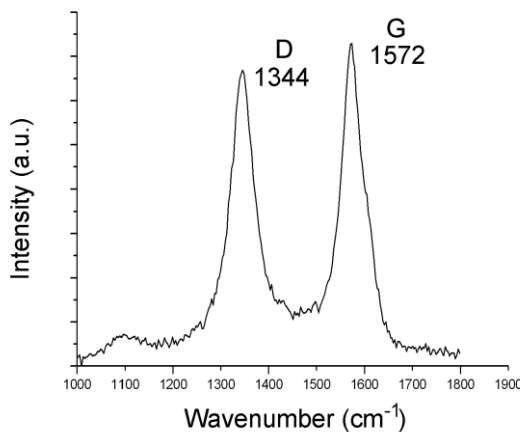


**Fig. 3-5** Raman spectrum of the as-purchased CNTs

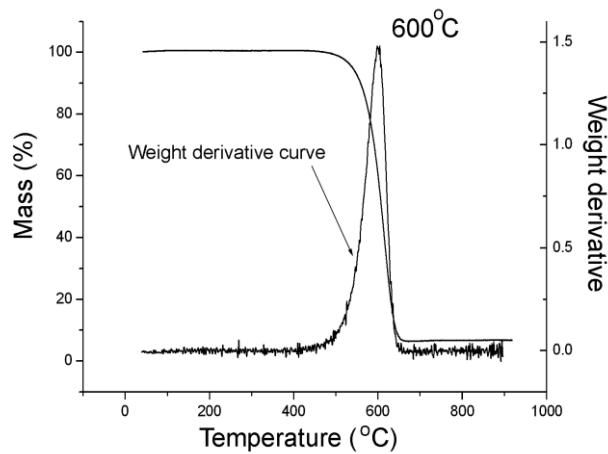


**Fig. 3-6** TGA curve for the as-purchased CNTs

● **Other raw materials and processing apparatus:**

The chemicals and processing apparatus used in this study are as follows:

Nitric acid (HNO<sub>3</sub>): Molecular weight: 63.01 g/mol; Purity 69.5%; from Scharlau Co.

Sulfuric acid (H<sub>2</sub>SO<sub>4</sub>): Molecular weight: 98.078 g/mol; Purity: 98%; from Fisher Chemical

O<sub>2</sub> gas Purity: 99.8%, from 新大氣體有限公司

H<sub>2</sub> gas Purity: 99.9%, from 新大氣體有限公司

Electronic balance: Mettler AB104

Hotplate: Shin Kwang

Ultrasonic agitator: Branson 1510; 40 kHz

### 3.3 Acid treatment procedures

When the MWCNTs were treated by the nitric/sulfuric acid treatment, 0.02 g as-purchased MWCNTs were immersed in 10 ml  $\text{HNO}_3/\text{H}_2\text{SO}_4$  (=1/3 (v/v)) solution and the CNTs/acid mixtures were then ultrasonicated for 6 and 9 h at room temperature. Alternatively, when MWCNTs were treated by the dilute acid treatment, CNTs were prepared with 0.02 g and immersed in 10 ml 0.25 M  $\text{HNO}_3$  solution. The CNTs/acid mixtures were then ultrasonicated for 2 h at room temperature. Subsequently, the mixtures were diluted with deionized water separately and filtered by using a 0.2  $\mu\text{m}$  porous polytetrafluoroethylene (PTFE) membrane disc to remove the excess acid from the solution. At last, all deposited black powder were washed from the disc filters using ethanol and then dried at 160 °C on a hotplate in air for 30 min. The details of the specimen designations for the MWCNTs treated by nitric/sulfuric or dilute nitric acid treatments, and the treatment conditions and sequences are listed in Table 3-1.

### 3.4 The ECR plasma system for ion treatment

Microwave discharge system can provide concentrated plasma with ion densities of more than  $3 \times 10^{11} \text{ cm}^{-3}$ . This can be used for many plasma processes highly efficiently. The frequency most often used is 2.45 GHz. It is the same as the often used microwave oven at home today. ECR plasma system has been a popular etching method in many applications because, with divergent magnetic flux and high bias voltage, this system can possess excellent features of high ionization efficiency, high density plasma generation in low-pressure vacuum, and effective plasma ion extraction and transportation <sup>[Matsuo-1982-L4]</sup>. These give the advantages

that the positive or negative ions can be easily extracted and transported toward the specimen with high incident energy; the specimen can be placed far from plasma sheath and then treated at relative low temperature. These advantages are very important for conducting highly efficient etching process to create high density free radical bonds on nanotube surface but causing no severely structural damage of the specimen.

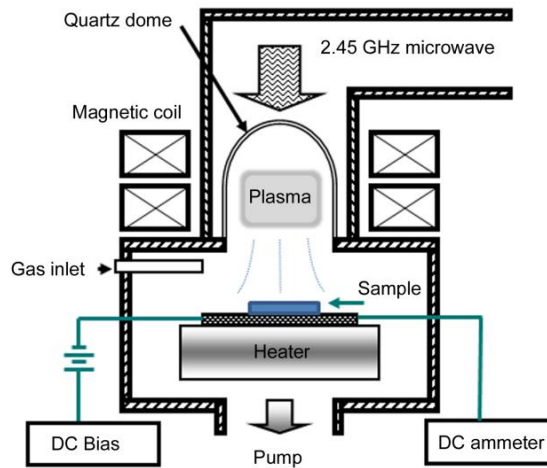


**Fig. 3-7** Schematic of the ECR plasma system for ion treatment

Figure 3-7 reveals the microwave ECR plasma system for the surface modification of CNTs. 2.45 GHz microwave was introduced into the plasma chamber through a quartz window. The output power of the microwave generator was set at about 750 W. The magnetic coil was arranged around the periphery of the chamber and the magnetic flux density was 875 Gauss to meet the ECR condition at the microwave frequency used. Before treatment, the system was pumped down to  $10^{-6}$  Torr first. To ensure a sufficient density of plasma and an adequate mean free path, during the treatment process, chamber pressure was held at  $4.2 \times 10^{-3}$  Torr. A bias voltage of -250 V was applied to the stage, which is 28 cm below plasma zone, to extract and accelerate the hydrogen and oxygen cations with high incident energy [Ni-2000-R16343]. Resistance heater is wired around the process stage. Thermocouple is also connected to process stage to measure the process temperature set.

**Table 3-1** Specimen designations and their treatment conditions and sequences

Specimen designation	Ion treatment <sup>a</sup>		Acid treatment <sup>b</sup>			Drying <sup>c</sup>	
	H <sub>2</sub> /O <sub>2</sub> flow ratio (sccm/sccm)	Process time (min)	solution	Sonication Temperature (°C)	Sonication time (min)	Set temperature (°C)	Heating time (min)
A1	No ion treatment		HNO <sub>3</sub> /H <sub>2</sub> SO <sub>4</sub> =1/3 (v/v)	Room temp	360	160	30
A2					540		
A3			0.25 M HNO <sub>3</sub>	Room temp	120	160	30
B1	50/0	5	No acid treatment				
B2	40/10						
B3	25/25						
B4	10/40						
B5	0/50						
B6	25/25						
C1	50/0	5	0.25 M HNO <sub>3</sub>	Room temp	120	160	30
C2	40/10						
C3	25/25						
C4	10/40						
C5	0/50						

<sup>a</sup> Other ion treatment conditions: crucible temperature and bias voltage : 400 °C and -250 V;

base pressure : 10<sup>-6</sup> Torr; working pressure : 4.2×10<sup>-3</sup> Torr; microwave power : 750 W

<sup>b</sup> MWCNT concentration: 0.002 g in 10 ml solution

<sup>c</sup> D.I. water cleaning and drying by a hotplate in air after acid treatment

### **3.5 Ion treatment procedures**

As shown in Fig. 3-7, 0.05 g samples of as-purchased MWCNTs were transported in a 304 stainless steel crucible and placed on the process stage in the vacuum chamber of the ECR plasma system. H<sub>2</sub>/O<sub>2</sub> gas flows were fed as etching gases with controlled ratios of 50/0, 40/10, 25/25, 10/40, and 0/50 (sccm/sccm), which are equivalent to H<sub>2</sub> concentrations of 100, 80, 50, 20, and 0 vol %, respectively. Once the stage temperature reached 400 °C, the plasma treatment was conducted for 5 and 20 min.

The details of the specimen designations for the MWCNTs treated by the ion treatment and the two-step process combining the ion and dilute nitric acid treatments, and the treatment conditions and sequences are also listed in Table 3-1.

### **3.6 CNTs characterization**

#### **3.6.1 Scanning electron microscopy (SEM)**

In order to observe the morphology changes, the samples of pristine MWCNTs and the MWCNTs treated by the ion and acid treatments were measured by using a SEM (JOEL, JSM-6500F). Before the measurement, each sample was sonicated in ethanol for 30 min and dispersed onto a silicon wafer.

#### **3.6.2 Transmission electron microscopy (TEM)**

The microstructures of the MWCNTs samples were characterized by TEM (JEOL JEM-2100). The samples were prepared by dispersing and then depositing the black powder on lacy carbon grids by using ethanol. Prior to characterization, all samples were dried by a hot plate for 30 min at temperature of 160 °C.



### 3.6.3 X-ray photoelectron spectrometer (XPS)

XPS (Perkin-Elmer model PHI 1600) was performed to determine the chemical changes on the surface of nanotubes. Prior to measurement, each specimen was attached to Scotch tape to avoid dispersion of the nanotubes in the vacuum chamber. Monochromated Al K $\alpha$  radiation ( $h\nu=1486.6$  eV) was used as the photon source and photoelectrons were collected at an angle of  $54.7^\circ$  relative to the normal direction of the specimen surface. The energy resolution of the system was set to 0.2 eV. During C<sub>1s</sub> spectrum analysis (Spectral Data Processor (SDP) v4.0, XPS international, LLC), background noise was subtracted by using the “Linear” mode in the range between 281.5 and 293 eV, and the component peak fitting was performed by using Gaussian line shapes.

### 3.6.4 Raman spectroscopy

In this study, Raman spectroscopy (Jobin YVON LabRam HR800) is used as a rapid way to monitor the structure change of MWCNTs before and after treatments. As-purchased MWCNTs and the MWCNTs treated by various treatments are deposited on silicon wafers by using ethanol and dried on hot-plate in air for 30 min at temperature, 160 °C. The exciting source was an Ar laser (514 nm) focused (50x) to a 2  $\mu$ m spot size. All spectra were collected with five accumulations of 3 s each.

### 3.6.5 Thermogravimetric analysis (TGA)

TGA (TA Q500) was used to characterize the changes in thermal stability. Sampling weight of 0.01 g of each sample was placed in a platinum pan balance. A heating rate was set as 10 °C/min and ramped from room temperature to 800 °C under air flow (60 mL/min).

## Chapter 4

### Results and discussion

#### 4.1 Effect of treatment time and solution composition on morphologies of the acid-treated MWCNTs

The SEM morphologies on the MWCNTs treated by the nitric/sulfuric acid for 6 and 9 h are in Figs. 4-1(a) to (b), respectively, under two magnifications. After the nitric/sulfuric acid treatment for 6 and 9 h, the morphologies of the acid-treated MWCNTs can be observed a significantly changed. It is observed that the nanotubes are cut by the treatment as the process time increases. In contrast to the as-purchased MWCNTs (Fig. 3-2a), the diameter distributions are also changed from original range between 15 and 40 nm to range between 25 to 40 nm when the MWCNTs are treated for 9 h. This leads to a larger mean diameter than that of the as-purchased MWCNTs. These results match previous studies which suggest that the harshness of the acid treatment reduces the length, narrows the diameter distribution, and increases the average tube diameter of the CNTs [\[Zhang 2004-149, Dumitrescu 2007-12944\]](#). In addition, it was also observed that more impurities are introduced by this treatment. It is suggested that, because the acid treatment often combines the unwanted side effects of damage to the sidewalls as well as length reduction of the nanotubes, these impurities may be by-products resulted from the severe structural damage [\[Hu 2003-13838, Zhang 2004-149\]](#).

Alternatively, as shown in Fig. 4-2, the SEM images show that, when the as-purchased MWCNTs are only treated by 0.25 M HNO<sub>3</sub> for 2 h, a slightly greater number of larger diameter nanotubes can be seen in the mild acid treated sample. This also results in a slightly larger mean value of the diameter distribution than that of the as-purchased MWCNTs. However, the diameter distribution and morphology change of the MWCNTs treated by the dilute acid is insignificant.

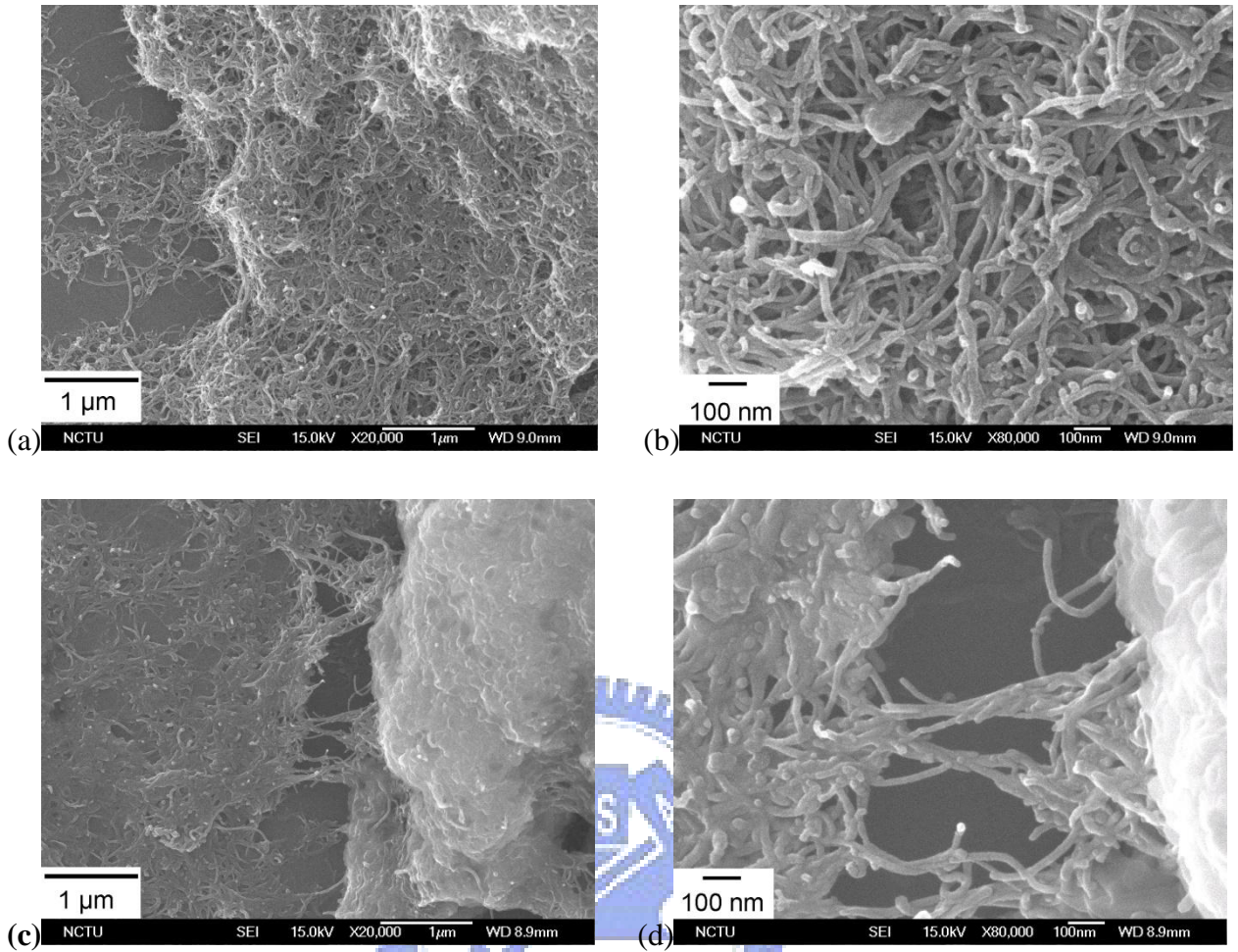


**Fig. 4-1** SEM morphologies of MWCNTs after different acid treatment times, (a) 6 h; (c) 9 h (Specimens A1 and A2, respectively), where (b) and (d) are corresponding SEM images of (a) and (c) respectively at higher magnification.

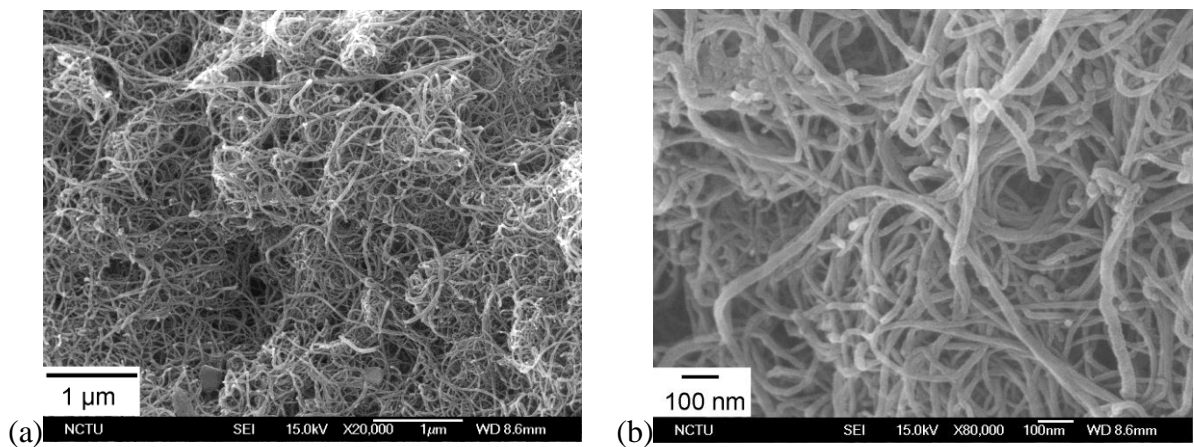
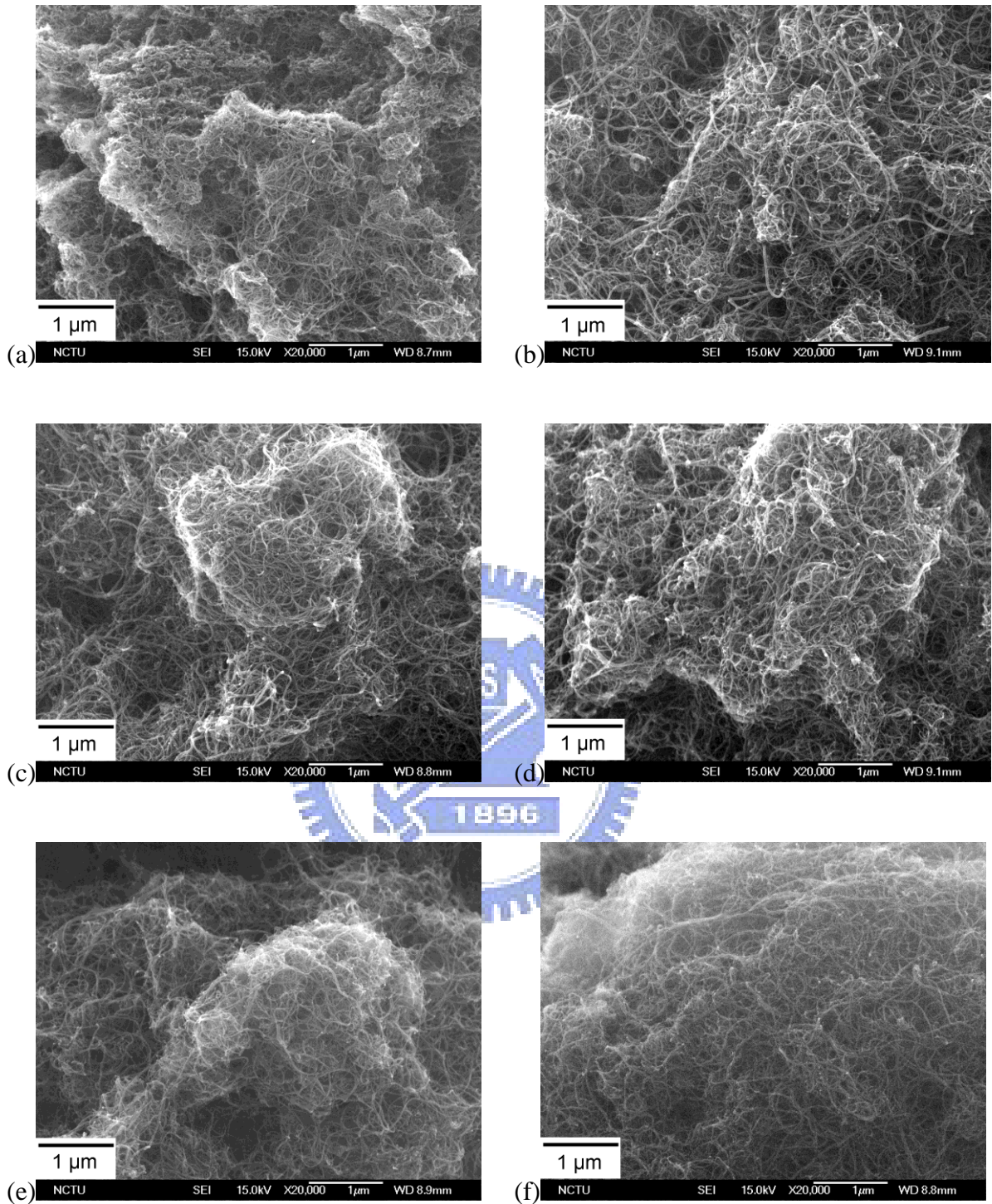


**Fig. 4-2** SEM images of the 0.25 M HNO<sub>3</sub> acid-treated MWCNTs (Specimen A3).

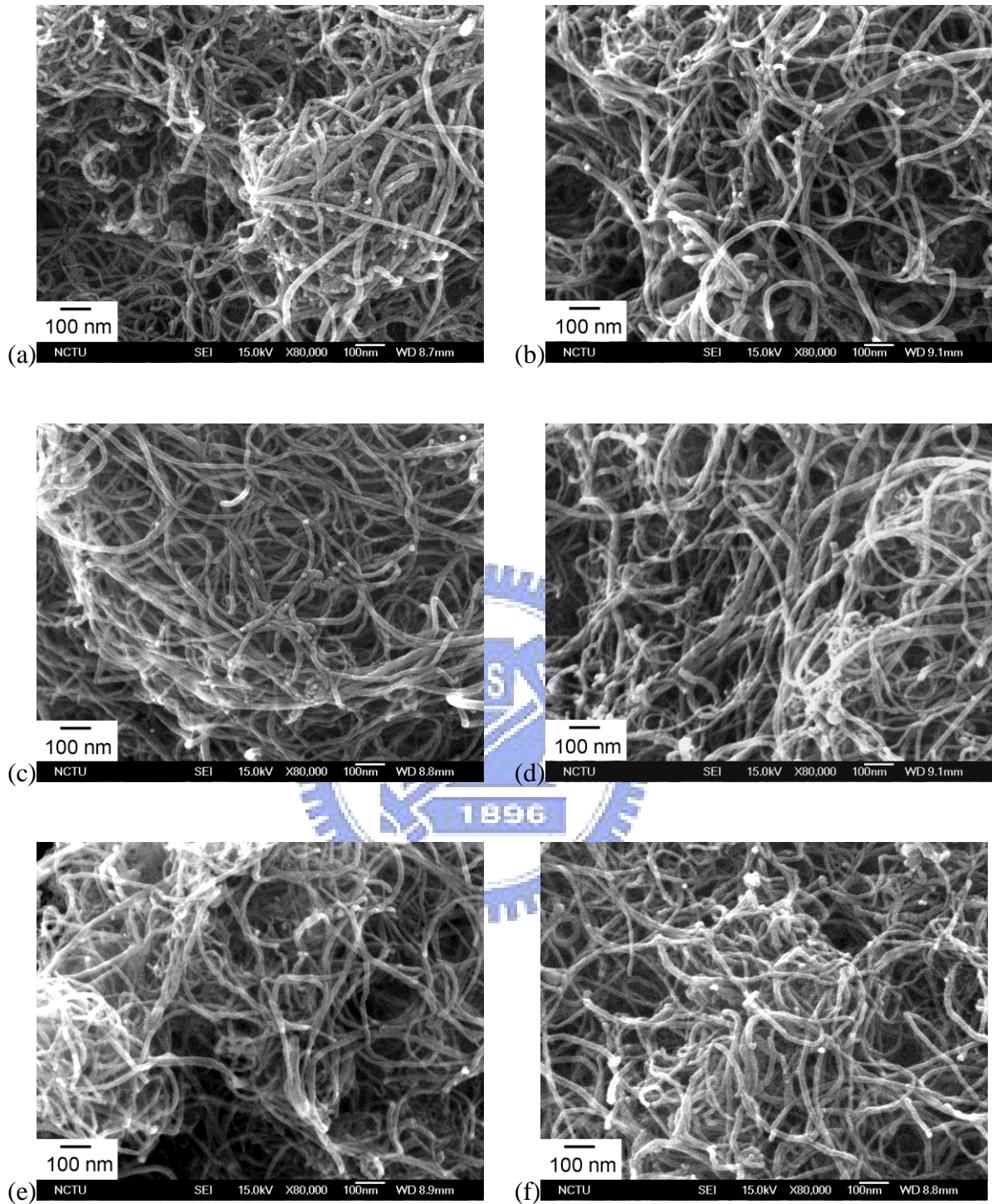




(a) 50/0 (sccm/sccm)	(b) 40/10 (sccm/sccm)
(c) 25/25 (sccm/sccm)	(d) 10/40 (sccm/sccm)
(e) 0/50 (sccm/sccm)	(f) 25/25 (sccm/sccm)

**Fig. 4-3** SEM images for the ion-treated MWCNTs specimens for different H<sub>2</sub>/O<sub>2</sub> flow ratios, (a) 50/0, (b) 40/10, (c) 25/25, (d) 10/40, (e) 0/50 and (f) 25/25 (sccm/sccm), (Specimen B1 to B6, respectively).





(a) 50/0 (sccm/sccm)	(b) 40/10 (sccm/sccm)
(c) 25/25 (sccm/sccm)	(d) 10/40 (sccm/sccm)
(e) 0/50 (sccm/sccm)	(f) 25/25 (sccm/sccm)

**Fig. 4-4** SEM images for the ion-treated MWCNTs specimens for different H<sub>2</sub>/O<sub>2</sub> flow ratios, (a) 50/0, (b) 40/10, (c) 25/25, (d) 10/40, (e) 0/50 and (f) 25/25 (sccm/sccm) (Specimen B1 to B6, respectively) at higher magnification.

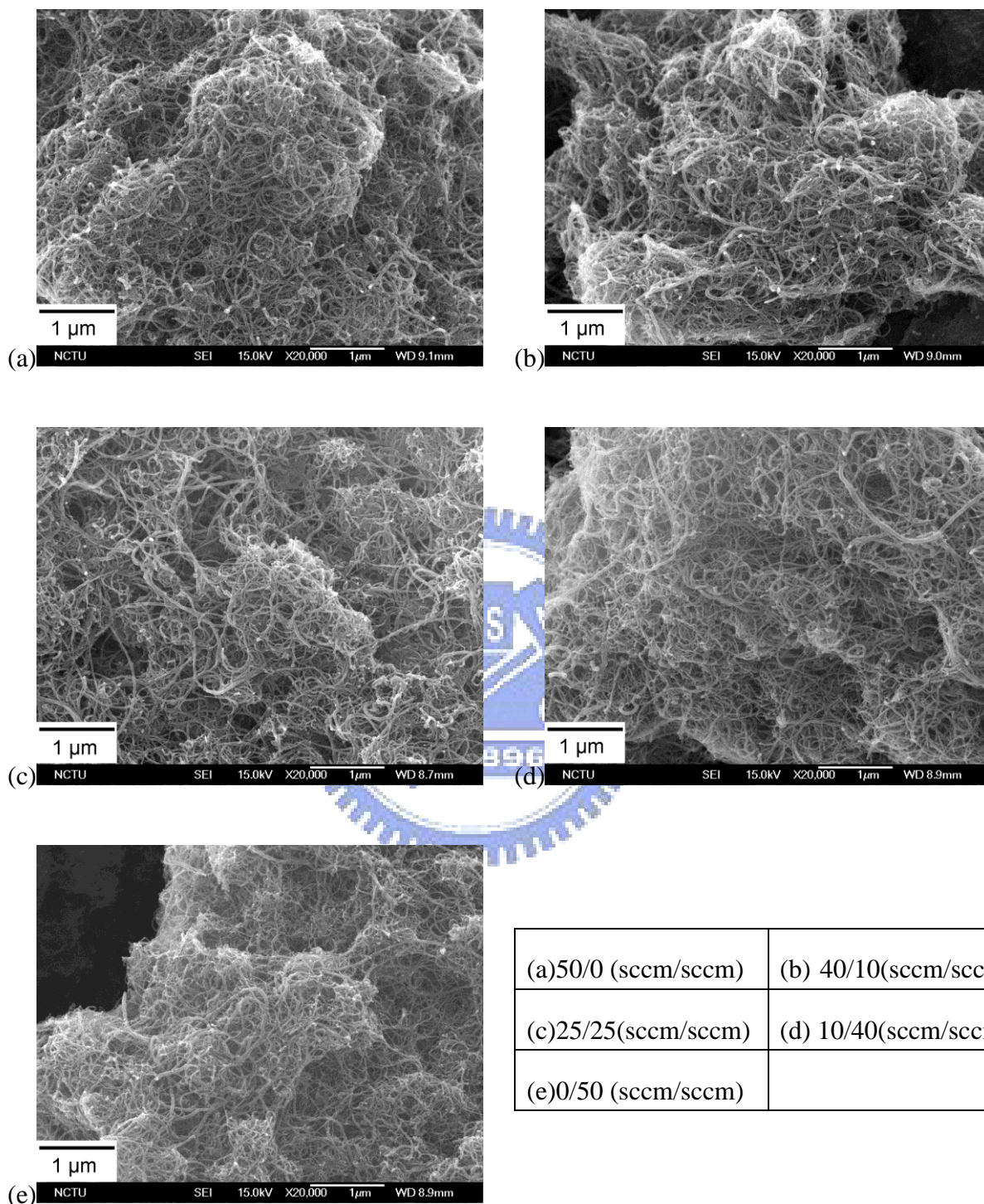
## **4.2 Effect of H<sub>2</sub>/O<sub>2</sub> flow ratio on morphologies of the ion-treated MWCNTs**

In contrast to the SEM characterization results of the nitric/sulfuric and dilute nitric acid-treated MWCNTs, after the ion treatment with various H<sub>2</sub>/O<sub>2</sub> flow ratios, as depicted in Figs. 4-3 and 4-4 with different magnifications, the morphologies and the diameter distributions of the ion-treated samples do not show any observable difference in comparison with those of the as-purchased sample (Fig. 3-2a). This depicts that the ion treatment has no negative effects on morphology of the MWCNTs.

## **4.3 Effect of ion pretreatment on MWCNTs morphologies by two-step process**

Figures 4-5 and 4-6 reveals the SEM images when the ion-pretreated MWCNTs by using various H<sub>2</sub>/O<sub>2</sub> flow ratios are further ultrasonicated in a dilute acid (0.25 M HNO<sub>3</sub>) for 2 h. As shown in the Fig. 4-5, the MWCNTs treated by the two-step process are observed to be with no difference in morphology as compared to that of the as-purchased MWCNTs. Meanwhile, further observing the figures at higher magnification (Fig. 4-6), the results show that, after being treated by the process under various H<sub>2</sub>/O<sub>2</sub> gas flow ratios, a slightly greater number of larger diameter nanotubes can be seen in the samples treated by the process. This results in a larger mean value of the diameter distribution. This could be because, after the ion pretreatment, the nanotubes can be with higher density free radical bonds so that nanotubes with smaller diameter could be more easily destructed in the dilute nitric acid due to their relatively low oxidation stability. However the effect is shown to be insignificant. This shows that, although the two-step process, combining the ion pretreatment and a 0.25 M HNO<sub>3</sub> acid treatment, may also possibly damage the side walls of the nanotube but this side effect is almost negligible.





(a)50/0 (sccm/sccm)	(b) 40/10(sccm/sccm)
(c)25/25(sccm/sccm)	(d) 10/40(sccm/sccm)
(e)0/50 (sccm/sccm)	

**Fig. 4-5** SEM images for the ion-pretreated MWCNTs specimens for different H<sub>2</sub>/O<sub>2</sub> flow ratios, (a) 50/0, (b) 40/10, (c) 25/25, (d) 10/40 and (e) 0/50 (sccm/sccm) (Specimen C1 to C5, respectively), and followed by a 0.25 M HNO<sub>3</sub> acid-treatment.

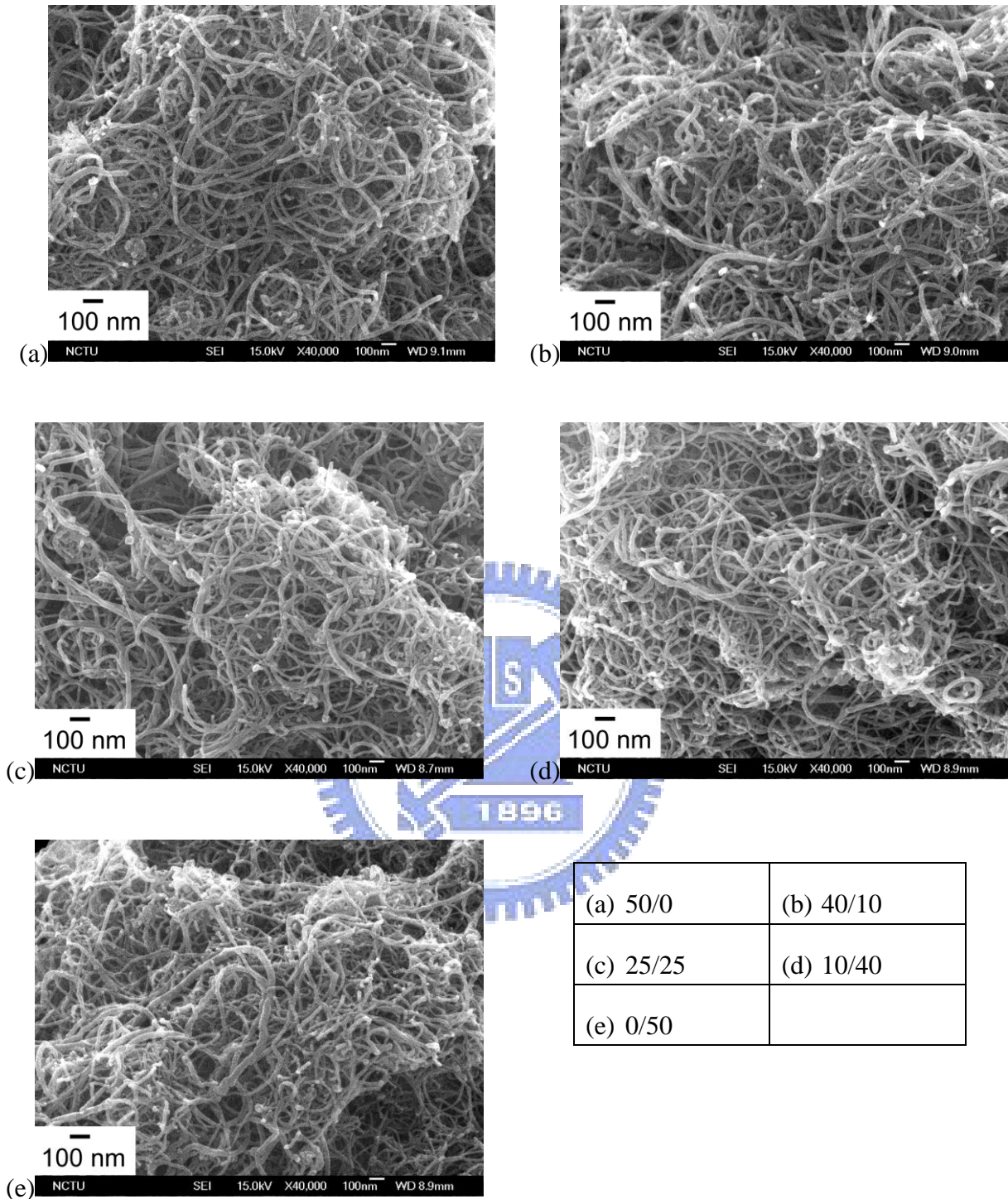


**Fig. 4-6** SEM images for the ion-pretreated MWCNTs specimens for different  $H_2/O_2$  flow ratios, (a) 50/0, (b) 40/10, (c) 25/25, (d) 10/40 and (e) 0/50 (sccm/sccm), (Specimen C1 to C5, respectively), and followed by a 0.25 M  $HNO_3$  acid-treatment at higher magnification.

Furthermore, in contrast to the results of the MWCNTs only treated by the dilute acid for 2 h in Fig. 4-2, the diameter distribution change, which results in more nanotube with large



diameter, of the two-step process is relative higher. This further supports that the free radical bonds introduced by the ion treatment can increase the size distribution change while the ion-pretreated MWCNTs are further treated in the dilute acid. In addition, it is also found that, with and without the ion treatment, the nanotube reductions in length for all samples are observed to be insignificant when MWCNTs are treated in the dilute acid treatment.

#### 4.4 TEM microstructures

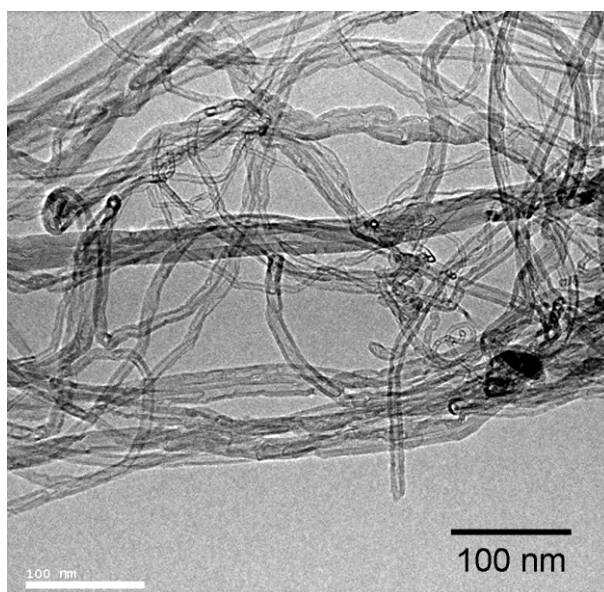


**Fig. 4-7** TEM image of merely ion-treated MWCNTs (Specimen B3).

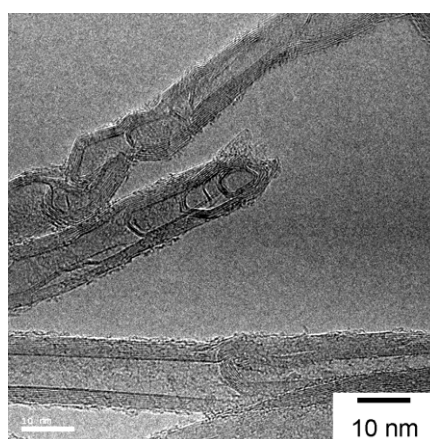


**Fig. 4-8** TEM image of merely ion-treated MWCNT (Specimen B3) at higher magnification.

Figure 4-7 and 4-8 shows the TEM image of the MWCNTs (Specimen B3) treated by the ion treatment with  $H_2/O_2$  gas flow ratio of 25/25 (sccm/sccm) for 5 min. As revealed in Fig.

4-8, the images at higher magnification support the fact that, after the ion treatment, the microstructure of the nanotubes are shown no difference compared with that of the as-purchased sample (Fig. 3-3b).

The SEM and TEM results depict that the effect of ion treatment and the two-step process on MWCNTs morphology and structure are insignificant. However, it is noted that, theoretically, SEM and TEM can not observe the functional groups nor precisely predict the formation of the free radical bonds if the “very small” defects are formed in the chemical structure of the surface.

#### 4.5 XPS spectra

In order to investigate the functionalization extent, the  $C_{1s}$  spectra of the nitric/sulfuric acid-treated MWCNTs are shown in Fig. 4-9, and the deconvolution results are given in Table 4-1. Note that the [O]/[C] ratio in the table is based on the relative percentage of three carboxyl groups to all the carbon species detected [\[Ago 1999-8116, Xu 2007-8945\]](#). As can be seen in Fig. 4-9 and Fig. 3-3, it is observed that when the as-purchased MWCNTs (Fig. 3-3) are treated by  $HNO_3/H_2SO_4$  solution for 6 and 9 h, the  $C_{1s}$  spectrum is apparently shift to higher binding energy. More specifically, the deconvolution results reveal that the share percentages of the oxygenated carbon species are higher after the nanotubes are treated by the acid treatment; and the [O]/[C] ratio increases as the process time increases from 6 to 9 h (46.2% to 52.7% respectively) while the  $sp^3$  carbon are reduced to 26.4% and 24.5% and  $sp^2$  are reduced to 27.5% and 22.6%, respectively. Suggested by Felten et al. [\[Felten 2005-074308\]](#), the  $sp^3$  content peaking at 281.5 can be attributed to amorphous carbon.

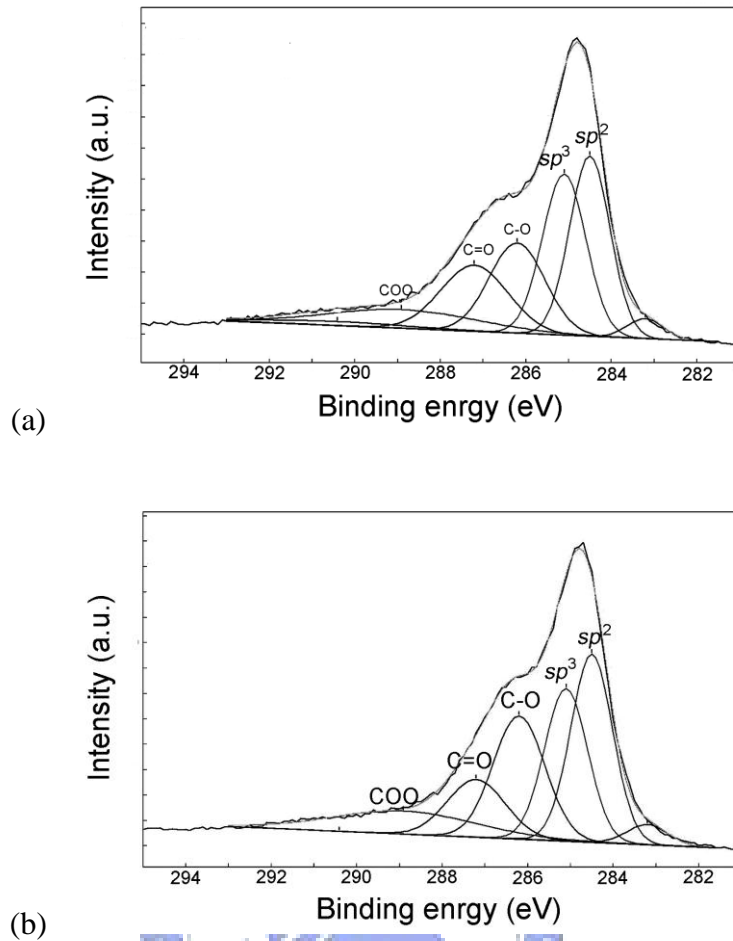


**Fig. 4-9** XPS  $C_{1s}$  spectra of the acid-treated MWCNTs under different treatment times, (a) 6h, and (b) 9 h (for Specimens A1 and A2, respectively).

After the as-purchased MWCNTs are treated by the ion treatment for 5 min using various  $H_2/O_2$  gas flow ratios, the XPS survey spectra are shown in Fig. 4-10. It is noted that the spectra showing the presence of carbon and oxygen on the treated and untreated samples are normalized with respect to  $C_{1s}$  intensity for comparison purposes. In contrast to the spectrum of the as-purchased MWCNTs, a higher concentration of oxygen is introduced to the surface of the nanotubes treated by the ion treatment using any gas flow ratio.

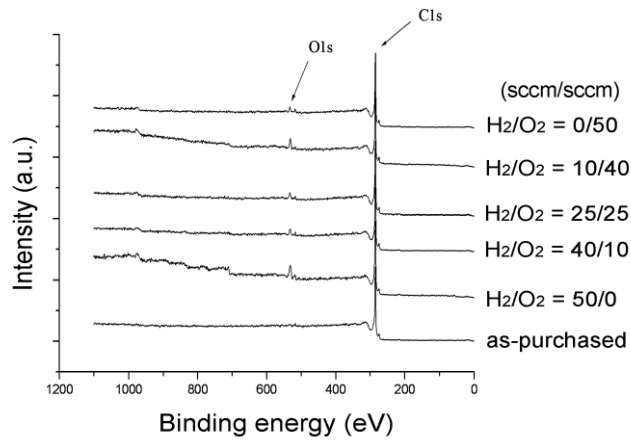


**Fig. 4-10** XPS survey spectra of the 5 min ion-treated MWCNTs under different H<sub>2</sub>/O<sub>2</sub> flow ratios (for Specimens B1 to B5).

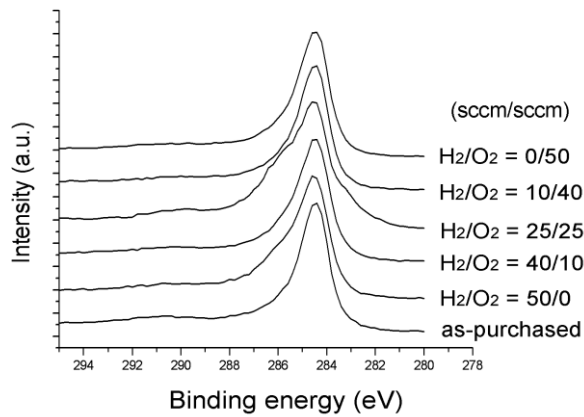


**Fig. 4-11** XPS C<sub>1s</sub> spectra of the 5 min ion-treated MWCNTs under different H<sub>2</sub>/O<sub>2</sub> flow ratios (for Specimens B1 to B5).

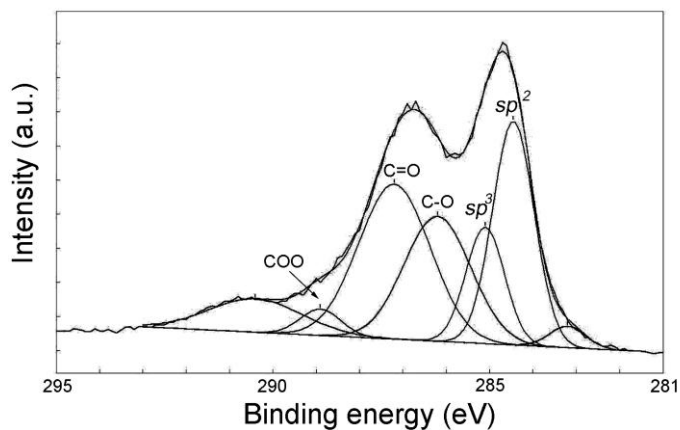


**Fig. 4-12** XPS C<sub>1s</sub> spectrum of the 20 min ion-pretreated MWCNTs (Specimen B6) and its deconvoluted spectra.

**Table 4-1** Comparisons of the XPS, Raman  $I_D/I_G$ , and TGA peak temperature for MWCNTs specimens merely treated by ion and/or acid processes.

Specimens designation	XPS*						Raman ( $I_D/I_G$ )	TGA Decomposition temperature <sup>+</sup> (°C)
	$sp^2$ (%)	$sp^3$ (%)	C-O (%)	C=O (%)	COO (%)	[O]/[C] <sup>#</sup> (%)		
As-purchased	48.8	40	1	8.4	1.8	11.2	0.89	600
A1	27.5	26.4	19	16.7	10.5	46.2	0.96	635
A2	22.6	24.5	15.7	28	9	52.7	0.96	638
A3	23.5	57.1	6.4	4.3	14.1	24.8	0.91	684
B1	30.8	54	2.1	11	2.2	15.3	1.08	596
B2	36.8	49.1	0.6	0.5	12.9	14	1.27	594
B3	42.8	26.1	13.8	17.3	< 0.1	31.1	1.07	595
B4	40.5	39.5	11.9	0.8	7.3	20	1.05	599
B5	44.2	44.6	< 0.1	9.4	1.7	11.1	1.03	598
B6	27.1	13.1	24.3	32.3	3.2	59.8	1	594
C1	59.5	21.1	1.4	9.2	8.9	19.5	1.06	651
C2	43.6	32.3	10.7	2.7	10.7	24.1	0.95	677
C3	37.1	10.6	32	18.2	2.2	52.4	1.26	684
C4	33.4	19.1	26.2	18.8	2.5	47.5	1.13	682
C5	44.2	32.9	9.2	8.2	5.5	22.9	0.96	668

<sup>#</sup> [O]/[C]: total percentage of oxygenated carbon species to the total number of carbon species detected.

<sup>+</sup> Corresponding to the peak temperature of weight derivative curve.

\*Represents the percentage of each carbon containing species in the MWCNTs specimens.

For a detailed comparison, all  $C_{1s}$  spectra of the MWCNT samples are presented in Fig. 4-11 and the deconvolution results are summarized in Table 4-1. After the samples are treated by the ion treatment, the XPS measurements show that the concentrations of the graphite,  $sp^2$  and  $sp^3$  carbons, and oxygen-containing functional groups are different according to the gas

mixture composition. Also, it is clear that when the samples of the MWCNTs are treated with a H<sub>2</sub>/O<sub>2</sub> gas flow ratio of 25/25 (sccm/sccm), the highest concentration of oxygenated functional groups is achieved whilst the concentration of sp<sup>3</sup> carbon is minimized. Meanwhile, the sp<sup>2</sup> carbon is insignificantly decreased.

The C<sub>1s</sub> spectrum of the MWCNTs treated by the ion treatment with H<sub>2</sub>/O<sub>2</sub> gas flow ratio of 25/25 (sccm/sccm) for 20 min is presented in Fig. 4-12. The results listed in Table 4-1 reveal that the [O]/[C] ratio is extremely high up to 59.8% and the sp<sup>3</sup> carbon is only with 13.1% while the morphology (cf. Fig. 4-3f and 4-4f) is almost the same as that of the as-purchased MWCNTs (Fig. 3-2). In contrast to the results of the MWCNTs merely treated by nitric/sulfuric acid for 9 h, the MWCNTs treated by the ion treatment with H<sub>2</sub>/O<sub>2</sub> gas flow ratio of 25/25 (sccm/sccm) for 20 min are with higher [O]/[C] and sp<sup>2</sup> values (Table 4-1).

As shown in Fig. 4-13, all XPS C<sub>1s</sub> spectra of the MWCNTs pretreated by the ECR ion pretreatment with various H<sub>2</sub>/O<sub>2</sub> gas flow ratios and followed by a 0.25 M HNO<sub>3</sub> acid treatment for 2 h are presented. It is seen that there are shifting for all MWCNTs specimens on the carbon signals of XPS spectra varied by various flow ratios. The results in Fig. 4-13 and Table 4-1 also show that when the MWCNTs are pretreated with H<sub>2</sub>/O<sub>2</sub> gas flow ratios of 25/25 and 10/40 (sccm/sccm) (for Specimen C3 and C4 respectively) the [O]/[C] ratios are 42.4% and 52.4% while sp<sup>3</sup> carbon are reduced to 10.6% and 19.1% respectively. Meanwhile, the sp<sup>2</sup> carbon of both the specimen are significantly higher than the results of the MWCNTs only treated by nitric/sulfuric acid for 6 and 9 h (Specimen A1 and A2 specifically). These results depict that the two-step method is significantly capable of facially functionalization and purification for removing the carbon impurities generated by synthesizing process simultaneously on the nanotube surface. In contrast to the MWCNTs merely treated by the ion treatment with H<sub>2</sub>/O<sub>2</sub> gas flow ratio of 25/25 (sccm/sccm) for 5 min (Specimen B3, cf. Table 4-1), the results support the fact that the two-step method, which combines the ion

pretreatment with H<sub>2</sub>/O<sub>2</sub> gas flow ratio of 25/25 (sccm/sccm) for 5 min and followed by a 0.25 M HNO<sub>3</sub> acid treatment for 2 h (Specimen C3), has higher capability of facially functionalizing and purifying nanotubes. In addition, by comparing the results of the MWCNTs treated by the ion treatment with H<sub>2</sub>/O<sub>2</sub> flow ratio of 25/25 (sccm/sccm) for 20 min (Specimen B6), the [O]/[C] ratio and sp<sup>3</sup> values of the MWCNTs treated by the two-step process with using the same H<sub>2</sub>/O<sub>2</sub> gas flow ratio (Specimen C3) are almost the same as that of Specimen B6 but the sp<sup>2</sup> carbon of Specimen C3 is significantly higher than that of the Specimen B6. This further confirms that the functionalization and purification capability of this method is significant, only the process time is longer than that of the ion treatment.

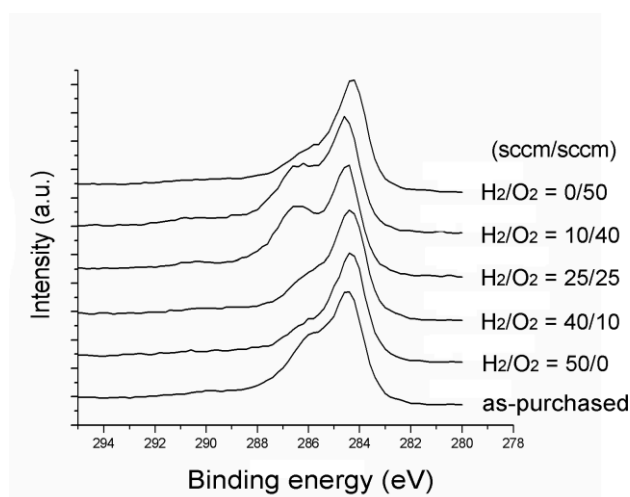


**Fig.4-13** XPS C<sub>1s</sub> spectra of the 5 min ion-pretreated MWCNTs and followed by a 0.25 M HNO<sub>3</sub> acid treatment (for Specimens C1 to C5).

As presented in Table 4-1, it is shown that the [O]/[C] ratio of the MWCNTs treated only with the 0.25 M HNO<sub>3</sub> acid treatment (Specimen A3) is obviously smaller than the results of the MWCNTs that underwent ion pretreatment alone by H<sub>2</sub>/O<sub>2</sub> flow ratio of 25/25 (sccm/sccm) for 5 min. This supports and confirms that in this case, the effect of the ion pretreatment is significant on the functionalization of MWCNTs by the dilute acid treatment.

As compared to the results of the MWCNTs treated by only ion treatment with H<sub>2</sub>/O<sub>2</sub> gas flow ratio of 25/25 and the two-step process with the same gas flow ratio, the HNO<sub>3</sub>/H<sub>2</sub>SO<sub>4</sub>

acid treatment reveals to be low facially functionalization and purification efficiencies. Thus, it is found that both the two presented methods are effective ways to graft polar functional groups onto the nanotubes while the removal of  $sp^3$  and the increase of  $sp^2$  are also significant.

## 4.6 Raman spectra

In general, functional groups are expected to be covalently bonded to free radical bonds on the surface of CNTs [Banerjee 2003-1899]. Therefore, higher density of free radical bonds is important for allowing more functional groups to form on nanotube surface. In order to evaluate the formation of free radical bonds on nanotube surface by the various treatments, the Raman spectra are presented in Figs. 4-14, 4-15, and 4-17.

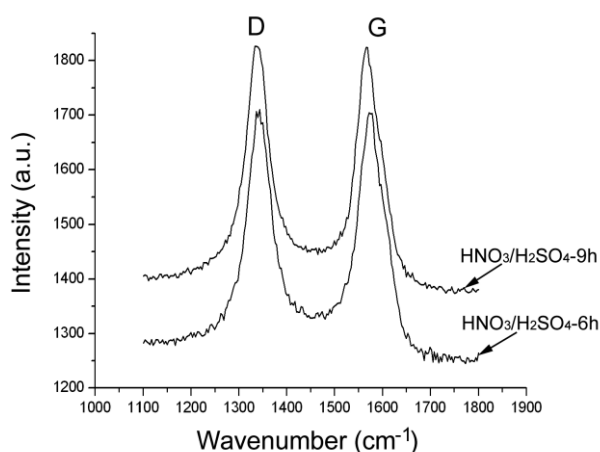


**Fig. 4-14** Raman spectra of the acid-treated MWCNTs under different treatment times (for Specimens A1 and A2).

As shown in Fig.4-14, the Raman spectra of the MWCNTs treated by HNO<sub>3</sub>/H<sub>2</sub>SO<sub>4</sub> solution for 6 and 9 h are presented with two characteristic peaks which are attributed to the D and G bands. The spectra have been normalized with respect to the G band for comparison. Suggested by previous studies, the intensity of the D band, at frequencies around 1,344 cm<sup>-1</sup>, is correlated with structural disorder of CNTs, which originates from the defects including disordered materials, poor graphitization, functionalized carbon, and the amorphous carbon on



the sidewall of nanotubes [Shaijumon 2007-75, Dillon 2004-691, Jian 2008-230]. The G band at frequencies around  $1,572\text{ cm}^{-1}$  is activated by the graphite signal [Jian 2008-230]. It is also suggested that the  $I_D/I_G$  ratio is closely associated with the defect density on the walls of the MWCNTs [Jian 2008-230]. Therefore, the intensity ratio can be used to evaluate the formation of free radical bonds which are preferential sites for functionalization. The results of the  $I_D/I_G$  ratio are also listed in Table 4-1. The results show that when the as-purchased MWCNTs are treated by the acid for 6 and 9 h, both the  $I_D/I_G$  ratios are 0.96.

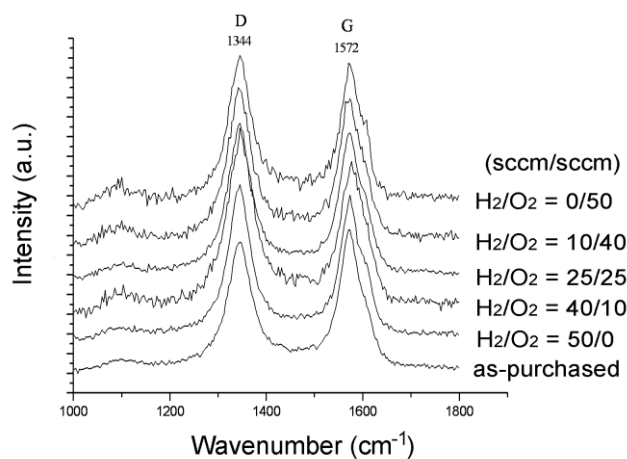


**Fig. 4-15** Raman spectra of the 5 min ion-treated MWCNTs under different  $H_2/O_2$  flow ratios (for Specimens B1 to B5).

In order to evaluate the effects of the  $H_2/O_2$  gas flow ratio on the formation of free radical bonds on the nanotube surface when the MWCNTs are treated by the ion treatment, the Raman spectra of the as-purchased and the ion-treated MWCNTs are presented in Fig. 4-15. As expected, in contrast to the as-purchased sample, all  $I_D/I_G$  ratios are increased after ion treatment with any  $H_2/O_2$  gas flow ratio. As shown in Fig. 4-16, the  $I_D/I_G$  ratio increases from 1.03 to 1.27 when  $H_2$  concentration increases from 0 to 80 vol. %. The  $H_2/O_2$  gas of 50/0, 40/10, 25/25, 10/40, and 0/50 (sccm/sccm) are equivalent to  $H_2$  concentrations of 100, 80, 50, 20, and 0 vol. %, respectively.

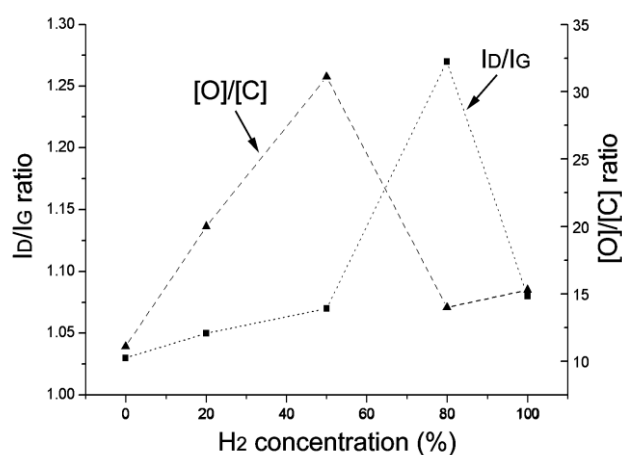


**Fig. 4-16** I<sub>D</sub>/I<sub>G</sub> ratio of the 5 min ion-treated MWCNTs vs. H<sub>2</sub> concentration in H<sub>2</sub>/O<sub>2</sub> flow.

Note that the ion density is very important for the formation of the free radical bonds on the surface and the oxygen cation in the ion stream is crucial for forming oxygen-containing functional groups. By comparing the ionic current, it is found that current increases from 0.12 to 0.47 A while the H<sub>2</sub> concentration increases from 0 to 100%. Note that the ionic current correlates with the ion density and is measured by an ammeter connected to the 150 mm diameter process stage. This shows that the ion density of the cation stream increases as H<sub>2</sub> concentration increases. This leads to higher I<sub>D</sub>/I<sub>G</sub> ratio when H<sub>2</sub> concentration of the gas flow is higher. However, this simultaneously reduces [O]/[C] value due to the decreases on oxygen cations in the ion stream. Apart from their involvement in ion bombardment, the generated oxygen cations can also act as highly reactive chemical species which form covalent bonds with the amorphous carbon and then nanotube surface. More specifically, the amorphous carbon layer is more reactive than the cylindrical walls to form volatile products with the oxygen cations. The products are then pumped out by the vacuum system. Thus, as shown in Table 4-1, the ion treatment using a H<sub>2</sub>/O<sub>2</sub> mixture can increase the concentration of oxygenated functional groups whilst also reducing the sp<sup>3</sup> value. On the other hand, treatment with pure O<sub>2</sub> gas (with the exception of increasing the I<sub>D</sub>/I<sub>G</sub> ratio) does not yield any other obvious effects in regard to the sp<sup>2</sup> and [O]/[C] values of CNTs when compared with the

as-purchased MWCNTs. This indicates that a H<sub>2</sub>/O<sub>2</sub> mixture not only facilitates free radical bonds but also promotes covalent bonding in this case. Therefore, even with the addition of 20 vol. % H<sub>2</sub> (H<sub>2</sub>/O<sub>2</sub> = 10/40 (sccm/sccm)) in gas flow, there is still a significant removal of amorphous carbon and formation of oxygen-containing groups on the nanotube surface.

In contrast to the results of the MWCNTs treated by HNO<sub>3</sub>/H<sub>2</sub>SO<sub>4</sub> solution for 9 h (Specimen A2), as listed in Table 4-1, after the MWCNTs are treated by the ion with H<sub>2</sub>/O<sub>2</sub> gas flow ratio of 25/25 (sccm/sccm) for 5 min, the measurement of Raman spectroscopy displays a higher I<sub>D</sub>/I<sub>G</sub> ratio (1.07) than that of Specimen A2 (0.96). This increase may reflect the fact that the ion treatment can introduce higher density of free radical bonds than the nitric/sulfuric acid treatment on the surface of the nanotubes effectively. However, it is observed that when the process time of the ion treatment increases to 20 min (Specimen B6), the I<sub>D</sub>/I<sub>G</sub> ratio value decreases to 1.00. As suggested by Osswald et al. <sup>[Osswald 2007-728]</sup>, this decrease might be due to the removal of the impurities coating on the surface of the MWCNTs.

Raman spectra of the MWCNTs treated by merely dilute acid treatment for 2 h and the two-step process combining the 5 min ion treatment with various H<sub>2</sub>/O<sub>2</sub> gas flow ratios and the dilute acid treatment are presented in Fig. 4-17. The resultant I<sub>D</sub>/I<sub>G</sub> ratios are also listed in Table 4-1. The results show that, when the as-purchased MWCNTs are only treated by the dilute acid treatment, both the I<sub>D</sub>/I<sub>G</sub> and [O]/[C] ratios can only slightly increase. However, when the MWCNTs are treated by the ion pretreatment and further treated by the dilute nitric acid treatment for 2 h, the MWCNTs can be with much higher I<sub>D</sub>/I<sub>G</sub> values. The increase of the I<sub>D</sub>/I<sub>G</sub> ratio indicates that higher density of free radical bonds can be induced by the ion pretreatment. This also supports the hypothesis that the ion treatment is very effective in creating free radical bonds on the nanotubes; and free radical bonds could only be introduced on the outer surface by the treatment because the incident ions do not reach the inner shells of

the nanotubes.

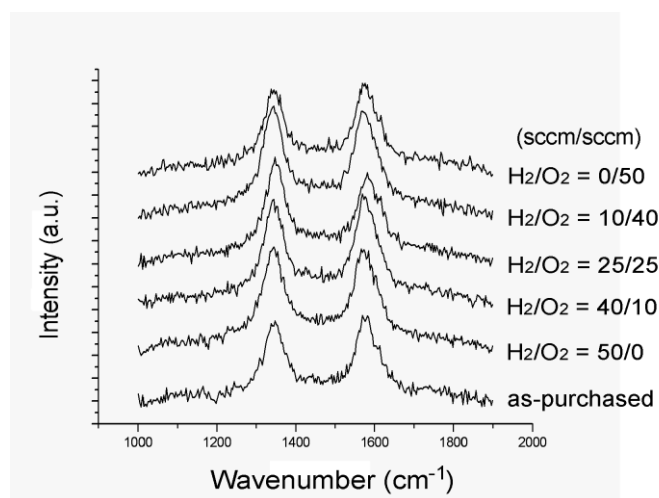


**Fig. 4-17** Raman spectra of the 5 min ion-pretreated MWCNTs and followed by a 0.25 M HNO<sub>3</sub> acid treatment (for Specimens C1 to C5).

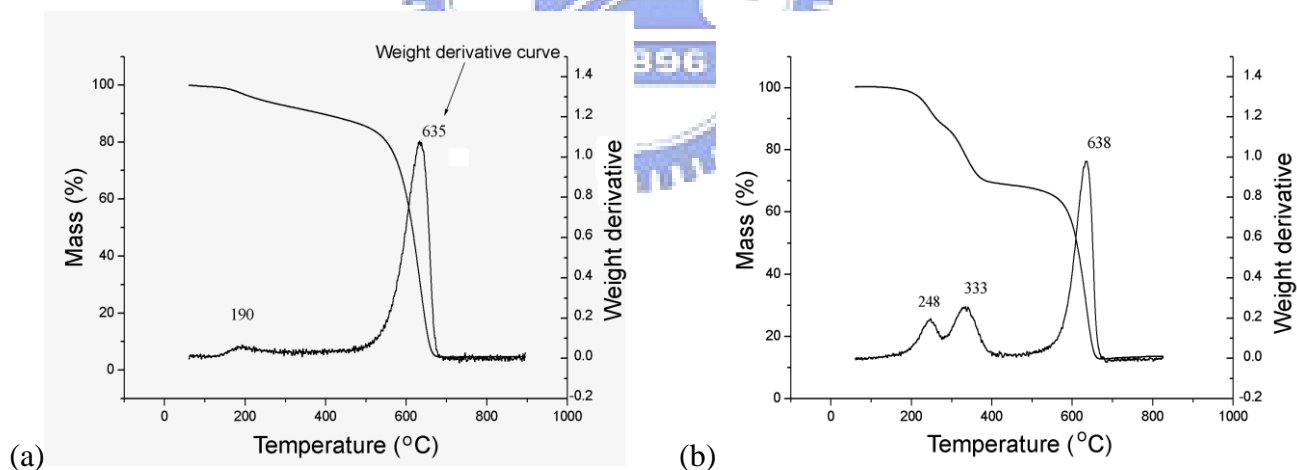
Additionally, as compared the results of Specimen B3 (cf. Table 4-1), when the MWCNTs are treated by the ion pretreatment with H<sub>2</sub>/O<sub>2</sub> gas flow ratio of 25/25 for 5 min and further treated by 0.25 M HNO<sub>3</sub> acid for 2 h (Specimen C3), the I<sub>D</sub>/I<sub>G</sub> ratio (1.26) of Specimen C3 is apparently higher than that of Specimen B3 (1.07). The [O]/[C] ratio is also increased from 31.1 % (Specimen B3) to 52.4 % (Specimen C3). These results support the fact that, with the ion pretreatment, high amount of oxygen-containing functional groups can be effectively introduced on nanotube surface by the dilute acid treatment. It is also shown that the I<sub>D</sub>/I<sub>G</sub> ratios of the MWCNTs treated by the two-step process are varied with different H<sub>2</sub>/O<sub>2</sub> gas flow ratio. However, it is found that there is no correlation between I<sub>D</sub>/I<sub>G</sub> ratio and H<sub>2</sub> concentration in gas flow.

It should be noted that, as the presence of measurement uncertainty is found to be relative high, Raman spectroscopy is invalid to quantify the formation of free radical bonds and there is still no sufficient evidence to support this. Therefore, in this study, we are using XPS for the functionalization quantification results. However, as suggested by previous studies [Dillon 2004-691, Osswald 2007-728, Jian 2008-230], it is still a good indicator to monitor the

formation of free radical bonds.

## 4.7 TGA results

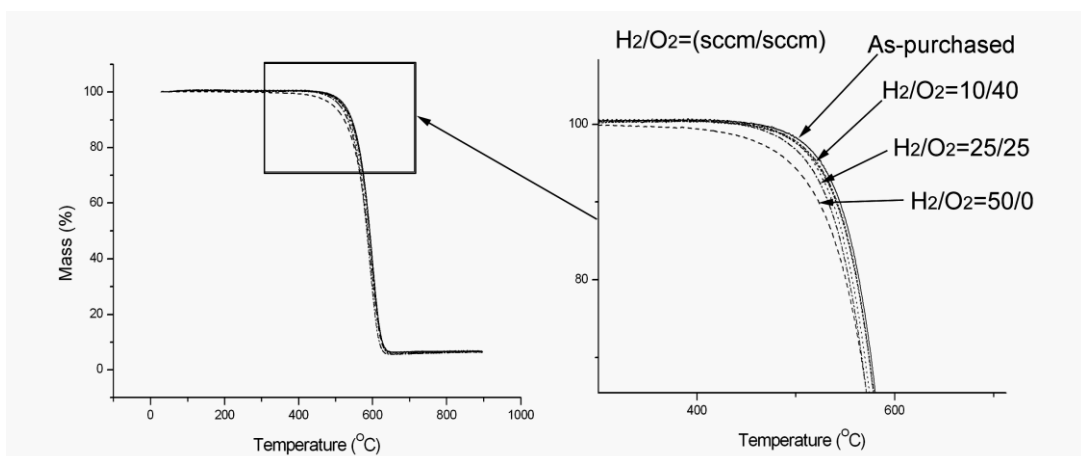
It is known that the oxidation stability correlates with the combing effect of defects and the diameter of the nanotubes [Zhang 2004-149, Xu 2007-8945, Liu 2007-5006, BOM 2002-615]. The presence of defects in graphite contributes to a decrease in the oxidative stability of the material [BOM 2002-615]. In addition, the larger the diameter is, the higher the oxidation stability of the nanotubes is [Zhang 2004-149, BOM 2002-615]. Theoretically, SEM and TEM can not observe the functional groups nor precisely predict the formation of free radical bonds if the “very small” defects are formed in the chemical structure of the surface. Because defects and derivatization moieties in nanotube walls result in lower structural integrity and can lower the thermal stability [Pillai 2007-3011, Liu 2007-5006], it is useful to confirm the results by using TGA.



**Fig. 4-18** TGA curves for the acid-treated MWCNTs under different treatment times, (a) 6 h, and (b) 9 h (for Specimens A1 and A2, respectively).

As revealed in Fig. 4-18, the mainly derivative peak temperatures of the MWCNTs treated by nitric/sulfuric acid process for 6 and 9 h are shown to be 635 and 638 °C, which are much higher than that of the as-purchased MWCNTs (600 °C). As supported by the results of SEM, it is suggested that the increase of the decomposition temperature may be dominated by

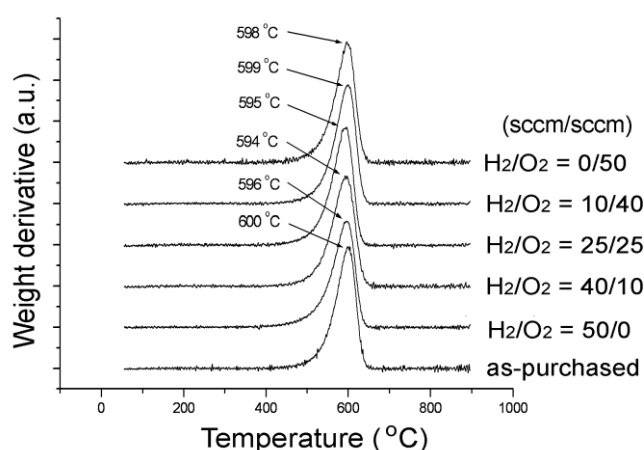
the significant diameter distribution change. Meanwhile, it is observed that there are satellite peaks presented at  $\sim 250$  and  $\sim 350$  °C in weight derivative TGA curves. The presence of the satellite peak of the derivative curve at  $\sim 350$  °C might have resulted from additional carbonaceous impurities which are introduced by the destruction of nanotubes during acid treatments [Zhang 2007-149, Hu 2003-13838, Harutyunyan 2002-8671, Shi-1999-35]. Additionally, the peak below 300 °C is typical of residual acid and absorbed water in the sample after treatment [Landi 2005-6819]. The presence of the satellite peaks are supporting the fact that the structural damage are severe when the nitric/sulfuric acid are used to facially modify the MWCNTs and this matches the SEM characterization results in Fig. 4-1. Meanwhile, as revealed in the figures, the TGA curve depicts that the carbon impurities introduced weight approximately 20% in 6 h acid-treated sample and 30% in 9 h acid-treated sample. The weight percentages of the catalysts are also found to be increased to 7% and 13% for the MWCNTS treated by acid for 6 and 9 h respectively (for Specimen A1 and A2 respectively). This shows that the structural damage increases as the acid treatment time increases. Therefore, the graphite structure are damaged and removed by filter during cleaning process. So the share percentage of catalyst is thus raised up.



**Fig. 4-19** TGA curves for the ECR ion-treated MWCNTs under different  $H_2/O_2$  gas flow ratio.

Figure 4-19 shows the TGA curves of the MWCNTs treated by the ion treatment for 5 min with various  $H_2/O_2$  gas flow ratios. It is found that all curves of the ion-treated MWCNTs

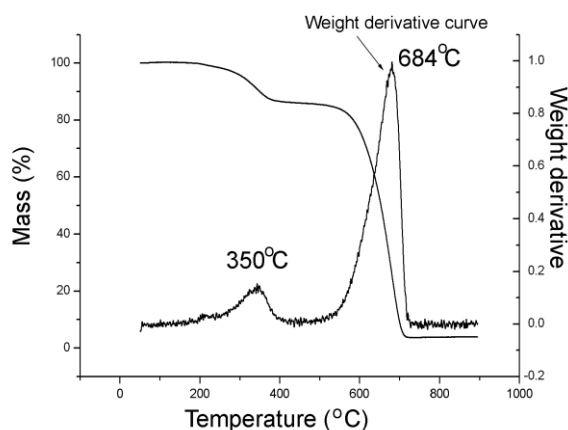
are almost overlapping on the curve of the as-purchased MWCNTS only the MWCNTS treated by H<sub>2</sub>/O<sub>2</sub> gas flow ratio of 50/0 (sccm/sccm) are slightly deviated from that of the as-purchased nanotubes because a very few percentage of the MWCNTS treated by H<sub>2</sub>/O<sub>2</sub> gas flow ratio of 50/0 (sccm/sccm) are decomposed from temperature at 300 °C. However, the deviation is insignificant.



**Fig. 4-20** Weight-derivative TGA curves for the 5 min ion-treated MWCNTs under different H<sub>2</sub>/O<sub>2</sub> flow ratios (for Specimens B1 to B5).

Figure 4-20 shows the weight-derivative curves of TGA analysis on the as-purchased MWCNTs and the 5 min ion-treated MWCNTs. The results show that with a main decomposition temperature of 600 °C, the as-purchased MWCNT samples are the most thermally stable with respect to oxidative degradation. Correspondingly, the MWCNTs treated by the ion treatment with a gas composition of 40/10 (sccm/sccm) have the lowest decomposition temperature (594 °C). Because the oxidation stability is a function of the combined effect of defects and the diameter of the nanotubes, with the same diameter distribution observed by the SEM characterizations in Fig. 4-3, the results are in agreement with the hypothesis that the decrease of the oxidation reaction temperature is mainly a result of the free radical bonds produced by the ion treatment. The marginal differences of the main decomposition temperature between as-purchased and ion-treated samples reflect the fact that

the effect of gas composition on structural integrity of the nanotubes is negligible in this case although the insignificant difference are varied with H<sub>2</sub>/O<sub>2</sub> gas flow ratio.



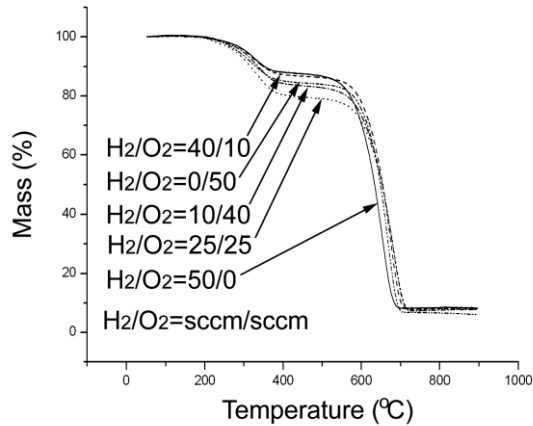
**Fig. 4-21** TGA curves for 0.25M HNO<sub>3</sub> acid-treated MWCNTs

Figure 4-21 reveals the TGA results of the MWCNTs are only treated by 0.25 M HNO<sub>3</sub> for 2 h. It is found that after the dilute acid treatment, carbon impurities including absorbed water are of approximately 15% in weight and the catalysts weight approximately 7% in the dilute acid-treated MWCNTs sample. Meanwhile, the main decomposition temperature peaks at 684 °C. This shows that this treatment is so moderate that the MWCNTS can be with high structural integrity and low free radical bonds introduced ( $I_D/I_G = 0.93$ ). This is also supported by SEM characterization (Fig. 4-2) in which the morphology change is insignificant after the dilute acid treatment while the diameter is slightly enlarged.

In order to evaluate the effects of the ion pretreatment on the decomposition temperature of the dilute acid-treated MWCNTs, all TGA and weight derivative TGA curves of the MWCNTs treated by the two-step process with various H<sub>2</sub>/O<sub>2</sub> gas flow ratios are presented in Fig. 4-22 and 4-23. As shown in the figures, the largest carbon impurities share percentage is approximately 22 % when the MWCNTs are pretreated by the ion treatment with H<sub>2</sub>/O<sub>2</sub> gas flow ratio of 25/25 (sccm/sccm) (Specimen C3) but the main combustion region is apparently shifted to higher temperature region. This leads to the highest main decomposition



temperature at 684 °C which is the same temperature as the MWCNTs only treated by 0.25 M HNO<sub>3</sub> acid for 2 h (Specimen A3). The results show that, with the ion pretreatment, the MWCNTs can be treated in dilute acid with high [O]/[C] ratio and thermal stability while the process time is relative low in contrast to the strong acid treatment.



**Fig. 4-22** TGA curves of the 5 min ion-pretreated MWCNTs and followed by a 0.25 M HNO<sub>3</sub> acid treatment (for Specimens C1 to C5).

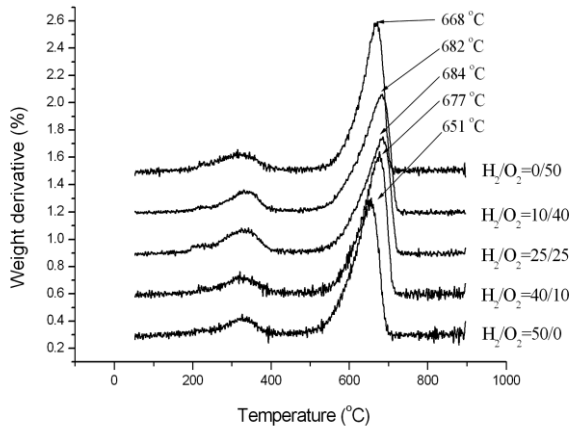


**Fig. 4-23** Weight-derivative TGA curves of the 5 min ion-pretreated MWCNTs and followed by a 0.25 M HNO<sub>3</sub> acid treatment (for Specimens C1 to C5)

For comparison, TGA and weight derivative TGA curves of the MWCNTs treated by various treatments and time conditions are presented in Figs. 4-24 and 4-25. As shown in Fig. 4-24, in contrast to the TGA curves of the as-purchased MWCNTs and the MWCNTs only

treated by the ion treatment (Specimen B3), all TGA curves of the MWCNTs treated by any acid treatment present oxidative reaction in lower temperature region ranging from 200 to 400 °C. As shown in Fig. 4-25, the satellite peaks of the weight derivative TGA curves show that this region could be contributed to carbon impurities. Meanwhile, the share percentage of the catalyst in the MWCNTs treated by HNO<sub>3</sub>/H<sub>2</sub>SO<sub>4</sub> acid for 9 h (Specimen A2) is significant higher than the specimens treated by other acid treatments.

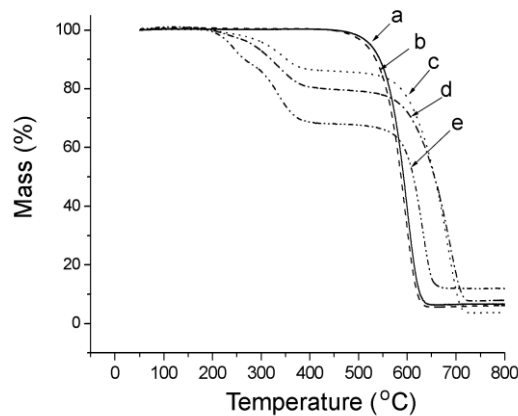


**Fig. 4-24** TGA curves of MWCNTs for different conditions, (a) as-purchased, (b) 5 min ion-treated (Specimen B3), (c) merely 0.25 M HNO<sub>3</sub> acid-treated (Specimen A3), (d) 5 min ion-pretreated and 0.25 M HNO<sub>3</sub> acid-treated (Specimen C3), and (e) merely acid-treated MWCNTs (Specimen A2).

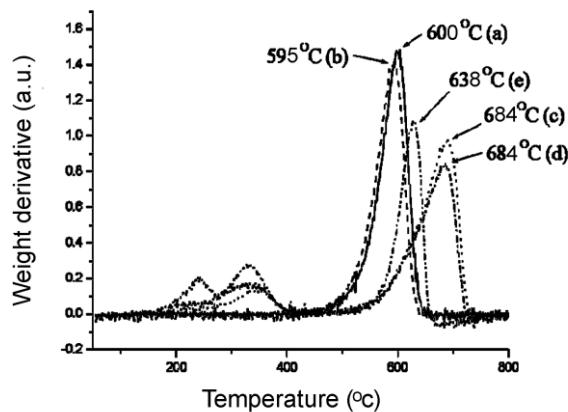


**Fig 4-25** Weight-derivative TGA curves of MWCNTs for different conditions, (a) as-purchased, (b) 5 min ion-treated (Specimen B3), (c) merely 0.25 M HNO<sub>3</sub> acid-treated (Specimen A3), (d) 5 min ion-pretreated and 0.25 M HNO<sub>3</sub> acid-treated (Specimen C3), and (e) merely acid-treated MWCNTs (Specimen A2).

According to the results of TGA, XPS and SEM characterization, although the

nitric/sulfuric acid treatment can introduce oxygenated functional groups on nanotube surface, the process is however censorable due to its high structural damage, long process time and solution wasting issues. This figure further depicts that, compared with the results of acid treatments, the ion treatment does not cause serious structural damage, and so the ion-treated sample can still be as the same thermal stability as the as-purchased sample.

According to the results of TGA, XPS in Table 4-1 and SEM characterization, the process combining the ion pretreatment applying H<sub>2</sub>/O<sub>2</sub> gas flow ratio of 25/25 (sccm/sccm) and a 0.25 M HNO<sub>3</sub> post acid treatment for 2 h can yield significant advantages such as a very high [O]/[C] ratio and high thermal stability MWCNTs although nanotubes with high density free radical bonds resulted from the ion pretreatment can be possibly damaged during the dilute acid treatment.

It is noted that the presence of the uncertainties in the results of XPS and TGA may slightly change the data provided above. Uncertainty analysis based on sufficient experiments data are required to revise the process parameters if the proposed method is to be applied for practical uses. Although the analysis has not been conducted yet, the present results are still reliable enough to characterize the performance of this method qualitatively.

# Chapter 5

## Conclusions

This study proposed two new processes and compared with the traditional processes to functionalize MWCNTs, in order to expand the potential applications of CNTs. The examined processes include the acid treatment by dilute or nitric/sulfuric acid solution, the ion treatment and the ion pretreatment followed by a dilute nitric acid treatment. Table 5-1 summarizes the experimental results in terms of efficiency of functionalization ( $[O]/[C]$ ,  $I_D/I_G$ ), facial purification ( $sp^2$ ), TGA decomposition temperature, and structure damage. From the experimental results, the following conclusions can be drawn:

1. By comparing the degree of functionalization and structure damage of CNTs by nitric/sulfuric with that by dilute acid treatments, the results show that sonicating CNTs in nitric/sulfuric acid treatment leads to a greater functionalization with  $[O]/[C]$  values of 52.7% but too much structure damage (i.e. higher  $I_D/I_G$  ratios and lower decomposition temperatures, up to 0.96 and down to 638 °C), though the values of  $[O]/[C]$ ,  $sp^2$  and  $I_D/I_G$  merely represent the near surface features due to limitation of penetration depth of XPS and Raman probes. Meanwhile, the chemical process is found to be with the drawbacks of pollution issue and too long treating time (up to 9 h).
2. When the MWCNTs are treated by the ion treatment, the results indicate that there are existence of maximum values of  $[O]/[C]$  and  $sp^2$ , and minimum values of  $I_D/I_G$  values at medium  $H_2/O_2$  ratios. The existence of maximum functionalization is due to the competition between the amounts of free radical bonds on nanotube surface and oxygen cations in the ion stream. Meanwhile, it is also shown that the ion treatment causes no significant structure damage, and at treatment times of 5 and 20 minutes, the maximum

values of the [O]/[C] values are 31.1% and 59.8% , respectively, at medium H<sub>2</sub>/O<sub>2</sub> ratio (= 25/25 (sccm/sccm)).

**Table 5-1** Comparisons of the performance of the modification processes on structure damage and the ranges of [O]/[C] ratio, sp<sup>3</sup> percentage, and decomposition temperature

Surface modification processes	structure damage	[O]/[C] (%)	sp <sup>2</sup> (%)	I <sub>D</sub> /I <sub>G</sub>	TGA decomposition temperature (°C)
No treatment	N.A.	11.2	48.8	0.89	600
Strong acid treatment only	Severe	46.2 ~ 52.7 (Max. for 9 h)	22.6 ~ 27.5 (Max. for 9 h)	0.96	635~ 638 (Min. for 6 h)
Dilute acid treatment for 2 h only	Light	24.8	23.5	0.91	684
Ion treatment only	Light	11.1 ~ 59.8 (Max. at H <sub>2</sub> /O <sub>2</sub> =25/25)	27.1 ~ 44.2 (Max. at H <sub>2</sub> /O <sub>2</sub> =10/40)	0.91 ~ 1.27 (Max. at H <sub>2</sub> /O <sub>2</sub> =40/10)	594 ~ 599 (Min. at H <sub>2</sub> /O <sub>2</sub> =40/10)
Two-step process	Light	19.5 ~ 52.4 (Max. at H <sub>2</sub> /O <sub>2</sub> =25/25)	33.4 ~ 59.5 (Max. at H <sub>2</sub> /O <sub>2</sub> =50/0)	0.95 ~ 1.26 (Max. at H <sub>2</sub> /O <sub>2</sub> =25/25)	651 ~ 684 (Min. at H <sub>2</sub> /O <sub>2</sub> =50/10)

- For the two-step process combining the 5 min ion pretreatment and a post dilute nitric acid treatment, the results show that the ion-treated MWCNTs at medium H<sub>2</sub>/O<sub>2</sub> ratio (= 25/25 (sccm/sccm)) can be further treated by dilute acid to increase the decomposition temperature from ~ 595 °C up to 684 °C without sacrificing the functionalization ([O]/[C]=52.4%). By comparing different process methods, both nitric/sulfuric and dilute acid treatments can enhance decomposition temperature by eliminating the impurities and the smaller CNTs to vary the size distribution of the tubes but it causes

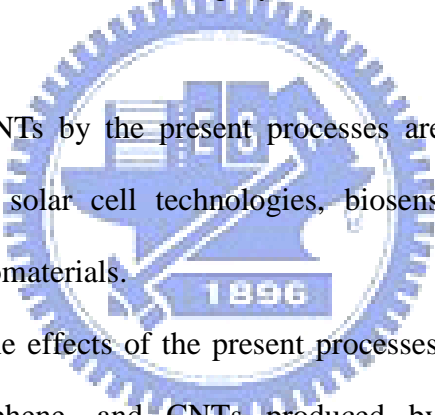
either too much structure damage or too long treating time. According to the results, the two-step process is relatively simple and efficient to functionalize CNTs, simultaneously enhance the decomposition temperature and cause no significant structure damage.



## Chapter 6

### Future Prospects

In this study, both the ion treatment, and the two-step process combining the ion pretreatment and a 0.25 M HNO<sub>3</sub> acid treatment are shown to be effective processes for surface modification of MWCNTs. The resulting nanotubes by the present ion treatment can be with very high polar functional groups and with insignificant structure and morphology changes while the process time is only with 20 min. When the MWCNTs are treated by the present two-step process, the nanotubes can be with high polar functional groups, high thermal stability, and high structural integrity. However, some subjects should be further studied:

- 
- (a) The functionalized CNTs by the present processes are further used for some specific applications, such as solar cell technologies, biosensors, drug and vaccine delivery vehicles, and novel biomaterials.
  - (b) In order to evaluate the effects of the present processes on various CNTs and graphene, different CNTs, graphene, and CNTs produced by various processes are to be functionalized by these two processes.
  - (c) Other process conditions including working pressure, positive bias voltage, and working distance between plasma zone and specimen are further studied because these conditions strongly correlate with the functionalization efficiency.
  - (d) According to the results, the thermal stability strongly correlates with the defects and the diameter of the nanotubes. It is important to find a method to measure the diameter distribution of the CNTs.

# References

## A

1. Ago, H., T. Kugler, F. Cacialli, W. R. Salaneck, M. S. P. Shaffer, A. H. Windle, and R. H. Friend, *J. Phys. Chem. B* 103 (1999) 8116-8121, "Work functions and surface functional groups of multiwall carbon nanotubes".
2. Ahn, K. S., J. S. Kim, C. O. Kim, and J. P. Hong, *Carbon* 41 (2003) 2481-2485, "Non-reactive rf treatment of multiwall carbon nanotube with inert argon plasma for enhanced field emission.
3. An, K. H., J. G. Heo, K. G. Jeon, D. Bae, C. S. Jo, C. W. Yang, C. Y. Park, Y. H. Lee, Y. S. Lee, and Y. S. Chung, *Appl. Phys. Lett.* 80 (2002) 4235-4237, "X-ray photoemission spectroscopy study of fluorinated single-walled carbon nanotubes".

## B

4. Bahr, J. L., J. P. Yang, D. V. Kosynkin, M. J. Bronikowski, R. E. Smalley, and J. M. Tour, *J. Am. Chem. Soc.* 123 (2001) 6536-6542, "Functionalization of carbon nanotubes by electrochemical reduction of aryl diazonium salts: A bucky paper electrode".
5. Banerjee, S., M. G. C. Kahn, and S. S. Wong, *Chem. Eur. J.* 9 (2003) 1899-18908 "Rational chemical strategies for carbon nanotube functionalization".
6. Bethune, D. S., C. H. Kiang, M. S. Devries, G. Gorman, R. Savoy, J. Vazquez, and R. Beyers, *Nature* 363 (1993) 605-607, "Cobalt- Catalysed growth of carbon nanotubes with single-atomic-layer wall".
7. Bianco, A., K. Kostarelos, and M. Prato, *Curr. Opin. Chem. Biol.* 9 (2005) 674, "Applications of carbon nanotubes in drug delivery".
8. Birkett, P. R., A. J. Cheetham, B. R. Eggen, J. P. Hare, H. W. Kroto, and D. R. M. Walton, *Chem. Phys. Lett.* 281 (1997) 111-114, "Transition metal surface decorated fullerenes as possible catalytic agents for the creation of single walled nanotubes of uniform diameter".
9. Bom, D., R. Andrews, D. Jacques, J. Anthony, B. L. Chen, M. S. Meier, and J. P. Selegue, *Nano Lett.* 2 (2002) 615-619, "Thermogravimetric analysis of the oxidation of

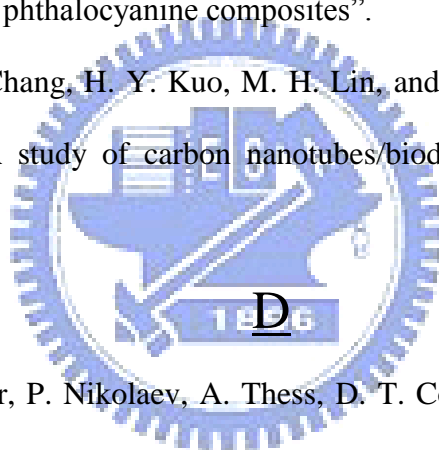


multiwalled carbon nanotubes: Evidence for the role of defect sites in carbon nanotube chemistry”.

10. Boul, P. J., J. Liu, E. T. Mickelson, C. B. Huffman, L. M. Ericson, I. W. Chiang, K. A. Smith, D. T. Colbert, R. H. Hauge, J. L. Margrave, and R. E. Smalley, Chem Phys. Lett. 310 (1999) 367-372, “Reversible sidewall functionalization of buckytubes”.
11. Briggs, D. and M. P. Seah, “Practical Surface Analysis”, (Jon Wiley & Sons, 1996), pp. 7.

## C

12. Cao, L., H. Z. Chen, M. Wang, J. Z. Sun, X. B. Zhang, and F. Z. Kong, J. Phys. Chem. B 106 (2002) 8971-8975, “Photoconductivity study of modified carbon nanotube/oxotitanium phthalocyanine composites”.
13. Chiu, W. M., Y. A. Chang, H. Y. Kuo, M. H. Lin, and H. C. Wen, J. Appl. Polym. Sci, 108 (2008) 3024, “A study of carbon nanotubes/biodegradable plastic polylactic acid composites”.



14. Dai, H., A. G. Rinzler, P. Nikolaev, A. Thess, D. T. Colbert, and R. E. Smalley, Chem. Phys. Lett., 260 (1996) 471-475, ”Single-walled nanotubes produced by metal catalyzed disproportionation of carbon monoxide”.
15. Dileo, R. A., B. J. Landi, and R. P. Raffaele, J. Appl. Phys. 101 (2007) 064307, “Purity assessment of multiwalled carbon nanotubes by Raman spectroscopy”.
16. Dillon, A. C., M. Yudasaka, and M. S. Dresselhaus, J. Nanosci. Nanotechnol. 4 (2004) 691-703, “Employing Raman spectroscopy to qualitatively evaluate the purity of carbon single-wall nanotube materials”.
17. Dresselhaus, M. S., G. Dresselhaus, R. Saito, and A. Jorio, Phys. Rep., 409 (2005) 47, “Raman spectroscopy of carbon nanotubes”.
18. Dresselhaus, M. S., G. Dresselhaus, A. Jorio, A. G. Souza, M. A. Pimenta, and R. Saito,

- Acc. Chem. Res. 35 (2002) 1070-1078, "Single nanotube Raman spectroscopy".
19. Dujardin, E., T. W. Ebbesen, A. Krishnan, and M. M. J. Treacy, *Adv. Mater.* 10 (1998) 1472-1475, "Wetting of single shell carbon nanotubes".
20. Dumitrescu, L., N. R. Wilson, and J. V. Macpherson, *J. Phys. Chem. C* 111 (2007) 12944-12953, "Functionalizing single-walled carbon nanotube networks: Effect on electrical and electrochemical properties".

## F

21. Felten, A., C. Bittencourt, J. J. Pireaux, G. Van Lier, and J. C. Charlier, *J. Appl. Phys.* 98 (2005) 074308, "Radio-frequency plasma functionalization of carbon nanotubes surface O<sub>2</sub>, NH<sub>3</sub>, and CF<sub>4</sub> treatments".
22. Flahaut, E., A. Peigney, C. Laurent, and A. Rousset, *J. Mater. Chem.* 10 (2000) 249, "Synthesis of single-walled carbon nanotube-Co-MgO composite powders and extraction of the nanotubes".
23. Fu, K. F. and Y. P. Sun, *J. Nanosci. Nanotechnol.* 3 (2003) 351-364, "Dispersion and solubilization of carbon nanotubes".

## G

24. Golovko, V. B., H. W. Li, B. Kleinsorge, S. Hofmann, J. Geng, M. Cantoro, Z. Yang, D. A. Jefferson, B. F. G. Johnson, W. T. S. Huck, and J. Robertson, *Nanotechnology.* 16 (2005)1636-1640, "Submicron patterning of Co colloid catalyst for growth of vertically aligned carbon nanotubes".
25. Gorbunov, O. Jost, W. Pompe, and A. Graff, *Carbon* 40 (2002) 113-118, "Solid-liquid-solid growth mechanism of single-wall carbon Nanotubes".
26. Guo T, P. Nikolaev, A. Thess, D. T. Colbert, and R. E. Smalley, *Chem. Phys. Lett.* 243 (1995) 49-54, "Catalytic Growth of Single-walled Nanotubes by Laser Vaporization".

## H

27. Harutyunyan, A. R., B. K. Pradhan, J. P. Chang, G. G. Chen, and P. C. Eklund, *J. Phys. Chem. B* 106 (2002) 8671-8675, "Purification of single-wall carbon nanotubes by selective microwave heating of catalyst particles".
28. Hassanien, M. Tokumoto, P. Umek, D. Vrbanic, M. Mozetic, D. Mihailovic, P. Venturini, and S. Pejovnik, *Nanotechnology* 15 (2005) 278-281, "Selective etching of metallic single-wall carbon nanotubes with hydrogen plasma".
29. Hofmann, S., R. Sharma, C. Ducati, G. Du, C. Mattevi, C. Cepek, M. Cantoro, S. Pisana, A. Parvez, F. Cervantes-Sodi, A. C. Ferrari, R. Dunin-Borkowski, S. Lizzit, L. Petaccia, A. Goldoni, and J. Robertson. *Nano Lett.* 7 (2007) 602, "In situ observations of catalyst dynamics during surface-bound carbon nanotube nucleation".
30. Hou, P. X., S. Bai, Q. H. Yang, C. Liu, and H. M. Cheng, *Carbon* 40 (2002) 81-85, "Multi-step purification of carbon nanotubes".
31. [http://en.wikipedia.org/wiki/Carbon\\_nanotube](http://en.wikipedia.org/wiki/Carbon_nanotube)
32. Hu, H., B. Zhao, M. E. Itkis, and R. C. Haddon, *J. Phys. Chem. B* 107 (2003) 13838-13842, "Nitric acid purification of single-walled carbon nanotubes".

## I

33. Ionescu, R., E. H. Espinosa, E. Sotter, E. Llobet, X. Vilanova, X. Correig, A. Felten, C. Bittencourt, G. Van Lier, J. C. Charlier, and J. J. Pireaux, *Sens. Actuators B* 113 (2006) 36, "Oxygen functionalisation of MWNT and their use as gas sensitive thick-film layers".
34. Itkis, M. E., D. E. Perea, R. Jung, S. Niyogi, and R. C. Haddon, *J. Am. Chem. Soc.* 127 (2005) 3439-3948, "Comparison of analytical techniques for purity evaluation of single-walled carbon nanotubes".

## J

35. Jian, S. R., Y. T. Chen, C. F. Wang, H. C. Wen, W. M. Chiu, and C. S. Yang, *Nanoscale*

- Res Lett. 3 (2008) 230-235, "The influences of H-2 plasma pretreatment on the growth of vertically aligned carbon nanotubes by microwave plasma chemical vapor deposition".
36. Jishi, R. A., D. Inomata, K. Nakao, M. S. Dresselhaus, and G. Dresselhaus, J. Phys. Soc. Jpn. 63 (1994) 2252-2260, "Electronic and Lattice Properties of Carbon Nanotubes".
37. Jorio, A., C. Fantini, M. A. Pimenta, R. B. Capaz, G. G. Samsonidze, G. Dresselhaus, M. S. Dresselhaus, J. Jiang, N. Kobayashi, A. Gruneis, and R. Saito, Phys. Rev. B 71 (2005) 075401, "Resonance Raman spectroscopy (n,m)-dependent effects in small-diameter single-wall carbon nanotubes".
38. Joy, D. C., Curr. Opin. Solid State Mater. Sci. 2 (1997) 465-468, "Scanning electron microscopy for materials characterization".
39. Juan, C. P., C. C. Tsai, K. H. Chen, L. C. Chen, and H. G. C. Cheng, Jpn. J. Appl. Phys. 44 (2005) 8231-8236, "Effects of high-density oxygen plasma posttreatment on field emission properties of carbon nanotube field-emission displays".
40. Kataura H, Y. Kumazawa, Y. Maniwa, I. Umez, S. Suzuki, Y. Ohtsuka, and Y. Achiba, Synth. Met. 103 (1999) 2555-2558, "Optical properties of single-wall carbon nanotubes".
41. Khare, B. N., P. Wilhite, R. C. Quinn, B. Chen, R. H. Schingler, B. Tran, H. Imanaka, C. R. So, C. W. Bauschlicher, and M. Meyyappan, J. Phys. Chem. B 108 (2004) 8166-8172, "Functionalization of carbon nanotubes by ammonia glow-discharge: Experiments and modeling".
42. Khare B, P. Wilhite, B. Tran, E. Teixeira, K. Fresquez, D. N. Mvondo, C. Bauschlicher, and M. Meyyappan, J. Phys. Chem. B 109 (2005) 23466-23472, "Functionalization of carbon nanotubes via nitrogen glow discharge".
43. Khare, B. N., P. Wilhite, and M. Meyyappan, Nanotechnology 15 (2004) 1650, "The fluorination of single wall carbon nanotubes using microwave plasma".

44. Kurt, R., J. M. Bonard, and A. Karimi, Carbon 39 (2001) 1723-1730, "Morphology and field emission properties of nano-structured nitrogenated carbon films produced by plasma enhanced hot filament CVD".

## L

45. Landi, B. J., C. D. Cress, C. M. Evans, and R. P. Raffaele, Chem. Mater. 17 (2005) 6819-6834, "Thermal oxidation profiling of single-walled carbon nanotubes".

46. Landi, B. J., H. J. Ruf, C. M. Evans, C. D. Cress, and R. P. Raffaele, J. Phys. Chem. B 109 (2005) 9952-9965, "Purity assessment of single-wall carbon nanotubes, using optical absorption spectroscopy".

47. Landi, B. J., R. P. Raffaele, S. L. Castro, and S. G. Bailey, Prog. Photovolt. 13 (2005) 165-172, "Single-wall carbon nanotube-polymer solar cells".

48. Lee, C. J., S. C. Lyu, Y. R. Cho, J. H. Lee, and K. I. Cho, Chem. Phys. Lett. 341 (2001), 245-249, "Diameter-controlled growth of carbon nanotubes using thermal chemical vapor deposition".

49. Li, C. H., K. F. Yao, and J. Liang, Carbon 41 (2003) 858-860, "Influence of acid treatments on the activity of carbon nanotube-supported catalysts".

50. Lian, Y., Y. Maeda, T. Wakahara, T. Akasaka, S. Kazaoui, N. Minami, T. Shimizu, N. Choi, and H. Tokumoto, J. Phys. Chem. B 108 (2004) 8848, "Nondestructive and high-recovery-yield purification of single-walled carbon nanotubes by chemical functionalization".

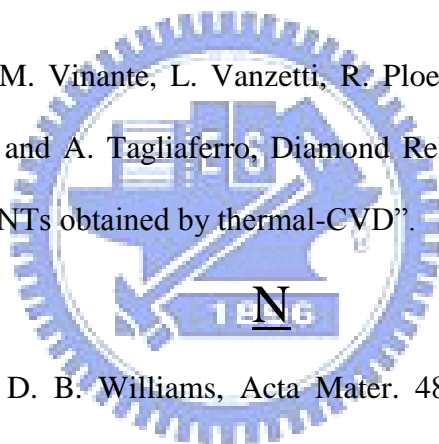
51. Liu, J., A. G. Rinzler, H. J. Dai, J. H. Hafner, R. K. Bradley, P. J. Boul, A. Lu, T. Iverson, K. Shelimov, C. B. Huffman, F. Rodriguez-Macias, Y. S. Shon, T. R. Lee, D. T. Colbert, and R. E. Smalley, Science, 280 (1998) 1253-1256, "Fullerene pipes".

52. Liu, Q. F., W. C. Ren, F. Li, H. T. Cong, and H. M. Cheng, J. Phys. Chem. C 111 (2007) 5006-5013, "Synthesis and high thermal stability of double-walled carbon nanotubes

using nickel formate dihydrate as catalyst precursor”.

## M

53. Maultzsch, J., S. Reich, C. Thomsen, S. Webster, R. Czerw, D. L. Carroll, S. M. C. Vieira, P. R. Birkett, and C. A. Rego, *Appl. Phys. Lett.* 81 (2002) 2647-2649, “Raman characterization of boron-doped multiwalled carbon nanotubes”.
54. Matsuo, S. and Y. Adachi, *Jpn. J. Appl. Phys.* 21 (1982) L4-L6, “Reactive Ion Beam Etching Using a Broad Beam ECR Ion Source”.
55. Mickelson, E. T., C. B. Huffman, A. G. Rinzler, R. E. Smalley, R. H. Hauge, and J. L. Margrave, *Chem. Phys. Lett.* 296 (1998) 188-194, “Fluorination of single-wall carbon nanotubes”.
56. Musso, S., S. Porro, M. Vinante, L. Vanzetti, R. Ploeger, M. Giorcelli, B. Possetti, F. Trotta, C. Pederzoli, and A. Tagliaferro, *Diamond Relat. Mater.* 16 (2007) 1183-1187, “Modification of MWNTs obtained by thermal-CVD”.



57. Newbury, D. E. and D. B. Williams, *Acta Mater.* 48 (2000) 323-346, “The electron microscope: The materials characterization tool of the millennium”.
58. Ni, B. and S. B. Sinnott, *Phys. Rev. Lett.* 61 (2000) R16343-R16346, “Chemical functionalization of carbon nanotubes through energetic radical collisions”.

## O

59. O'Connell, P. Boul, L. M. Ericson, C. Huffman, Y. H. Wang, E. Haroz, C. Kuper, J. Tour, K. D. Ausman, and R. E. Smalley, *Chem. Phys. Lett.* 342 (2001) 265, “Reversible water-solubilization of single-walled carbon nanotubes by polymer wrapping”.
60. Osswald, M. Havel, and Y. Gogotsi, *J. of Raman Spectrosc.* 38 (2007) 728-736, “Monitoring oxidation of multiwalled carbon nanotubes by Raman spectroscopy”.
61. Ovejero, G., J. L. Sotelo, M. D. Romero, A. Rodriguez, M. A. Ocana, G. Rodriguez, and J.

Garcia, *Ind. Eng. Chem. Res.* 45 (2006) 2206, "Multiwalled carbon nanotubes for liquid-phase oxidation. Functionalization, characterization, and catalytic activity. *Industrial & Engineering Chemistry Research*".

## P

62. Park, Y. S., J. Wilkinson, S. Banda, Z. Ounaies, K. E. Wise, G. Sauti, P. T. Lillehei, and J. S. Harrison, *Carbon* 39 (2001) 655-661, "High yield purification of multiwalled carbon nanotubes by selective oxidation during thermal annealing".

63. Park, T. J., S. Banerjee, T. Hemraj-Benny, and S. S. Wong, *J. Mater. Chem.* 16 (2006) 141-154, "Purification strategies and purity visualization techniques for single-walled carbon nanotubes".

64. Pillai, S. K., S. S. Ray, and M. Moodley, *J. Nanosci. Nanotechnol.* 7 (2007) 3011-3047, "Purification of single-walled carbon nanotubes".

65. Qin, L. C., D. Zhou, A. R. Krauss, and D. M. Gruen, *App. Phys. Lett.* 72 (1998) 3437-3439, "Growing carbon nanotubes by microwave plasma-enhanced chemical vapor deposition".

## R

66. Raravikar, N. R., P. Keblinski, A. M. Rao, M. S. Dresselhaus, L. S. Schadler, and P. M. Ajayan, *Phys. Rev. B* 66 (2002), 235424-1-9, "Temperature dependence of radial breathing mode Raman frequency of single-walled carbon nanotubes".

67. Rao, A. M., E. Richter, S. Bandow, B. Chase, P. C. Eklund, K. A. Williams, S. Fang, K. R. Subbaswamy, M. Menon, A. Thess, R. E. Smalley, G. Dresselhaus, and M. S. Dresselhaus, *Science* 275 (1997) 187-191, "Diameter-Selective Raman Scattering from Vibrational Modes in Carbon Nanotubes".

## S

68. Saito, R., M. Fujita, G. Dresselhaus, and M. S. Dresselhaus, *Appl. Phys. Lett.* 60 (1992) 2204-2206, "Electronic-structure of Chiral Graphene Tubules".
69. Saito, R., Dresselhaus, G., and Dresselhaus, M. S., "Physical Properties of Carbon Nanotubes", (Imperial College Press, 2004), pp. 25, 35, 38, 46, 47, 59, 60.
70. Saito, Y., M. Okuda, N. Fujimoto, T. Yoshikawa, M. Tomita, and T. Hayashi, *Jpn. J. Appl. Phys.* 33, (1994), L526-L529, "Single-wall carbon nanotubes growing radially from Ni fine particles formed by arc evaporation".
71. Saito, Y, *Carbon* 33 (1995) 979-988, "Nanoparticles and filled nanocapsules".
72. Y. Saito, K. Nishikubo, K. Kawabata, and T. Matsumoto, *J. Appl. Phys.* 80 (1996) 3062-3067 "Carbon nanocapsules and single-layered nanotubes produced with platinum-group metals (Ru, Rh, Pd, Os, Ir, Pt) by arc discharge".
73. Shaijumon, M. M., N. Bejoy, and S. Ramaprabhu, *Appl. Surf. Sci.* 242 (2005) 192, "Catalytic growth of carbon nanotubes over Ni/Cr hydrotalcite-type anionic clay and their hydrogen storage properties".
74. Shi, Z. J., Y. F. Lian, F. H. Liao, X. H. Zhou, Z. N. Gu, Y. G. Zhang, and S. Iijima, *Solid State Commun.* 112 (1999) 35-37, "Purification of single-wall carbon nanotubes".
75. Smart S. K., A. I. Cassady, G. Q. Lu, and D. J. Martin, *Carbon* 44 (2006) 1034, "The biocompatibility of carbon nanotubes".
76. Smith, E. and G. Dent, "Modern Raman Spectroscopy- A practical Approach", (John Willey & Sons, Ltd. 2005), pp. 2.

## T

77. Tohji K., T. Goto, H. Takahashi, Y. Shinoda, N. Shimizu, B. Jeyadevan, I. Matsuoka, Y. Saito, A. Kasuya, T. Ohsuna, H. Hiraga, and Y. Nishina, *Nature* 383 (1996) 679-679, "Purifying single-walled nanotubes".
78. Tsai, M. H., M. S. Thesis, (2001), Mat. Res. Lab., MSE, NCTU, "Deposition mechanisms



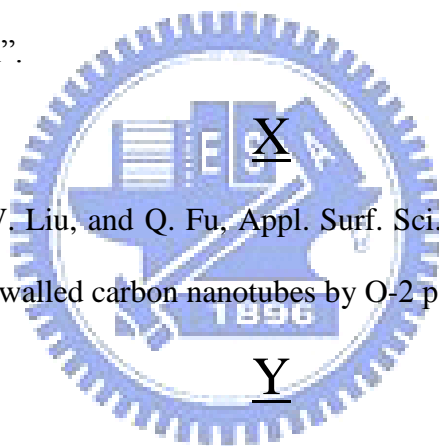
and properties of large area well-aligned carbon nanotubes by catalyst-assisted ECR-CVD method”.

## V

79. Venkatesan, N., J. Yoshimitsu, Y. Ito, N. Shibata, and K. Takada, *Biomaterials* 26 (2005) 7154-7163, “Liquid filled nanoparticles as a drug delivery tool for protein therapeutics”.

## W

80. Wiltner, A. and C. Linsmeier, *Phys. Status Solidi A* 201 (2004) 881-887, “Formation of endothermic carbides on iron and nickel”.
81. Wu, Z. Y., Y. Y. Xu, X. L. Zhang, G. L. Shen, and R. Q. Yu, *Talanta* 72 (2007) 1336-1341, “Microwave plasma treated carbon nanotubes and their electrochemical biosensing application”.



82. Xu, T., .H. Yang, J. W. Liu, and Q. Fu, *Appl. Surf. Sci.* 253 (2007) 8945-8951, “Surface modification of multi-walled carbon nanotubes by O-2 plasma”.

83. Yu, K., Z. Q. Zhu, Y. S. Zhang, Q. Li, W. M. Wang, L. Q. Luo, X. W. Yu, H. L. Ma, Z. W. Li, and T. Feng, *Appl. Surf. Sci.* 225 (2004) 380-388, “Change of surface morphology and field emission property of carbon nanotube films treated using a hydrogen plasma”.

## Z

84. Zhang, M., M. Yudasaka, and S. Iijima, *J. Phys. Chem. B.* 108 (2004) 149-153, “Diameter enlargement of single-wall carbon nanotubes by oxidation”.
85. Zhang, J. H., T. Feng, W. D. Yu, X. H. Liu, X. Wang, and Q. Li, *Diamond Relat. Mater.* 13 (2004) 54-59, “Enhancement of field emission from hydrogen plasma processed carbon nanotubes”.
86. Zhang, Y., S. L. Yuan, W. W. Zhou, J. J. Xu, and Y. Li, *J. Nanosci Nanotechnol.* 7 (2007)

2366-2375, “Spectroscopic evidence and molecular simulation investigation of the pi-pi interaction between pyrene molecules and carbon nanotubes”.

87. Zheng, G., Q. Q. Li, K.L. Jiang, X. B. Zhang, J. Chen, Z. Ren, and S. S. Fan, Nano Lett. 7 (2007) 1622-1625, “Transition of single-walled carbon nanotubes from metallic to semiconducting in field-effect transistors by hydrogen plasma treatment”.

88. 郭正次, 朝春光, “奈米結構材料科學”, (全華科技圖書股份有限公司), 2004, pp. 9-2, 9-9.



# Vita

姓名：曾文綬 Wen-Shou Tseng  
出生年月日：民國 57 年 04 月 25 日  
聯絡電話：0937840271  
通訊住址：320 中壢市西園路 8-11 號 6 樓  
電子郵件信箱：wstseng.mse92g@nctu.edu.tw

## 學歷：

博士：國立交通大學材料科學與工程學系 民國 92 年 9 月 ~ 民國 98 年 6 月  
碩士：英國曼徹斯特大學(University of Manchester)材料中心高階工程材料組 民國 90 年 9 月 ~ 民國 91 年 12 月  
大學：國立中央大學機械工程學系 民國 76 年 9 月 ~ 民國 80 年 6 月

## 經歷：

1. 41 期預官 裝甲兵少尉連絡官 民國 80 年 7 月 ~ 民國 82 年 6 月
2. 永大機電股份有限公司 機械設計工程師 民國 82 年 6 月 ~ 民國 84 年 2 月
3. 台達電子自動化工程處 高級工程師及專案計劃主持人 民國 84 年 2 月 ~ 民國 90 年 8 月
4. Unaxis PECVD 工程師 民國 92 年 1 月 ~ 民國 92 年 7 月
5. 訊倉科技 LCM 製程及設備部經理 民國 92 年 7 月 ~ 民國 93 年 5 月
6. 統寶光電 AMOLED 量產規劃部副理 民國 93 年 7 月 ~ 民國 95 年 2 月
7. 東捷科技 總經理室技術經理 民國 97 年 10 月 ~ 民國 98 年 2 月

## 期刊論文：

1. W.S. Tseng, C.Y. Tseng, P.K. Chuang, A.Y. Lo, C.T. Kuo, "A High Efficiency Surface Modification Process for Multi-walled Carbon Nanotubes by Electron Cyclotron Resonance Plasma", Journal of Physical Chemistry C 112 (2008) 18431-18436.
2. W.S. Tseng, C.Y. Tseng, C.T. Kuo, "Effects of gas composition on highly efficient surface modification of multi-walled carbon nanotubes by cation treatment", Nanoscale Research Letters 4 (2009) 234-239.
3. W.S. Tseng, C.Y. Tseng, C.T. Kuo, "Functionalizing Multi-Walled Carbon Nanotubes Using ECR Plasma and a Mild Nitric Acid Treatment", Feb 15, 2009, Accepted by Journal of Nanoscience and Nanotechnology.
4. W.S. Tseng, W.H. Wang, T.H. Hong, C.T. Kuo, "Metal Oxide Film for Growing Vertically Aligned Single-walled Carbon Nanotubes", May 25, 2009, Accepted by Japanese Journal of Applied Physics.

國際研討會論文：

1. W.S. Tseng, W.H. Wang, T.H. Hong, C.T. Kuo, “Effect of catalyst thickness on the chirality of SWNTs deposited by MPCVD”, New Diamond and Nano Carbons International Conference, Osaka, Japan (2007)

國內研討會論文：

1. 曾文綬, 王威翔, 洪蔡豪, 郭正次, “以新型微波輔助化學氣相沉積法成長不同旋度單壁碳奈米管, 2007年台日材料熱處理計術研討會, Taipei, Taiwan (2007) 口頭報告
2. 曾文綬, 王威翔, 洪蔡豪, 郭正次, “金屬氧化層厚度於利用微波輔助化學氣相沉積法成長單壁碳奈米管時對於其旋度及結構之影響”, 2008年台灣鍍膜科技協會年會暨國科會專題計劃研究成果發表會, Changhua, Taiwan (2008)

